Eindhoven University of Technology

MASTER

An experimental and numerical (vortexmethod) simulation of the mixing of two gasflows with large densityratio

de Kruiff, G.T.

Award date:
1986

Link to publication

Disclaimer
This document contains a student thesis (bachelor's or master's), as authored by a student at Eindhoven University of Technology. Student theses are made available in the TU/e repository upon obtaining the required degree. The grade received is not published on the document as presented in the repository. The required complexity or quality of research of student theses may vary by program, and the required minimum study period may vary in duration.

General rights
Copyright and moral rights for the publications made accessible in the public portal are retained by the authors and/or other copyright owners and it is a condition of accessing publications that users recognise and abide by the legal requirements associated with these rights.

- Users may download and print one copy of any publication from the public portal for the purpose of private study or research.
- You may not further distribute the material or use it for any profit-making activity or commercial gain

An experimental and numerical (vortexmethod) simulation of the mixing of two gasflows with large densityratio.

G.T. de Kruiff

Koninklijke/Shell-Laboratorium Amsterdam

nov 1984 - jan 1986

Afstudeerverslag

Afstudeer hoogleraar: Prof. ir. G. Vossers
Vakgroep: Transportfysica

Afdeling: Technische Natuurkunde

Technische Hogeschool Eindhoven

言天下之至動而不可亂也 周易繫辭[1]

[1] *Speaking of the most restless phenomenon in the universe, one should not be distracted by its randomness*

I Chin

Op deze plaats wil ik mijn dank uitspreken aan J.H.M. Disselhorst, H.J.A. Hasenack en R.J.M. van Dam voor de begeleiding en steun die ik van hen heb gekregen tijdens dit afstuderen.

SUMMARY

An important part of a coal gasification plant is the quench. In the quench hot particles containing reactorgas has to be cooled down by mixing it with cold gas. This must be done in such a way that no hot particles can reach a cold quench wall.
This report contains a theoretical and experimental investigation of a (so-called) A-type quench in which through an annular slit the cold gas is mixed into the hot gas.
In the theoretical part the applicability for this flow of a two dimensional vortex method is investigated. The conclusion is that only the first part of the mixing layer, which is dominated by large scale two dimensional phenomena, can thus be modelled.
A first step in the development of a vortexmethod has been made.
In the experimental part the flow is simulated in the Quench Test Unit. Nitrogen with temperatures of 90 K and 350 K has been used as modelgas. The results of three experiments, visualisation and slow- and fast temperature measurements, can produce enough information to optimalize the A-type quench design.

PART B THE QUENCH TEST UNIT

CHAPTER 1 INTRODUCTION

1.1 Background and purpose

In a coal-gasification plant coal is being gasified into syngas, a mixture of CO and H_2. Two important parts of such a plant are the gasification-reactor and the tube, connected to this reactor, through which the produced syngas flows.
In the gasification-reactor coal is injected together with oxygen. The coal is partly oxydized in order to create a temperature of a ca. 1800 K. At this temperature the reaction will continue and the final product is syngas. This gas contains a large number of ashparticles (diameter=ca. 20 micrometer) which at this temperature are liquid and very sticky. A part of these particles is captured by the reaction vessel wall and flows down into a slag tap. The rest of these particles will be convected with the gasflow and will stick to the cooler walls of the outlet pipe and probably will grow into big lumps and block the gasflow.
Several options to prevent this have been studied in the past.
The syngas has to be cooled before it can be produced further and cooled gasparticles lose their stickyness. So the problem is how to cool the ashladen syngas without the sticky ashparticles blocking the flow.
Shell has chosen a device in which the reactor gas is quickly cooled by mixing it with cold gas. Such a device is called a quench. (quenching means cooling very quickly).
A quench that has already operated used the principle of envelopping the ash-laden gasstream in a cold gasmantle. This is the so-called H-type quench. This quench performed quite well but did not fully prevent for all coal types the outlet-pipe wall from fouling.
A more recent idea is the so-called A-type quench. In such a quench the hot reactorgas is intensely mixed with a cold quenchgas that is injected at high speed into the hot flow through an annular slit at the bottom of the outletpipe (quenchshaft). The purpose of this cool gas addition is to cool the sticky ashparticles enough to remove their stickyness and thus preventing them from fouling the quench-shaft. The special feature of the A-type quench is its aerodynamic throat (fig.1.1) that prevents hot particles to reach the wall during the cooling proces.

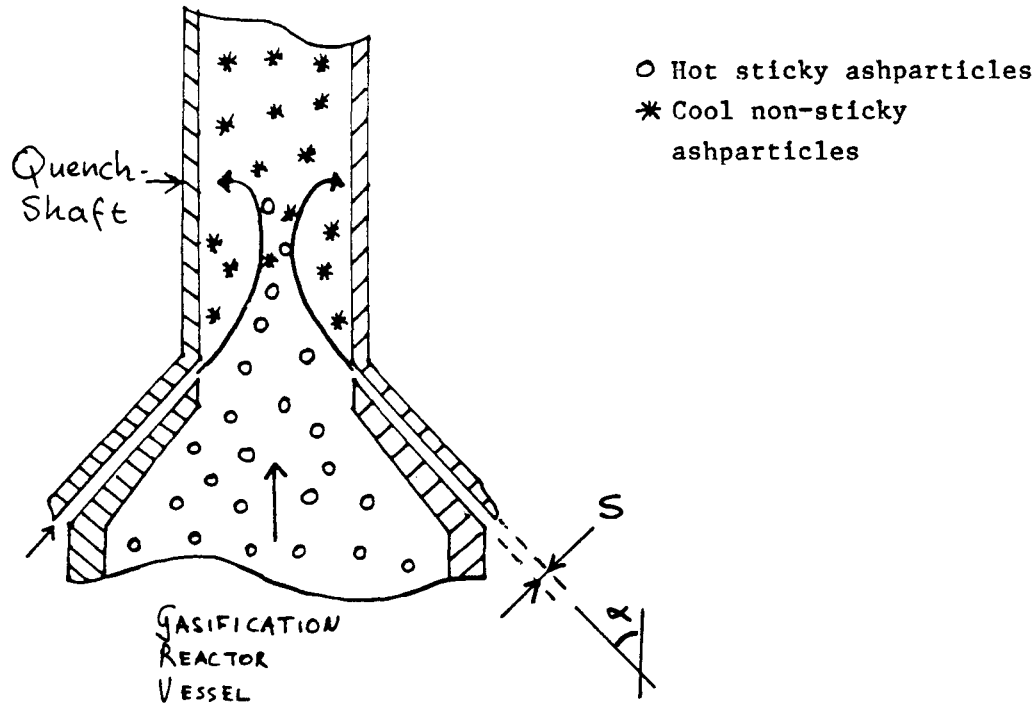

Fig.1.1 The A-type quench on top af the gasificationreactor

The investigations decribed in this report contribute to the understanding of the flow behavior in an A-type quench.
The designers of the coalgasification plant are primarily interested in an answer to the following question:
"Can an A-type quench be operated such that no slagging/fouling of the quench by ashparticles occurs?"
If this appears to be the case the second question becomes relevant:
"Can we reduce the shaftlength by increasing the mixing/quenching-speed?"
If normal operating condition exist in a quench with one annular slit only two parameters are left to optimize quenchperformance:

- The slitwidth (S)
- The angle between the annular slit and the quenchshaft (α)

This paper contains a theoretical (part A) and an experimental (part B) investigation of the A-type quench flow. In the theoretical part a vortexmethod is used to model a mixing-flow.
As a first step in investigating mixing in the complex A-type geometry a more simple geometry was studied. This is the geometry of the plane mixing layer. In chapter 2 a literature overview of the experimental knowledge of the plane mixing layer is given. In chapter 3 some basic theory concerning the vortexmethod and in chapter 4 a literature overview of the vortexmethod is given.

In chapter 5 a description of a vortexmethod by the author is given. As a first step the plane mixing layer was simulated with the vortexmethod. The simulation of the A-type quench flow was not completed, and some problems concerning this simulation are not yet solved. The basic outline for this simulation however is already given.
The experimental part of the investigation consists of the designing, building and testing of a scalemodel of the A-type quench. In this model it is possible to study as well the effect of the slitwidth S as the effect of the angle on the quenchperformance. Details about the design of this so-called Quench Test Unit (Q.T.U.) can be found in chapter 6. The description and some examples of the the results of the actual experiments are given in chapter 7. Due to delays in the building of the Q.T.U. this paper will not give all the results available nor an extensive discussion of the results.
Finally in part C a final conclusion will be given.

PART A THEORETICAL DESCRIPTION OF THE MIXING LAYER

CHAPTER 2 PENOMENOLOGY OF THE PLANE MIXINGLAYER; LITERATURE

2.1 Introduction

In chapter 1 the study of parallel mixing was announced as a first step of understanding the quenchflow in a A-type quench. A mixing flow is a very good example of a turbulent flow. So understanding a mixing flow means having some understanding of turbulence.
Turbulence is described by Hinze 5) as follows:

1.) Turbulent fluid motion is an irregular condition of flow in which the various physical quantities show a random variation with time- and spacecoordinates, so that statistically average values can be discerned.

2.) Turbulence is a continuum phenomena, that is characterized by a strong diffusive nature with respect to any transferable property.

3.) Turbulence exists of the superposition of eddies of various sizes. There is a strong interaction between these eddies resulting in an energytransfer from the bigger eddies to the smaller ones.

Various models for describing turbulence, based on these conceptions, have been developed in the last 100 years. Well known is the mixing-length model of Prandtl and more recent the k-ϵ models.
Recent investigations, of which we will describe some examples, have shown that turbulent motion is not as chaotic as had been thought. It seems that coherent structures of deterministic nature are an essential feature of turbulence. Such coherent structures have been observed for a long time. Famous are for example the drawings of Leonardo Da Vinci (1452-1519), see figure 2.1.1.

Fig. 2.1.1 Drawing by Leonardo Da Vinci with coherent structures.

The existence of these coherent structures however has been attributed to the geometric configuration of the flowdomain. Only recently it has become clear that by using only statistical information of a turbulent flow important information is lost. Stated differently, a lot af properties of turbulent flow can be explained with the concept of coherent structures.
The vortexmethod, to decribe turbulent flow, makes use of this concept. Most flows of high Reynolds number are characterized by areas with high vorticity and areas with low vorticity. Coherent structures nearly always coincide with the areas of high vorticity. A good example of such a turbulent flow and the flow that is of great importance to the A-type quench is the mixing layer.
The most simple form of a mixing layer is the plane mixing layer. In the plane mixing layer two fluidstreams *) of different velocities meet eachother after a sharp separation point. The x-coordinate starts at the origin in the separation point and goes in streamwise direction, the y-coordinate is perpendicular to the splitter plate (figure 2.1.2).

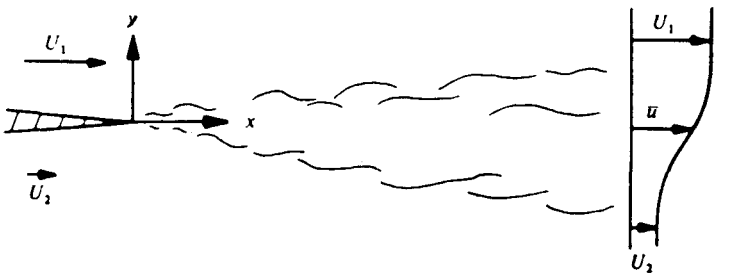

figure 2.1.2 The plane mixing layer

Since it is the aim of this work to model the mixing layer in the A-type quench with a vortexmethod the first step would be to model the plane mixing layer with a vortexmethod, and preferably with a two-dimensional vortexmethod.
In order to get a good idea of how the plane mixing layer looks like in reality paragraph 2.2 describes experimental results about the plane mixing layer as presented in literature.
In paragraph 2.3 a synthesis of the descriptions of the plane mixing layer based on paragraph 2.2.

*) The definition of plane mixing layer also includes the plane one-stream mixing layer, where U_1 or U_2 is 0.

2.2 Experimental evidence

In this paragraph we will describe the experimental work on the plane mixing layer by Winant & Browand 4), Brown & Roshko 3), Chandrsuda 7), Wygnanski 8), Breidenthal 11), Jimenez 13), Fiedler 14) and Dziomba 15).
The first two investigations descibe the mixinglayer as a two-dimensional phenomena, Chandrsuda stresses the three-dimensionality of the mixing-layer, Wygnanski attacks the view of Chandrsuda, Breidenthal & Jimenez reconcile these views and the last two articles are concerned with the effect that initial conditions have on the development of the mixing layer.

Winant and Browand 4) formed a plane mixing layer by bringing two streams of water, moving at different velocities, together in a walled channel. Dye was injected between the two streams just before they were brought together, marking the vorticity-carrying fluid. Unstable waves grew (Kelvin-Helmholtz-instability) and the wavelength of the system was that of the most unstable wave. Fluid was observed to roll up into discrete two-dimensional vortical structures.
These turbulent vortices interacted by rolling around eachother and they often formed a single vortical structure, see also figure 2.2.3. This repeatedly ocurring pairingprocess controlled the growth of the mixinglayer. Pairing was promoted by small variations in the strength and spacing of the vortical structures.

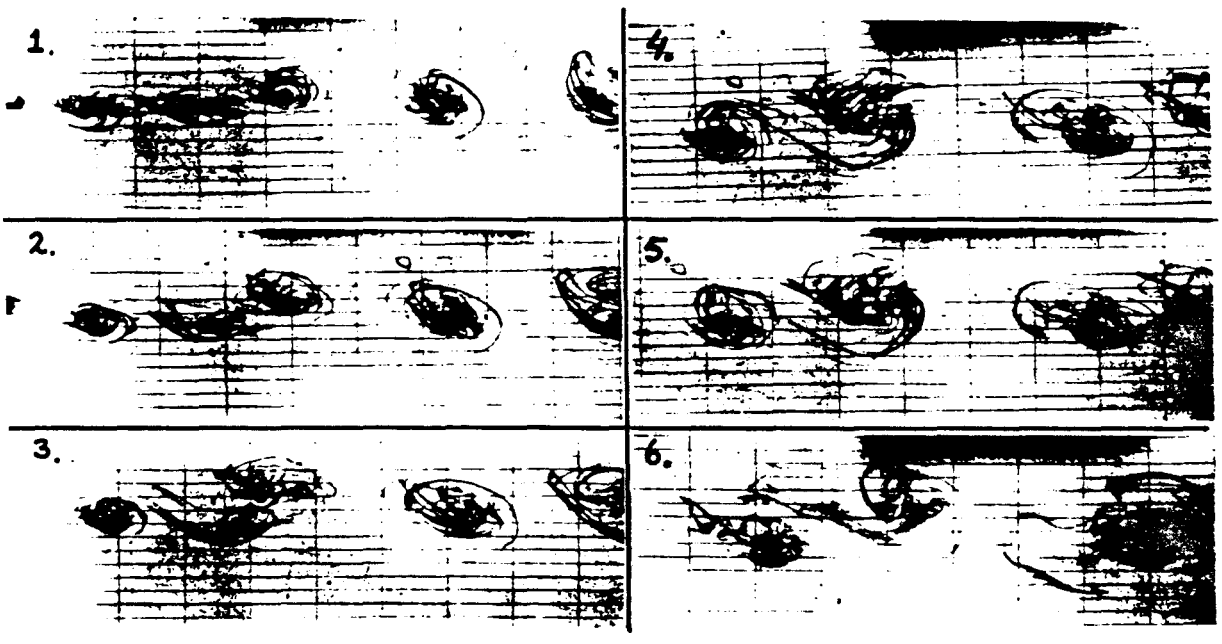

Fig. 2.2.1 Dye-photo's in a watertunnel demonstrating the rolling-up and pairing process of vortices in the plane mixing layer, by Winant & Browand 4).

In cases where the instability was mechanically forced the frequency of the wave was fixed by the frequency of the forcing-mechanism. This appeared to delay the proces of vortexpairing. In figure 2.2.1 a sequence of dye photograph's is presented.

Brown & Roshko 3) studied the plane mixing layer between two streams of different gases (nitrogen and helium).
With spark shadowpictures they showed that for all density-ratios the mixinglayer was dominated by large coherent structures, see figure 2.2.2.

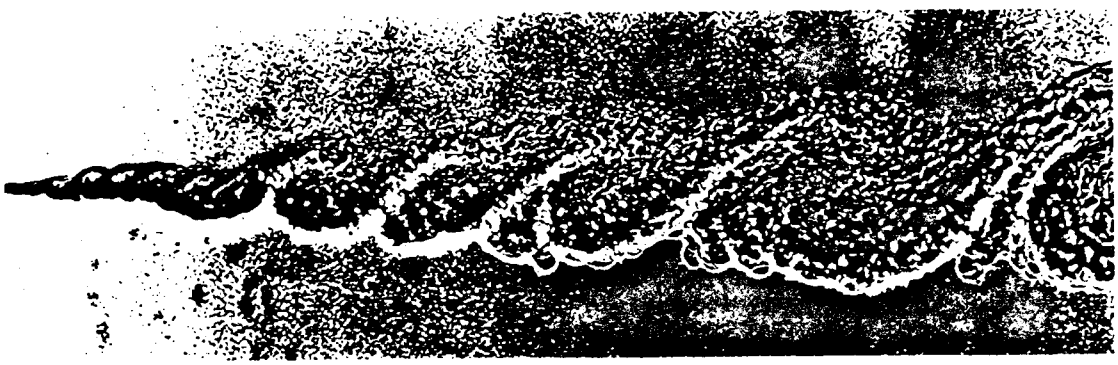

Fig.2.2.2 Shadowpicture of plane mixinglayer by Brown & Roshko 3).

High speed film showed that these structures were convected at nearly constant speed and increased their size and spacing discontinuously by amalgamation with neighbouring ones. In figure 2.2.3 the timehistory of a number of these coherent structures is given.

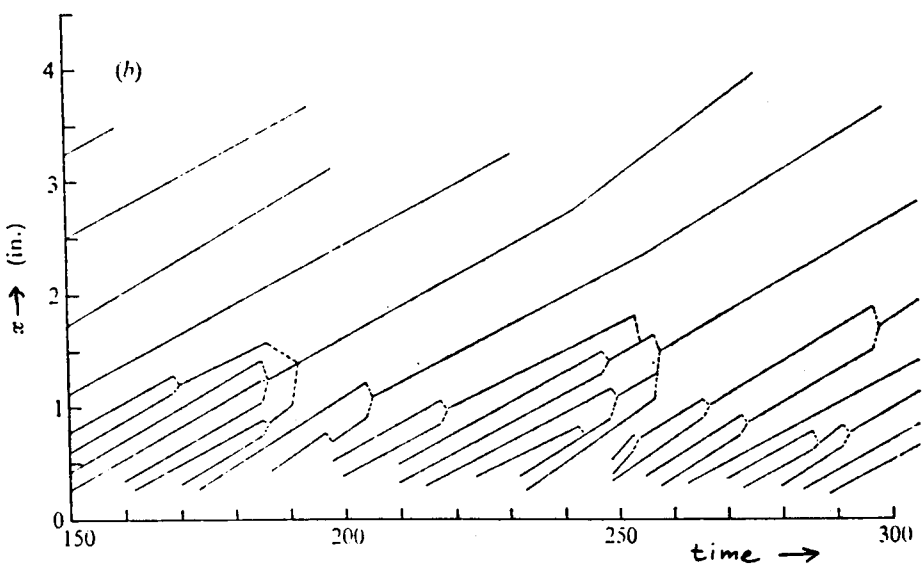

Fig.2.2.3 Timehistory of coherent structures by Brown & Roshko.

The pictures and measurements of density fluctuations suggest that turbulent mixing and entrainment (the process of dragging the surrounding fluid into the mixinglayer) is a process of entanglement on the scale of large structures.
Brown & Roshko defined the vorticity-thickness as a measure for the thickness of the mixinglayer:

$$\delta_\omega = \frac{U_1 - U_2}{\left(\frac{\partial U}{\partial y}\right)_{max}} \qquad (2.2.1)$$

The dependence of the vorticitythickness on the velocity-difference parameter $\lambda^* = (U_1-U_2)/(U_1+U_2)$ and on the density ratio $r = \rho_1/\rho_2$ is shown in figure 2.2.4.

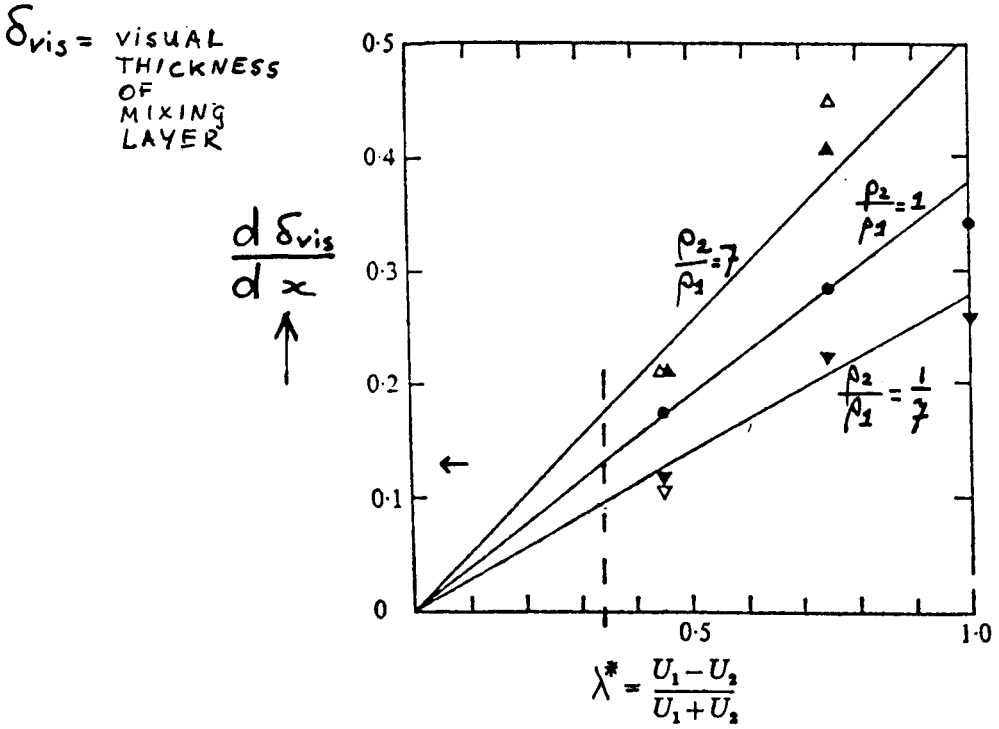

Fig.2.2.4 The grow of the vorticitythickness by Brown & Roshko 3).

-Influence of density difference-
Brown & Roshko found that in all mixing layers the spreading angle of the density profile was greater than the spreading angle of the velocity profile. This was particularly marked for the case where the massflows ($\rho_1 \cdot U_1 = \rho_2 \cdot U_2$) of flow 1 and 2 were equal, see figure 2.2.5. This implied significantly different diffusionrates for mass and momentum. When the data was compared with a simple eddy-viscosity model the Schmidtnumber Sc ($Sc = \gamma_T/D_T$ —> momentum diffusion / mass diffusion) for which the best correspondence was found lied between 0.2 and 0.3.

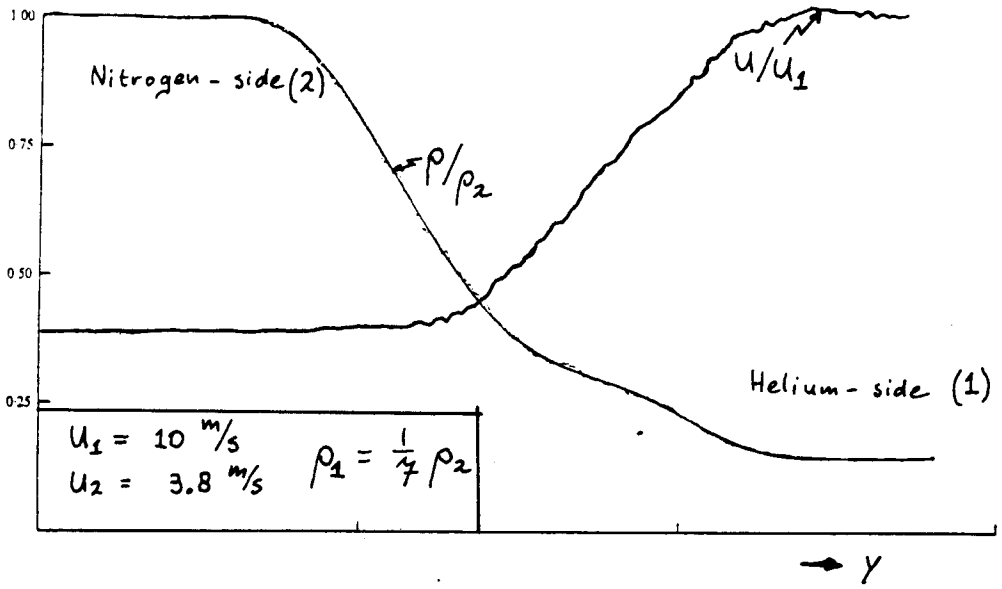

Fig.2.2.5 Averaged velocity- and densityprofile by Brown & Roshko.

This considerable difference in the diffusivities is related to the large structures in the flow. Owing to the large-amplitude excursions of the layer helium on one side was convected with little mixing to the nitrogen side and vice-versa. These velocity perturbations will be much less in the heavy than in the light gas, due to the requirement of continuity of the corresponding pressure-perturbation. Consequently, in traversing away from the low velocity dense gas on one side there will be a considerable change in mean composition before the mean velocity changes significantly.

-Entrainment-

Brown & Roshko also presented a simple model for the entrainment rate based on the concept that entrainment is caused by the entanglement of non-turbulent fluid by the large coherent structures. They assumed each eddy to be a cilindrical structure with diameter d_{viz}. When U_{avc} is the average convectionspeed of the eddies, and l_{av} is their average spacing then the averaged entangled flow-rate $\dot{Q}_e$ per unit span is given by:

$$\dot{Q}_e = \tfrac{1}{4} \cdot \pi \cdot d_{viz}^2 \cdot U_{avc} / l_{av} \qquad (2.2.2)$$

From experimental realations for d_{viz} and l_{av} they finally derived:

$$\dot{Q}_e = 0.104 \cdot \frac{1 - r_u}{1 + r_u} \cdot U_1 \cdot x \qquad (2.2.3)$$

with : $r_u = U_2/U_1$

This formula (2.2.3) accounts for all entangled fluid and does not distinguish between the two sides. They found reasonable agreement with entrainmentdata of other authors.

Chandrsuda et.al 7) performed a two-stream mixing layer experiment in a suck-down smoke tunnel. Turbulence-levels in the two streams were of order 0.2 %. They found that the persistance of the two-dimensional structures increased as the velocity-ratio departed from unity. The persistance of two-dimensional structures decreased however with increasing turbulence-level of the low velocity-stream. The mechanism of this break-down of two-dimensionality is the distortion by weak oscillations in the transition-region of the mixing layer. But even in the three-dimensional mixing-layer fairly regular large scale structures existed having a spatial distribution that was not radically different from the later stages of the Brown-Roshko flow.
The conclusion of Chandrsuda et.al. was that the 2-D Brown-Roshko vortex-roll disturbances will only arise in the rare situation of a plane mixing layer with laminar boundary layers at the nozzle exit and low turbulence-level in the external flow.
Other evidence suggested that the 2-D Br&R structure won't appear if the exit boundary layer is turbulent. They thought there was also reason to believe that the small-scale turbulence in the Br&R mixing layer will eventually break down the 2-D structures to three-dimensionality.
So they concluded there is only one asymptotic state of the plane mixing layer and its large structure is fully 3-D.

Wygnanski et.al 8) set out to test the sensitivity of the large eddy structure of the plane mixing layer to outside influences. They wanted to see how long these structures remained two-dimensional. Experiments were performed in a windtunnel with U_2 =15 m/s and U_1/U_2 = 0.4 with a turbulence-level of 0.2 %.
They introduced different kinds of disturbances on the initial conditions and also on the boundaryconditions of the mixinglayer. Spanwise correlation measurements were done at different downstream position for u'- and v'-velocities and also for a scalar contaminant (temperature). The conclusion was that an initial turbulent boundary layer did not influence the two-dimensionality of the mixing layer. Forcing improved the spanwise regularity of the large eddies.
Increasing the free-steam turbulence with a factor 15 to 3% caused the spanwise correlation to decrease quickly just after the splitterplate but its final value was not much less than in non-turbulent cases. It was thus concluded that the two-dimensional

turbulent cases. It was thus concluded that the two-dimensional character of the coherent eddies perseveres in spite of strong external small-scale buffeting.

Breidenthal et.al. 11) studied the plane mixing layer in a blow-down watertunnel. The free-stream turbulencelevel was around 0.5%. The maximum Reynoldsnumber achieved, based on the vorticitythickness of the mixing layer (δ_ω) and the velocitydifference between the two streams, was around 10^4.
An important goal of this investigation was to study the mixing at an intimate molecular level. This was done by letting a diffusion limited chemical reaction between the two streams produce an easily detectable reaction product.
It was concluded that if diffusion is the limiting factor in mixing then the mixing (the amount of product) is dependent of the Reynoldsnumber and the Schmidtnumber. However if (large scale) entrainment is the limiting factor (at high Reynoldsnumbers) then mixing is independent of Re and Sc. After transition (small-scale laminar to small-scale turbulent) mixing is esentially independent of Re.
Transition was influenced by the initial conditions. For example the transition Reynoldsnumber of the mixing layer ($\Delta U x/\nu$) decreased with increasing velocityratio.
In figure 2.2.6 the (speculative) effect of the initial Reynolds-number ($U_1 \theta_1/\nu$ (θ_1 = momentumthickness of boundarylayer at end of splitterplate) and the non-dimensional distance downstream x/θ_1 on the small-scale mixing (normalized product-thickness P/θ_1; P=thickness of productlayer) is given.

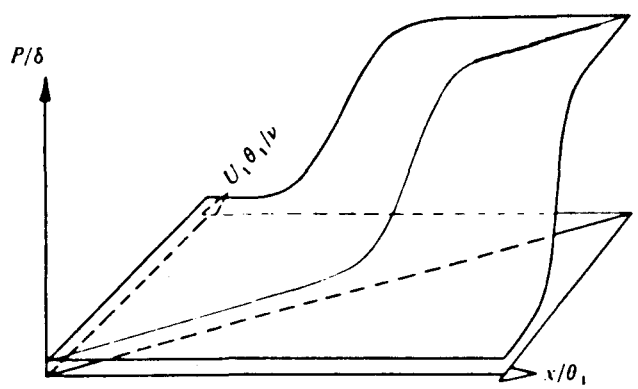

Fig.2.2.6 Speculative effect of the initial conditions on the transition in the mixing layer, by Breidenthal et.al.11)

What was clear was that there was no mixing in the initial 2-D disturbance region. Depending on the initial Reynoldsnumber sooner or later transition took place in the mixinglayer and mixing increased very quickly. After this transition the mixing was again Re-independent.
From the flow-pictures of the reaction product it appeared that next to the primary 2-D disturbance there were so-called span-wise wiggle-disturbance, These disturbances can maybe interpreted as streamwise vortices of alternating sign. The average wavelenth of this wiggle was about 1.1 times the wavelenth of the initial 2-D Kelvin-Helmholtz waves. Despite these three-dimensional effects and strong three-dimensional small-scale turbulence the large structure remained basically two-dimensional.

Jimenez et.al. 13) performed a mixing layer experiment in 7x11 cm water tunnel. One of the streams -the low speed one- contained a dye that fluoresced when illuminated with a sheet of laserlight perpendicular to the streamdirection. A film was made on a fixed position in the mixing layer. The dimension time, as represented by the sequence of filmframes, was converted to a space-dimension by supposing a certain convection velocity. Thus it was possible to create 3-D pictures of the mixing layer, see figure 2.2.7. Reynoldsnumbers, based on the mixinglayer thickness, were of order 300-600, corresponding (Breidenthal 4)) to the growth of 3-D instabilities and the well-developed region of 3-D instabilities.

Fig.2.2.7 The low-reynolds number mixing layer seen from the low-speed side, looking downstream. Flow is from bottom left to top right.

Out of these pictures it appeared that next to the primary spanwise vortices the plane mixing layer contained secondary structures who deformed these spanwise vortices.
These secondary vortices were in sign alternating longitudinal vortices, that were produced early in the evolution of the mixing layer as a result of the deformation of the 2-D eddies by a secondary instability.
At very low Re the vorticity field was 2-D, concentrated in the spanwise cores, and the mixing was low. During transition to 3-D the stream-wise longitudinal vortices appeared in the braids of the primary vortices (figure 2.2.8) but the vorticity was still largely 2-D in the cores. The only three dimensionality was in those places in which both systems intersected, above and below the classical cores. It was only there that mixing was enhanced. Further downstream small-scale turbulence was either produced or convected throughout the layer and mixing was more uniform.

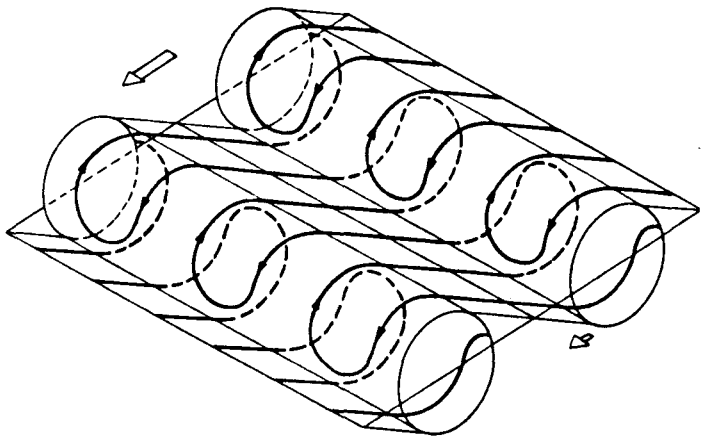

Fig. 2.2.8 Model for streamwise vorticity distribution

Jimenez et.al. devised a system to estimate vorticity strengths from concentration measurements. The strength of the longitudinal vortices was a large percentage of the local circulation in the spanwise vortexsystem. This suggested that their origin is some 3-D instability of the spanwise structure, either before or after the first pairing interaction.

Fiedler & Mensing 14) investigated the effect of excitation on the one-stream mixing layer in air with a turbulent boundary layer before separation.
The unexited free stream turbulence level in the 300x300 mm exit nozzle was smaller than 0.15 %. Exitation was applied near the separation point through a slit with the help of a loudspeaker.
They concluded that the neutral shear layer is unstable for

periodic perturbations. The perturbation wave was amplified along x, forming two-dimensional vortices of elliptical cross-section. Amplification is defined as the ratio between the amplitude of the disturbance at a downstream position and at the separation point. The rate of amplification was highest at the onset of vortexformation, it was zero at the saturation point x_s (near $x=U_o/f_o$ where U_o was the main stream velocity and f_o the excitation-frequency) and further downstream it was negative.
The maximum value of amplification depended on the strength of excitation. It was around 53 for exitationstrength -> 0.
It was observed that the sequence of periodic events in the stream was sensitive to the separation condition at the trailing edge. When forcing was applied such that the separation remained at all times fixed to the trailing edge only vortices of basic frequency were formed. After the saturation point the energy in the excitation frequency decayed exponentially, while the vortices lost coherence without pairing.
When on the other hand at strong forcing the separation point was no longer fixed to the trailing edge but moved periodically upstream, a stable condition of repeated pairing set in.
Formation of vortices -be it with or without pairing- was always accompanied by strong increase of spread and thus of entrainment. After saturation the spread rate strongly decreased. In the mean exited flows experienced approximately twice the spread compared to neutral flow. The turbulent shear stress had a maximum at vortex formation and a minimum at the beginning of decay.
The different ways of vortex formation, rolling-up of the sheet OR pairing of vortices, had no different effect on the flow properties, i.e. increase in spread, shear stress or entrainment)
The wavelengths of the disturbed vortexsheet (kelvin Helmholtz-wavelength) compared well with the values found by Hernan & Jimenez 1982 15):

Fiedler & Mensing: $\Lambda / \lambda (x-x_o) = 0.56$
Hernan & Jimenez: $\Lambda / \lambda (x-x_o) = 0.578$
with: Λ = wavelength, $\lambda = (U_1-U_2)/(U_1+U_2)$ and x_o = origin of mixing layer.

Dziomba et.al. 15) investigated both in a suction tunnel and in a blower tunnel the turbulent free shear layer. They made an effort to remove all resonance frequencies of the wind tunnel and if this was not possible to estimate their effect on the flow. Free stream turbulence levels were below .4 %.
They concluded that the initial conditions played an important role in the development of the free shear layer. One of the most crucial influences was a periodic oscillation forced upon the shear layer immediately downstream of the trailing edge. Other resonance

frequencies like those of the windtunnel influenced the shear layer in a similar, but moderate way. The shear layer reacted on this periodic disturbance only if the exited waves were close or identical to the natural wavelenth in the flow. In this case the corresponding vortices became stabilized over a certain distance while the spreading angle of the shear layer deviated from the linear.

Also Dziomba et.al. concluded that the discrete coherent vortex is not a typical constituent of the undisturbed free shear layer, only in the case of periodic forcing they become apparent.

Unintended forcing increased the spreading rate of the shear layer with more than 20 %. When the laminar-turbulence transition took place on the splitter-plate, i.e. the leaving boundary-layer was fully turbulent, the modulation forced upon the flow at the trailing edge was not weakened or cancelled by the transition process. Thus the effect of forcing was increased.

While disturbing frequencies could disturb the shear layer at almost any downstream position, only the developing region was influenced by the splitter-plate boundary layers or the trailing edge thickness.

Dziomba et.al. concluded that it is extremely difficult to create a shear layer whose characteristics are not influenced by outside disturbances.

2.3 Synthesis

In this paragraph it is tried to make a synthesis of the experimental evidence presented in paragraph 2.2.
The plane mixing layer can be divided in five regions:
(1) the boundary layer on the splitting plate,
(2) the free stream region,
(3) the linear region,
(4) the transition region and
(5) the fully turbulent region.

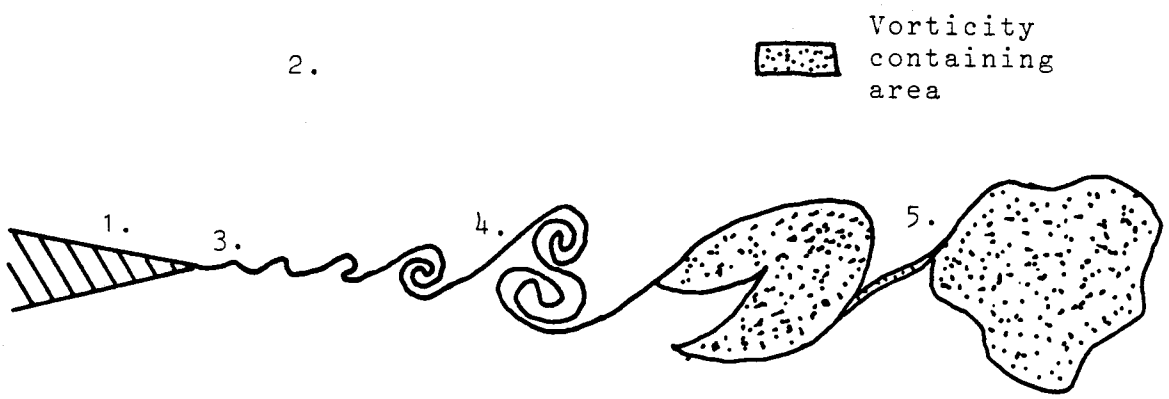

Figure 2.3.1 The division of the plane mixing layer in five regions

Also we will discern two different length-scales:
(1) The small-scale of the Kolmogorov vortices. On this scale molecular mixing takes place, and the
(2) The large-scale of the momentum thickness of the boundary layer or the mixinglayer. This is the scale on which large scale mixing, entrainment and mixing layer growth occurs.
The conditions existing in the boundarylayer (region 1) and in the free stream region (region 2) fully determine the development of the mixing layer in the regions 3,4 and 5. The different conditions possible are stated in table 2.3.2

Region	Condition	Parameter
1	The boundary layer is turbulent	$\frac{U \cdot \theta}{\nu}$
1	The boundary layer is laminar	$\frac{U \cdot \theta}{\nu}$
1	Angle between the two streams	α
1	Radius of splitterplate point	R_s/θ
2	The difference in the free stream velocities $U_1 - U_2 = \Delta U$ divided by the average velocity $\frac{1}{2}(U_1 + U_2) = \bar{U}$	$\frac{\Delta U}{\bar{U}}$
2	Excitations in the free stream	$\frac{u'}{\bar{U}}$, $\frac{v'}{\bar{V}}$
2	The existence of walls	
2	Density difference between the two streams	ρ_1/ρ_2

Table 2.3.2 Parameters determining the plane mixing layer

Despite the fact that all these conditions have different effects on the mixing layer it is possible to see some 'universal' structure in the development of the mixing layer.
These universal properties refer predominantly to large scale happenings in the mixing layer.

In region 3 two fluids with different velocities meet eachother. Every small disturbance on the interface of the two fluids, the so-called vortexsheet, will grow. This primary instability is called the Kelvin Helmholtz instability. Until the waves on this interface start to roll up a very simple two dimensional linear inviscid theory as presented by Michalke 1) is able to predict the growth-rates and the frequencies of this waves. The growth of these waves causes the increase in spread of the mixing layer. Under all conditions of table 2.3.2 the large scale structure of the mixing layer is essentially two dimensional in this region.

In region 4 the vortex sheet starts to roll up and form elliptical vortices or eddies. These vortices are responsible for the entrainment and also by amalgamating/pairing cause the mixing layer to grow. This region is called a transition region because in this region a secondary instability creates large scale 3-D

fluctuations. The exact nature of this instability is not known but it seems to be triggered by small-scale 3-D motions. It appears that the moment of transition depends on the Reynoldsnumber of the initial boundary layer (region 1) and also on the level of free stream turbulence (region 2). The 2-D spanwise vortices form helical structures and in the braids of these helices there appear streamwise counterrotating vortices. Where the streamwise and the spanwise vortices intersect small scale 3-D mixing is enhanced. Finally the mixing layer becomes fully turbulent in region 5. Large scale fluctuations are fully three dimensional. But even now there often is some spanwise coherence in the large eddies. It is still a point of discussion where and how the mixing layer flow becomes self preserving and if there is only one self preserving state for the mixing layer.

-Excitation-

In region 3, just downstream of the separation point the mixing layer is most sensitive to outside disturbances/excitation. This sensitivity is so great that it is very difficult to create a pure neutral mixing layer. One can safely assume that in every industrial mixing layer these disturbances play a role. They always increase the spreading rate of the mixing layer. Excitation with velocities that are only 0.5% of the main stream velocity can increase the growth rate of the mixing layer with a factor 2. Coherent excitations always increase the spanwise regularity of the primary vortices and they seem to move the large scale transition further downstream.

Suppose the mixing layer is excited by a frequency f_o. In the area $0 < \lambda^* \cdot f_o \; x/U_c < 1$, where $\lambda^* = (U_1 - U_2)/(U_1 + U_2)$ and $U_c = .5\ (U_1 + U_2)$, more or less corresponding with region 1, the vortexformation and amalgamation is strongly stimulated by excitation. When the exitation is weak this process will continue further downstream. With strong excitation however the mixing layer seems to resonate in the area $1 < \lambda^* f_o \cdot x/U_c < 2$ with the excitation frequency f_o. This causes the 2-D spanwise vortices to stabilize and it prevents amalgamation. A decrease in the spread rate of the mixing layer is then observed.

CHAPTER 3 FLUID DYNAMIC BACKGROUND FOR THE VORTEXMETHOD

3.1 Introduction

In chapter 2 it became clear that coherent structures play an important role in the evolution of the mixinglayer. Because these coherent structures can be seen as more or less discrete vorticity containing areas surrounded by a fluid that contains no vorticity the vortexmethod seems a promising approach for a description of this flow. Before a description of the vortexmethod in chapter 4 some of the fluid dynamic background of the vortexmethod is presented in this chapter.
In paragraph 3.2 the Kelvin-Thomson theorem is treated. This theorem states that in flow without viscosity circulation (circle integral of vorticity) is preserved and that vorticity moves with the fluid.
In paragraph 3.3 the complex velocity potential is presented. With the help of the complex velocity potential it is possible to describe the vortexmethod in an elegant and clear way.

3.2 The Kelvin-Thomson circulation theorem.

Suppose we have a velocity field $\vec{u}(\vec{x})$. The circulation (strenth) Γ around a closed material curve drawn in the fluid is defined as:

$$\Gamma = \oint \vec{u} \cdot d\vec{s} \qquad (3.2.1)$$

with S the closed material (fixed to the fluid elements) curve and $d\vec{s}$ a material line element of the curve.

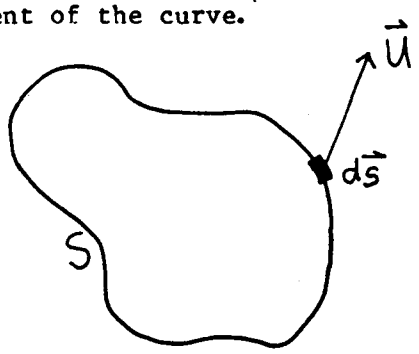

The change of circulation through S is given by:

$$\frac{d\Gamma}{dt} = \frac{d}{dt} \oint \vec{u} \cdot d\vec{s} \qquad (3.2.2)$$

This integral can be split in two:

$$(1)\quad \oint \vec{u} \cdot d\left(\frac{d\vec{s}}{dt}\right) \qquad \text{and (2)} \quad \oint \frac{d\vec{u}}{dt} \cdot d\vec{s} \tag{3.2.3}$$

It is easy to prove that the first integral is zero. Suppose we start the integration in point $\vec{x}_{S,1}$ and end in $\vec{x}_{S,2}$. Because the integration curve is closed $\vec{x}_{S,1} = \vec{x}_{S,2}$ and:

$$\oint_{\vec{x}_{s,1}}^{\vec{x}_{s,2}} \vec{u} \cdot d\left(\frac{d\vec{s}}{dt}\right) = \frac{1}{2}\left(\vec{u}\cdot\vec{u}\,\Big|_{\vec{x}_{s,1}}^{\vec{x}_{s,2}}\right) = 0$$

To solve integral 2 it is necessary to find an expression for $d\vec{u}/dt$. It is generally accepted the Navier-Stokes equation describes fluid motion in Newtonian fluids:

$$\frac{d\vec{u}}{dt} = \vec{F} - \frac{1}{\rho}\vec{\nabla}p + \nu\nabla^2\vec{u} \tag{3.2.4}$$

We substitute this in equation 2.2.3. First however we suppose that the outside force $\vec{F}$ can be described by a potential, so this term vanishes in a closed curve integration. Second we suppose that the pressure p is a function of alone or that is constant. Then it is possible to write integral (2) as:

$$\oint \frac{d\vec{u}}{dt} \cdot d\vec{s} = \oint \left[-\nabla\left\{\int \frac{dp}{\rho}\right\} + \nu\nabla^2\vec{u}\right] d\vec{s} \tag{3.2.5}$$

and, since $\int \frac{dp}{\rho}$ is a single valued scalar function:

$$\frac{d\Gamma}{dt} = \nu \oint \nabla^2\vec{u} \cdot d\vec{s} \tag{3.2.6}$$

Neglecting viscosity ν gives us Kelvin's circulation theorem:

$$\frac{d\Gamma}{dt} = 0 \tag{3.2.7}$$

The circulation round a closed material curve is invariant in an inviscid fluid. When the rotation operator is applied to the velocity the vorticity vector follows:

$$\vec{\omega} = \vec{\nabla} \times \vec{u} \tag{3.2.8}$$

With Stokes rule the relation between circulation and vorticity follows:

$$\Gamma = \iint \vec{\omega} \cdot \vec{n} \cdot dA \tag{3.2.9}$$

in which the integral is taken over a surface with normal vector n and bounded by the close curve S. We define a **vortexline** as a line in the fluid whose tangent is everywhere parallel to the local vorticity and we define a **vortextube** as a surface in the fluid formed by all vortexlines passing through a given closed curve. When we substitute equation 3.2.9 in the Kelvin circulation theorem the result suggests that vortex-tubes are in some sense permanent. As is shown by an argument in Batchelor 16), pp.274, we find one of the dynamical vorticity laws of Helmholtz:
A vortextube moves with the fluid and its strength remains constant.

3.3 The complex velocity potential

It is possible to write any velocity field $\vec{u}(\vec{x})$ as a summation of three velocities:

$$\vec{u} = \vec{u}_e + \vec{u}_v + \vec{u}_p \tag{3.3.10}$$

(e:stands for expansion, v for vorticity and p for potential) where $\vec{u}_e$, $\vec{u}_v$ and $\vec{u}_p$ obey the following relations:

$$\vec{\nabla} \cdot \vec{u}_e = \Delta \quad , \quad \vec{\nabla} \times \vec{u}_e = 0 \tag{3.3.11}$$

$$\vec{\nabla} \cdot \vec{u}_v = 0 \quad , \quad \vec{\nabla} \times \vec{u}_v = \vec{\omega} \tag{3.3.12}$$

$$\vec{\nabla} \cdot \vec{u}_p = 0 \quad , \quad \vec{\nabla} \times \vec{u}_p = 0 \tag{3.3.13}$$

$\vec{u}_e$ describes that part of the velocity field that is caused by expansion of the fluid. Since we are only concerned about

incompressible fluids $\vec{u}_e = 0$.
The solution to equation 3.3.12 is the well known Biot-Savart equation. When $\vec{\omega}(\vec{x})$ is known throughout the velocityfield it is possible to calculate $\vec{u}(\vec{x})$. Biot-Savart sais that the velocity $\vec{u}_v(\vec{x})$ caused by a fluid element at $\vec{x}'$ with vorticity $\omega(\vec{x}')$ is given by ($\vec{s} = \vec{x} - \vec{x}'$):

$$\delta\vec{u}_v(\vec{x}) = - \frac{\vec{s} \times \vec{\omega}(\vec{x}')\ \delta V(\vec{x}')}{4\pi |\vec{s}|^3} \qquad (3.3.14)$$

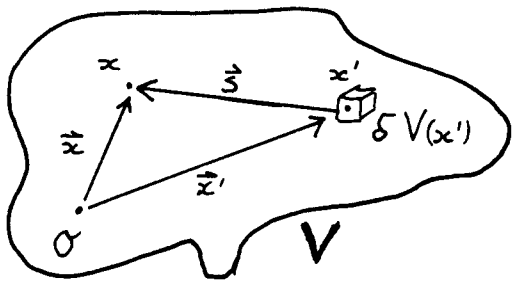

Fig.3.2.1 Flowfield picture belonging to equation 3.3.14

The total velocity field caused by the vorticity field $\vec{\omega}(x)$ is the integral of δu_v over the entire volume:

$$\vec{u}_v(\vec{x}) = -\frac{1}{4\pi} \iiint_V \frac{\vec{s} \times \vec{\omega}(\vec{x}')}{|\vec{s}|^3}\ \delta V(x') \qquad (3.3.15)$$

Because we can write $\nabla x\ \vec{u}_p = 0$ a velocity potential $\varphi(\vec{x})$ can be defined for $\vec{u}_p$ such that:

$$\vec{\nabla}\varphi(\vec{x}) = \vec{u}_p(\vec{x}) \qquad (3.3.16)$$

This is a very handsome simplification because by knowing the scalar field $\varphi(\vec{x})$ it is possible to derive the velocity field $\vec{u}(x)$. The continuity equation for incompressible fluids $\nabla \cdot \vec{u} = 0$ requires that at all points the Laplace equation holds:

$$\nabla^2\varphi = 0 \qquad (3.3.17)$$

The properties of the solution of the Laplace equation are strongly dependent on the topology of the region of space in which the equation holds. When this region is "single valued" this means that we can write:

$$\varphi(\vec{x}) = \varphi(\vec{x}_o) + \int_{\vec{x}_o}^{\vec{x}} \vec{u}_p(\vec{x}')\, d\vec{x}' \qquad (3.3.18)$$

where the solution is independent of the integration path between $\vec{x}_o$ and $\vec{x}$ as long as this path remains inside the fluid.
In the particular case of a two-dimensional velocity field $\vec{u}_p$ satisfies relations of such a form that is possible to make use of the theory of functions of complex variables in a way that is both elegant and effective. The components u_p and v_p of $\vec{u}_p$ can be written as:

$$u_p = \frac{\partial \varphi}{\partial x} \quad , \quad v_p = \frac{\partial \varphi}{\partial y} \qquad (3.3.19)$$

Because $\nabla \cdot \vec{u}_p = 0$ we also can define a streamfunction ψ such that:

$$u_p = \frac{\partial \psi}{\partial y} \quad , \quad v_p = -\frac{\partial \psi}{\partial x} \qquad (3.3.20)$$

We now define a complex potential w(z) (z=x+iy) as:

$$w(z) = \varphi + i\,\psi \qquad (3.3.21)$$

By taking the complex derivative of this potential we find the velocity:

$$\frac{dw}{dz} = u_p - i\, v_p \qquad (3.3.22)$$

In this way we have a powerful tool, the complex function theory, to describe our velocity field $\vec{u}_p$.
It is possible to combine the advantages of the complex potential description with the vorticity distribution description and tackle velocityfields $\vec{u} = \vec{u}_v + \vec{u}_p$. This is most easily demonstrated with an example, e.g. the pointvortex. A pointvortex in the point $\vec{x}_i$ is decribed by its streamfunction:

$$\psi_i(\vec{x}) = \frac{-\Gamma_i}{2\pi} \cdot \ln(x - x_i) \qquad (3.3.23)$$

The velocity field connected with this stream function obeys everywhere $\vec{\nabla}.\vec{u} = 0$ and everywhere, except on the point $\vec{x}_i$ itself, $\vec{\nabla} \times \vec{u} = 0$. The velocity potential, connected with the pointvortex is not single valued anymore. There is a 'cyclic constant' Γ_i, and everytime we choose our path of integration to go around point $\vec{x}_i$ this cyclic constant is added to the velocitypotential. This does not prevent us from deriving a velocity field from it. The complex velocity potential of the point vortex i is given by:

$$w_i(z) = \frac{-i\Gamma_i}{2\pi} \ln(z - z_i) \tag{3.3.24}$$

and the velocities dw/dz:

$$u_i - i\,v_i = \frac{-i\Gamma_i}{2\pi} \cdot \frac{1}{(z - z_i)} \tag{3.3.25}$$

In this way we defined a complex velocity potential for a flow field with circulation. The Kelvin theorem applied on a pointvortex in a velocity field states that the circulation of the pointvortices (Γ_i) is a preserved quantity and that the pointvortex position moves with the local velocity.

CHAPTER 4 THE VORTEXMETHOD; LITERATURE

4.1 Introduction

A variety of fluid flows of high Reynolds number are characterized by the coexistence of high-vorticity areas and low-vorticity areas. The two major classes of such flows are boundarylayers on solid surfaces and free shear layers. The mixing layer in the Quench Test Unit is a good example of such a shear layer. Shearlayers come into existence when the boundarylayer on a bodysurface sperates from this surface. This is called shedding. The way in which the layer separates from the surface is determined by the so-called Kutta-condition. The layer is unstable for disturbances and tends to roll-up into concentrated vortices, see chapter 2. This instability is called, as we have seen, the Kelvin Helmholtz instability. These vortices are sometimes indicated with the more general name coherent structure. Owing to the interest in these coherent structures during the last decade much effort has been spent to describe the motion and the structure of the shear layer. These studies could be devided into three different types:

1) Studies that model the shear layer with an isolated vortexsheet of zero thickness. (isolated means: placed in a unbounded fluid)
2) Studies that model the shear layer with as an isolated vortexsheet of small but finite thickness.
3) Studies that model the separation of the shearlayer from a solid surface and also look into the interaction of the layer with walls.

Inspirated by the discrete nature of the coherent structures a vortexmethod describes the high vorticity areas with more or less discrete vorticity building blocks (VBB's).
These VBB's are solutions of the inviscid Navier Stokes equation, the so called Euler equation. The summation of the velocity potentials of these VBB's is still a solution to the Euler equation. The Thomson-Kelvin theorem, presented in chapter 3, states that, when the viscosity is zero, the circulation of these VBB's is preserved and that they move with the local velocity. Those VBB's can have different forms, depending on the flow under investigation. For two-dimensional flows we want to suggest the following division going from a not so abstract physical VBB to very abstract mathematical VBB's. This division is presented in figure 4.1.1.

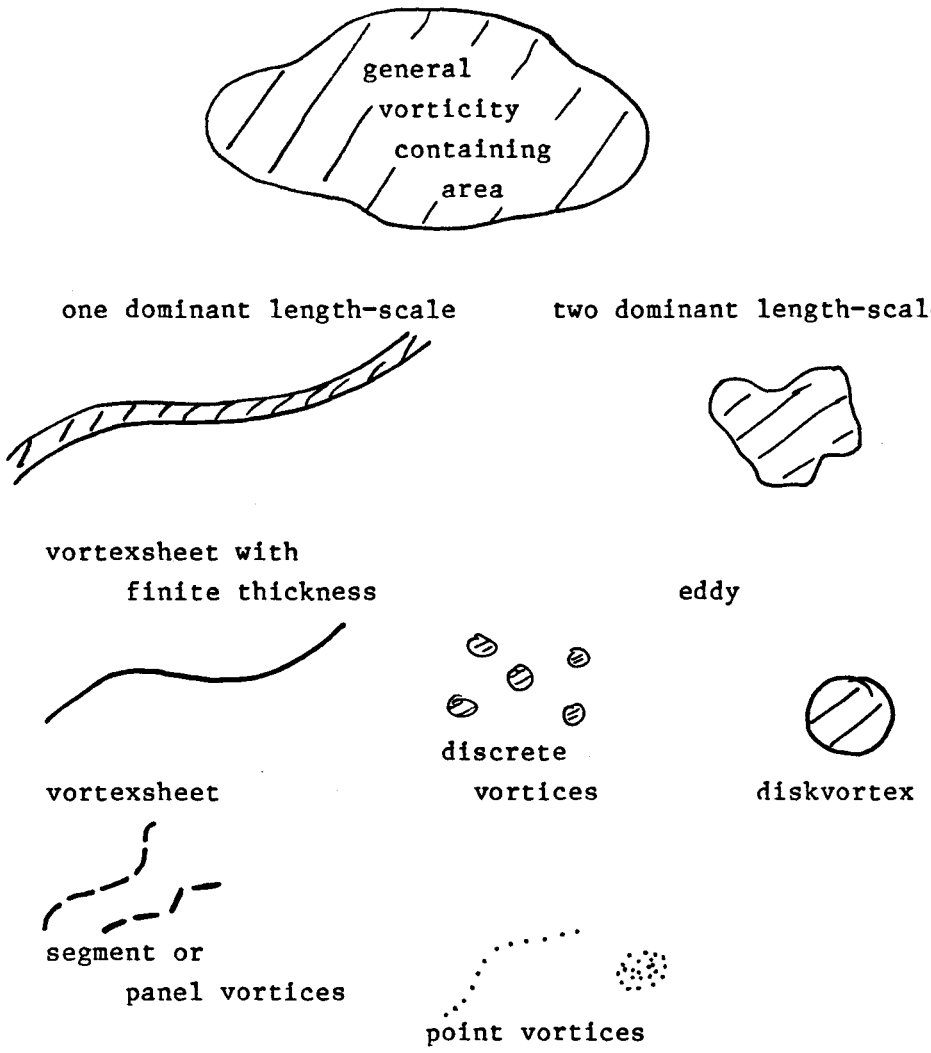

Figure 4.1.1 Schematic presentation of two dimensional vorticity building blocks

The definitions of the most used terms in the vortexmethod are:

Vortex ; A vortex is a finite element of fluid containing vorticity. It is surrounded with vorticity free fluid or walls.

Vortexsheet ; A vortexsheet is a surface (in two dimensional fluids a line !) over which there is discontinuous change of the velocity component along the surface. The pressure and the normal component of the velocity are continuous when crossing the sheet. The term vortexsheet is also used to describe the ´physical´ vortex- or shearlayer in which the discontinuity always is stretched over some distance because of viscosity. In this paper when the attention is focussed on the thickness of the vortexsheet this will always be mentioned.

Pointvortex ; A pointvortex is a position in a two dimensional flowfield with a fixed circulation Γ. At some distance its

velocityfield is that of a cicular vortex with uniform vorticity-distribution. As we have seen in par. 3.3 the velocity, induced by a pointvortex, has a singularity (goes to infinity) in the point vortex itself.

Discrete vortex ; Some authors call the discrete vortex a vortex blob or use the term discrete vortex to denote a point vortex. A discrete vortex is a pointvortex in a two dimensional flow field except for a small region around the vortexposition. In this region the singularity in the velocity potential has been removed and is replaced by a potential without a singularity. See for more details paragraph. 4.4.

Segment- or Panel- or sheetvortex ; This kind of vortex is a short line with some mathematically easy to describe form, e.g. a straight line or a circle-arc. Also the vorticitydistribution on this line is given by a relatively simple expression. These facts allow an analytical determination of the velocity potential of this segement- or panel- or sheetvortex.

Other less commonly used VBB's have been used in literature.
An example is the FAVOR (finite area vortex region) presented by Melander et.al. 74). It is elliptically formed and the authors claim that it has several advantages above the more usual point- or discrete vortices, when describing coalescence of vorticity.

In the following paragraphs a review is given of the two dimensional vortexmethod presented in the literature. The attention will be focussed on the description of the shearlayer and the vortexsheet. In paragraph 4.2 an analytical mathematical description of the isolated vortexsheet and several of the analytic or similarity solutions that are known for this vortexsheet are given.
Paragraph 4.3 describes how the vortexmethod tries to give a numerical solution to the equations presented in paragraph 4.2. An history is given of the trials of several authors to solve the equations of motion of the vortexsheet. One of the methods, the discrete vortex method, deserves a separate treatment. This is given in paragraph 4.4.
In paragraph 4.5 walls are introduced in the fluid that is described by the vortexmethod. Paragraph 4.6 deals with the problem of vortexshedding. In paragraph 4.7 a much used way of introducing artificial viscosity in the flow will be presented. Paragraph 4.8 describes a vortexmethod modified to include the effects of gravity and surface tension. Applications of the vortexmethod and combined experimental/vortexmethod studies are the subject of paragraph 4.9. Finally in paragraph 4.10 a conclusion is formulated.

4.2 An analytical description of the vortexsheet.

A convenient description for the equation of motion of an isolated vortexsheet is, among others, given by Moore 54).
Suppose P is a typical fluid particle of the sheet and Q is reference fluid particle on the sheet. If the vorticity in the sheet is of one sign the net vorticity or circulation C in the arc QS is a monotone function of the arcdistance between Q and S, and C is a Lagrangian intrinsic coordinate.

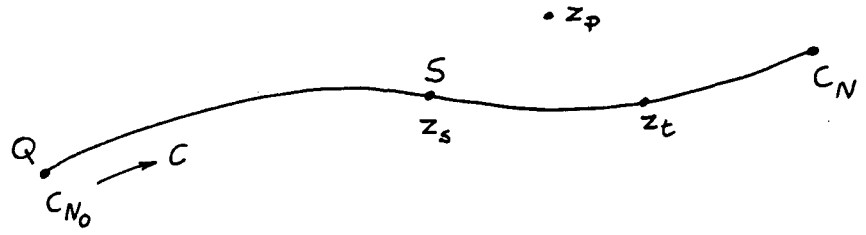

Fig. 4.2.1 The vortexsheet, belonging to equation 4.2.1 - 4.2.4

If $z_s(C,t)$ is the complex coordinate of a point on the sheet as a function of time then the complex velocity of the particle at position z_p in the plane is given by the twodimensional Biot Savart integral (see also par.3.3):

$$\frac{dz_p^*}{dt} = \frac{1}{2\pi i} \int_{C_{N_0}}^{C_N} \frac{dC'}{z_p - z_s(C',t)} + U_E - iV_E \qquad (4.2.1)$$

where U_E, V_E denote the components of an external irrotational velocity field.
The self-induced motion in a point z_t on the vortexsheet is the average of the velocities on both sides of the sheet:

$$\frac{dz_t^*}{dt} = \frac{1}{2}\left\{ \frac{dz^*}{dt}\Big|_{z \downarrow z_t} + \frac{dz^*}{dt}\Big|_{z \uparrow z_t} \right\} \qquad (4.2.2)$$

These velocities are given by:

$$\frac{dz^*}{dt}\Big|_{z \updownarrow z_t} = \pm \frac{1}{2}\left(\frac{\partial z_t}{\partial C}\right)^{-1} + \frac{1}{2\pi i} \int_{C_{N_0}}^{C_N} \frac{dC'}{z_t - z_s(C',t)} + U_E - iV_E \qquad (4.2.3)$$

where the slash in the integral sign denotes the Cauchy principal value. From 4.2.2. and 4.2.3 follows the selfinduced velocity of the vortexsheet in point z_t:

$$\frac{dz_t^*}{dt} = \frac{1}{2\pi i} \int_{C_{N_0}}^{C_N} \frac{dC'}{z_t - z_s(C';t)} + U_E - iV_E \qquad (4.2.4)$$

The strength γ of the sheet, which denotes the velocityjump across the sheet, is given by:

$$\gamma = \frac{dC}{ds} \qquad (4.2.5)$$

where s is a pathlength parameter along the sheet.
Moore 34) has generalized equation 4.2.4 to a vortexsheet of small thickness. If ω denotes a large but constant value of the vorticity in a thin sheet the equation of motion of this sheet becomes:

$$\frac{dz_t^*}{dt} = \frac{1}{2\pi i} \int_{C_{N_0}}^{C_N} \frac{dC'}{z_t - z_s(C';t)} - \frac{i}{6\omega} \frac{\partial}{\partial C} \left\{ \frac{\frac{\partial z}{\partial C}}{\left|\frac{\partial z}{\partial C}\right|^4} \right\}_{z_t} + U_E - iV_E \qquad (4.2.6)$$

Equations 4.2.4 would seem suitable for numerical treatment. But in spite of a lot of attempts by various authors no consistent and easy to use solutions have yet been obtained.

-Analytical solution-

A. A simple exact solution of equation 4.2.4. is that of a cicular vortexsheet with a uniform vorticity distribution. When the strength and the radius of the sheet are unity the solution of $z_t(C,t)$ is given by:

$$z_t(C,t) = \exp\{i(C + \tfrac{1}{2}t)\} \qquad (4.2.7)$$

B. Prandtl demonstrated the existence of self-similar unsteady spiral vortex sheets with the shape of logaritmic spirals. A physical example of such a sheet is the so called Kaden-sheet. An initial flow for t<0 is defined as a steady attached potential flow around a semi-infinite flat plate ($z_p = x + 0\cdot i$; $x<=0$; $w=-iaz^{1/2}$, a=constant). At t=0 the plate is removed, leaving a semi-infinite vortexsheet. At its end the selfinduced velocity is infinite and the the singularity is resolved through a self-similar spiral-like roll-up of the form:

$$z_p(c,t) = (a.t)^{2/3} \cdot \omega(\lambda) \qquad (4.2.8)$$

where t=time and $\omega(\lambda)$ the nondimensional self similar shape function of the sheet. Several authors have attempted, with mixed succes, to simulate Kaden's problem with a vortexmethod. We mention van de Vooren 19), Chorin 20), Moore 24), Pullin 36), Fink & Soh 40) and Baker 42). Outof the results of Pullin figure 4.2.2 is an example.

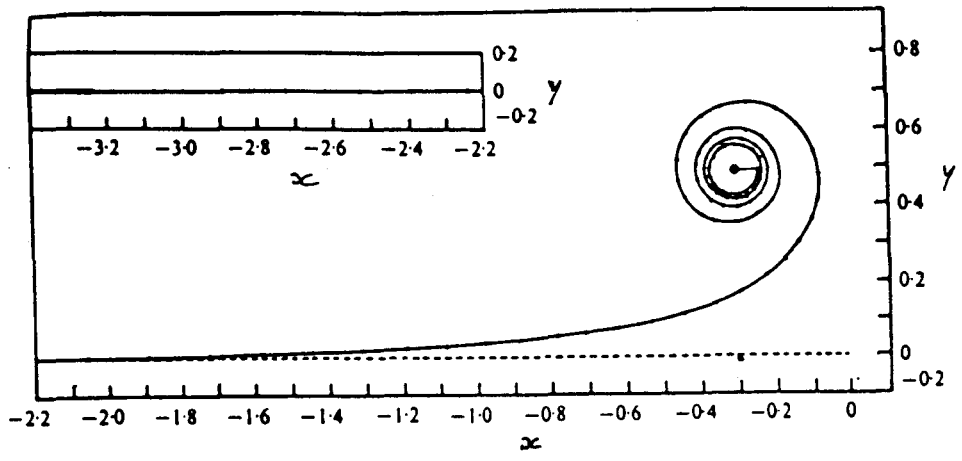

Fig. 4.2.2 Solution of Kaden's problem with a vortexmethod, by Pullin 36).

C. The Kelvin Helmholtz instability of a vortexsheet shows that infinitesimal disturbances of wavelength λ on a plane sheet of strength γ, while the disturbances are so small that non-linear effects play no role, grow like $\exp(\pi \cdot \gamma \cdot t/\lambda)$, see Batchelor 16) The shorter the wave, the faster it grows. When, at larger amplitudes non-linear effects start to dominate, the growthrate reduces. Meiron et al. 64) studied the K.H.-instability of a vortexsheet of zero thickness. They applied a sinusoidal perturbation of the vorticity. By means of a high order Taylor series in time they showed that the sheet develops a curvature singularity at a finite time t_c. This indicates that the vortex-sheet of zero thickness as a model for the shearlayer is only valid for a limited period of time.

4.3 Discretization with pointvortices

Rosenhead 17) already in 1931 tried to solve the equation of self inuced motion of the two dimensional isolated vortexsheet by representing the vortexsheet with pointvortices.

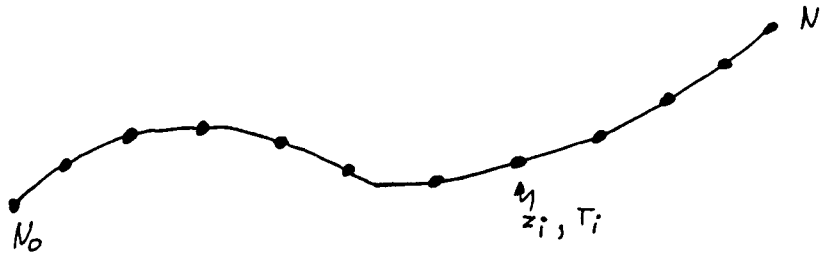

Fig.4.3.1 The vortexsheet represented by pointvortices.

He approximated the integral of equation 4.2.4 by a Riemann sum and used the fact that a pointvortex induces no motion on itself to cancel the infinite contribution from the local singularity of 4.2.4. If the circulation of the i^{th} pointvortex is denoted by Γ_i and its position by z_i then the velocity of the i^{th} pointvortex is given by:

$$\frac{dz_i^*}{dt} = \frac{1}{2\pi i} \int_{C_{N_0}}^{C_N} \frac{dc'}{z_i - z_s(c',t)} = \frac{1}{2\pi i} \sum_{\substack{j=N_0 \\ j \neq i}} \frac{\Gamma_j}{z_i - z_j} \qquad (4.3.1)$$

The motion of the sheet is followed by using a simple first order (or second order) scheme:

$$z_i(t + dt) = z_i(t) + \frac{dz_i}{dt} \cdot dt \qquad (4.3.2)$$

where dt is the timestep of the procedure.
Unfortunately this simple straightforward procedure leads to chaotic motion that does not accurately represent the behaviour of the continuous vortexsheet. Hama & Burke 18 recalculated Rosenheads result with finer timesteps and finer discretization. They found that chaos developped in those regions of the sheet where pointvortices came closer to eachother. They concluded that chaos was caused by the singularity in the velocitypotential which caused unrealistic high velocities on nearby vortices.
This happened in spite of the fact that because of conservation of energy the point vortices cannot come arbitrarly close to eachother. The Hamiltonian H is one of the four invariants of the vortexmethod in an unbounded flowfield:

1) $$H = -\frac{1}{2\pi} \sum_{\substack{\text{all} \\ \text{pairs}}} \Gamma_i \Gamma_j \ln |z_i - z_j| \qquad (4.3.3)$$

Other invariants are:

2) $$\sum_i \Gamma_i \qquad (4.3.4)$$

3) $$\sum_i \Gamma_i z_i \qquad (4.3.5)$$

4) $$\sum \Gamma_i z_i z_i^* \qquad (4.3.6)$$

Many authors have tried to solve the problem of erratic and chaotic movement of the vortexsheet. Many adhoc procedures were invented to prevent chaos. An example of such a strategy is the amalgamation of two vortices into one vortex with their combined strength when they come nearer to eachother than a certain arbitrary limit. With this procedure Clements et al. 25) simulated the flow around a circular cylinder.

Chorin 20) first suggested the use of discrete vortices (pointvortices with a viscous desingularized core). One has to realise that, by representing a vortexsheet with discrete vortices, one simulates a shear layer of small but finite thickness. Hald et al. 33) and Majda et al. 57) proved that under certain conditions the discrete vortex representation converges with arbitrary high order accuracy to the solution of the two-dimensional Euler equation. This subject will be described in greater detail in paragraph 4.4.
Fink & Soh 40) claimed that the point vortex method broke down into chaos because of an integration error. In support for this they established a theory of the integration error in the scheme of equation 4.3.1. They concluded that a pointvortex representation implicitly involved the neglect of logarithmic terms which represent the local contributions for the self induced velocity. They argue that these logarithmic terms, although in a regular represented and smooth sheet initially vanishingly small, amplify through small sheet distortions, leading eventually to chaotic motion. They introduced a repositioning technique aimed at removing these logarithmic terms, and they found that chaotic movement disappeared. In their technique each timestep the vortices are repositioned along the sheet in such a way that their spacings remain equal. The consequence of this intrusion in the development of the sheet is that each timestep each vortex must be attributed a new vorticity strength Γ. This is done in such a way that the cumulative vorticity C(s), when going along the sheet with path parameter s, remains the same before and after repositioning. A variant of this technique, used by the author, is described in paragraph 5.4.

accuracy.
Baker 48) disputed the results of Fink & Soh and proved them to be unreliable. He reproduced the work of van Vooren 19) and gave an accurate treatment of the pricipal value integral 4.2.4. This was done by subtracting from the integrand a function with the same singularity, which thus rendered the integrand regular. The canceling function could be integrated analytically. If trapezoidal integration is used van Vooren's procedure leads to:

$$\frac{1}{2\pi i}\int_{C_{N_0}}^{C_N}\frac{dc'}{z_t - z_s(c',t)} = \frac{1}{2\pi i}\sum_{\substack{j=N_0\\ j\neq t}}^{N}\frac{\Gamma_j}{z_t - z_j} - \frac{i\Gamma_t}{4\pi}\frac{\left(\frac{\partial^2 z_t}{\partial c^2}\right)}{\left(\frac{\partial z_t}{\partial c}\right)^2} \qquad (4.3.7)$$

This means that the error in Rosenhead's pointvortexmethod (and also in Fink & Soh 's vortexmethod), denoted by the first term on the right hand of 4.3.7 is less than e_N where:

$$e_N = \frac{C_N}{4\pi N}\cdot \mathrm{Max}\frac{\left|\frac{\partial^2 z}{\partial c^2}\right|}{\left|\frac{\partial z}{\partial c}\right|^2} \qquad (4.3.8)$$

and that therfore the integration procedure of Rosenhead was a consistent approximation because the truncation error goes to zero when the number of integration points goes to infinity.
The conclusion is that chaos is not caused by inaccurate integration.
Moore 54) showed that chaos in fact was caused by a discrete form of the Kelvin-Helmholtz instability and that the succes of Fink & Soh's method was due to the fact that it dampened this discrete K.H.instability. He compared the results of Rosenhead's and Fink & Soh 's vortexmethod applied on a circular vortexsheet with the analytical solution, see equation 4.2.7. The circular vortexsheet was represented by 60 pointvortices. The difference between the exact solution $z_j(t)$ and the calculated solution $\tilde{z}_j(t)$ was expressed by:

$$\tilde{z}_j(t) - z_j(t) = z_j(t)\cdot\varepsilon\cdot\exp(\sigma_p\cdot t)\exp(i\cdot j\cdot p\cdot\varphi) \qquad (4.3.9)$$

with j denoting the j^{th} vortex, p the label of the mode ($0<p<60$), ε the amplitude of the error and σ_p the growthrate of the error. The modes 30,20,15,12,10 have periodicities of 2,3,4,5,6 vortexspacings. He found that a disturbance with a spacing of 2 (pairing of neighbouring vortices) was the most unstable mode. In table 4.3.2 some growthrates for different modes are given.

Periodicity	σ_p
2 spacings	6.91
3 spacings	6.17
4 spacings	5.15
5 spacings	4.32
6 spacings	3.62

Table 4.3.2 Growthrate of the different modes of the discrete Kelvin Helmholtz instability.

Fink & Soh's solution against chaos was in fact the supression of these modes of disturbance. Its specific effect can be seen in the comparison of the two pictures of figure 4.3.3. In these pictures the 'mode-spectrum' of the error is given. In Rosenhead's method one sees clearly that the most unstable mode is mode 30. In the second picture the overall amplitude of the error is many orders lower. Intersesting is the fact that Fink & Soh's method is most effective for the most unstable p=30 mode.

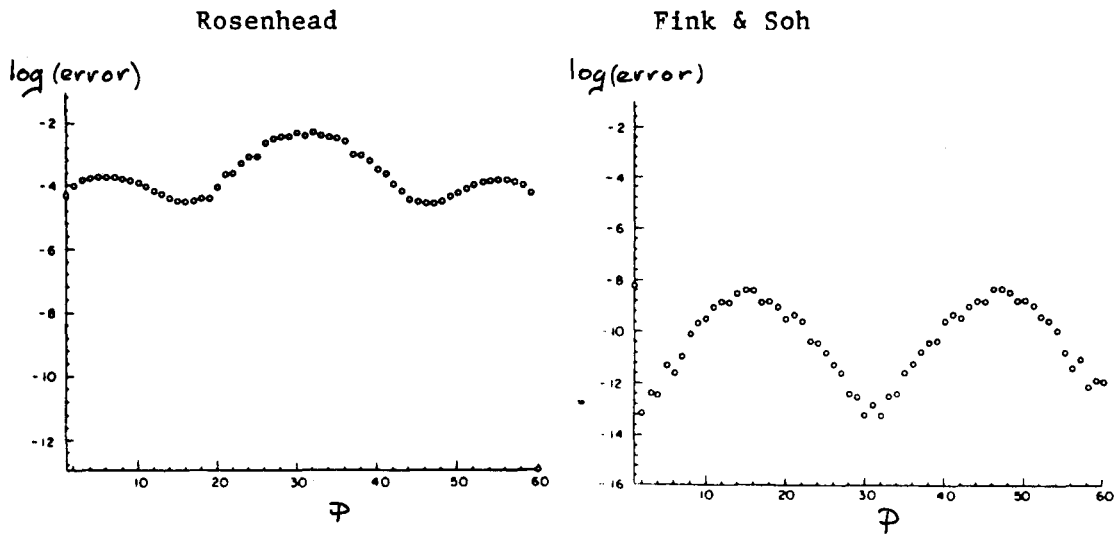

Fig. 4.3.3 Mode-spectrum of the error in the point vortexmethod solution of the circular vortexsheet using Rosenhead's version or Fink & Soh's version;

Fink & Soh's vortexmethod, when pursued long enough in time, eventually also develops chaotic behaviour and it even produces spurious waves in the vortexsheet. With this method not the equation of motion of a vortexsheet of zero thickness was solved but the equation of motion of a thin layer with an unknown thickness. Although it is not clear in general what the relationship is between the unkwown exact solution of the Gauchy principal value integral 4.2.4 and Fink & Soh's solution, the gross features of the developped vortexsheet can probably be accepted as real.

Only in more recent years more accurate ways of numerical treatment of equation 4.2.4 have been presented.
Hoeijmakers & Vaatstra 60) presented a panel-vortex method with a flexible timestep and a flexible vortex-representation of the sheet. When the curvature of the sheet increased, timesteps decreased and the number of dicretizations increased. This was done in such a way that second order accuracy was preserved all times. Moreover they calculated the short range self induced velocities by representing the sheet locally with a quadratic polynomial with a continuous quadratic vorticity distribution γ. However in the roll-up region the time-step decreased so much that the procedure ceased to advance in time. They chose therefore to amalgamate the inner part of the roll-up region into one pointvortex. In this way they achieved smooth and stable results. Through this amalgamation procedure they effectively turned the vortexsheet again in a thin layer.
The first authors who succeeded in finding a numerical solution to the equation of motion of an infinitly thin vortexsheet were Higdon & Pozrikidis 75). They used a similar procedure as Hoeijmakers & Vaatstra 60), with flexible representation and timestep. The difference was that they chose for their vortex segment, that represented the sheet for short-range selfinduced velocity calculations, the arc of a circle. They didn't apply an amalgamation procedure and they consequently found that the timestep reduced and converged to a finite t_c. At the same time the number of representations increased and a singularity evolved in the curvature of the sheet. This result is similar to the result obtained by Meiron et al. 64), mentioned in par. 4.3.
Higdon & Pozrikidis 76) succeeded also in simulating the Kelvin Helmholtz instability of a sheet with pre-defined thickness and constant vorticity. They found that the growthrate of the disturbances strongly was effected by the layer-thickness, but that the final amplitude is relatively insensitive to the thickness. For thin layers with thickness less than 3% of the wavelength, three different patterns were observed in the vortex core region. A compact elliptic core, an elongated S-shaped core and a bifurcation into two cores. For thicker layers stationary elliptic cores may develop if the thickness exeeds 15% of the wavelength.
A last contribution to the pointvortexmethod that we want to mention is one of Maskew 30). He observed that in the near-field (1-5 vortexspacings) of a straight vortexsheet represented by pointvortices the calculated induced velocities deviate from those of the exact solution. He presented an algoritm in which the vortexsheet between two pointvortices was subdivided in an array of subvortices, keeping ofcourse the total circulation constant. In this way, by choosing the number of subvortices, he in fact reduced the dimension of the 'near-field' and thus could reach arbitrary

accuracy in evaluation of velocities near the sheet. This procedure could have interesting applications in the roll-up region or in models with more than one vortexsheet.

4.4 Discrete vortices

Discrete vortices were first introduced by Chorin 20) as a way of preventing the erratic behaviour in the solutions of the vortexmethod. He introduced a viscous core that desinguralized the Biot-Savart integral. The complex velocity potential w at a point z caused by Chorin's discrete vortex in z_j with strength Γ_j and core radius δ is given by:

$$w(z) = \Gamma_j \cdot w_\delta (z - z_j)$$

$$w_\delta (z') = \begin{cases} \frac{1}{2\pi} \ln (z') & |z| \geq \delta \\ \frac{z}{2\pi\delta} + C_\delta & |z| < \delta \end{cases} \qquad (4.4.1)$$

where C is a constant chosen in such a way that $w_\delta (z')$ is continuous. This choice of $w_\delta(z')$ causes the velocity in the core to be constant. A cut-off that has been used by various other authors is the Gaussian cut-off:

$$w_\delta (z') \sim \exp (- |z|^2) , \quad z < \delta \qquad (4.4.2)$$

The discrete vortex method was critisized by among others Leonard 51) because of the arbitrary introduction of a core radius and because the method didn't allow for deformation of the core while surrounding fluidelements were distorted.
Hald & del Prete 33) found however that on certain conditions (concerning the choice of vortexspacing and cut-off function $w(z')$) the method converged for a limited time interval to the solution of the Euler equations. Their results were improved upon by Majda & Beale 57). They proved that discrete vortexmethods can have arbitrarily high order accuracy when the distance h between the vortices and the core size δ are well chosen. As the attractive computational features of the discrete vortexmethod Majda & Beale mentioned:

- The discrete vortices closely mimic the physical mechanisms in 2-D fluid flow.
- The discrete vortexmethod is adaptive; The discrete vortices automatically concentrate in regions with steep gradients.
- Vortexmethods do not have numerical viscosity like conventional

Euleruian difference methods.
- They can be designed to have higher order accuracy without substantially changing the basic algoritm.

The main disadvantage of the discrete vortex method is the fact that the computational cost is proportional to N^2, with N the number of vortices.

4.5 The vortexmethod and walls

For fluid flow two boundaryconditions must be satisfied at a solid surface:

1) $\vec{u} \cdot \vec{n} = 0$, the inpenetrability of the wall.

2) $\vec{u} \cdot \vec{s} = 0$, the no-slip condition

$\vec{n}$ is the normal vector on the wall and $\vec{s}$ is a vector along the wall. The vortexmethod essentially is an inviscid method specially suited for high Reynolds number flows. In a high Reynolds number flow the boundarylayer is very thin and the flow outside of the boundarylayer can be treated as an inviscid flow. Therefore in many cases the no-slip condition may be released. The most common way to satisfy the inpenetrability condition in two dimensional flow is by way of mirror vortices. Suppose a pointvortex with strength Γ approaches a flat plate. Introduction of a similar pointvortex but with opposite vortexstrength at the mirrorposition causes all normal velocities on the plate to cancel, see figure 4.5.1.

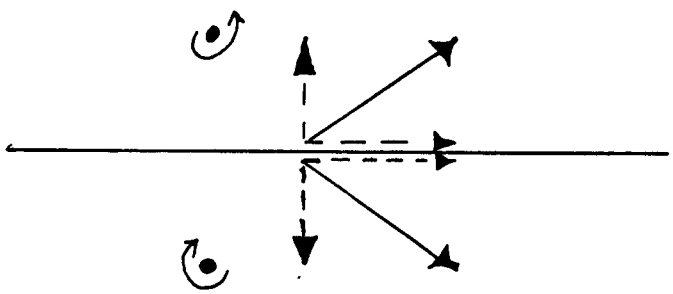

Fig. 4.5.1 Solving the inpenetrability condition by way of a mirrorvortex

With the help of conformal mapping, using for example a Schwartz Christoffel transformation (see Batchelor 16)), it is possible to transform a lot of flowgeometries to the flat plate geometry. If this plate is positioned along the real axis vortices and mirror-vortices are eachother's complex conjugates.
Suppose that a geometry in the z-plane is transformed to the upper

half ζ-plane with a transformation denoted by:

$$\frac{dz}{d\zeta} = f(\zeta) \tag{4.5.1}$$

The velocity induced on vortex i is derived from the total complex velocity potential (including all rotational and irrotational sources) minus its own velocity potential:

$$\frac{dz_i^*}{dt} = \lim_{z \to z_i} \left\{ \frac{dw}{dz} + \frac{i\Gamma_i}{2\pi} \cdot \frac{1}{z - z_i} \right\} \tag{4.5.2}$$

As is calculated in appendix 1 this expression can be written in terms of ζ where the position ζ_i in the ζ-plane corresponds with z_i in the z-plane:

$$\frac{dz_i}{dt}^* = \lim_{z \to z_i} \left\{ \frac{d\zeta}{dz} \left(\frac{dw}{d\zeta} + \frac{i\Gamma_i}{2\pi} \cdot \frac{1}{\zeta - \zeta_i} \right) + \frac{i\Gamma_i}{4\pi} \frac{\left(\frac{\partial^2 \zeta}{\partial z^2}\right)}{\left(\frac{\partial z}{\partial \zeta}\right)^2} \right\} \tag{4.5.3}$$

The potential $dw/d\zeta$ consists of the contribution of the vortices, the mirrorvortices and the irrotational flow Φ_E in the ζ-plane:

$$\left.\frac{dw}{d\zeta}\right|_{\zeta_i} = \Phi_{E,\zeta_i} + \sum_{j=1}^{N} \frac{i\Gamma_j}{2\pi} \left\{ \frac{-1}{\zeta_i - \zeta_j} + \frac{1}{\zeta_i - \zeta_j^*} \right\} \tag{4.5.4}$$

where ζ_j and ζ_j^* are the vortex- and mirrorvortexposition in the ζ-plane.

Inamuro et al.70) presented an alternative way of satisfying the $\vec{u} \cdot \vec{n} = 0$ condition. They distributed pointvotices on the walls in such a way that at the midpoints between the pointvortices the normal velocities were zero. They claim that their method is more easily adaplable to complex geometries. Several authors want to model the boundarylayer and have therefore to satisfy the no-slip condition $\vec{u} \cdot \vec{s} = 0$. Generally this is done by introducing vorticity at the walls, in the form of discrete vortices or vortexsegments, that compensate the velocitydifference between the fluid and the wall. Usually these boundarylayer vortices are given a random walk component in their velocities in order to simulate the diffusion of vorticity that takes place in a boundarylayer.

4.6 The shedding of vorticity

The shedding of vorticity from a sharp edge is uniquely determined by the Kutta condition, which requires that the velocity of the fluid is finite at the separation point and that the separated vorticity is convected away from this point. In the case of such a sharp edge the separationpoint is always fixed to this edge. The vortexsheet that develops after shedding is parallel to one of the surfaces when the wedge has a finite angle. The sign of the shed vorticity determines to which of the surfaces the sheet is parallel. Boundarylayer separation from smooth solid surfaces is determined by the pressure distribution along the surface and is therefore more difficyult to model with a vortexmethod.
The rate of vorticity shedding $d\Gamma/dt$ is given by:

$$\frac{d\Gamma}{dt} = \frac{1}{2}(U_1 - U_2)(U_1 + U_2) \qquad (4.6.1)$$

when $U_1 > U_2$. U_1 and U_2 are the velocities along the sheet on the one and on the other side just after the separation point. In the case of the shedding from a bluff body like a prism $U_2 = 0$ and $\frac{d\Gamma}{dt}$ becomes $\frac{1}{2} \cdot U_1^2$.
Several methods have been used to incorporate vortexshedding in a vortexmethod model. One of the earliest attempts was by Clements 21) who studied the two dimensional flow past a square. He evaluated U_1 at a point at a distance Y_I above the square's separation point, see figure 4.6.1.

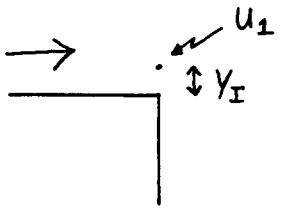

Fig.4.6.1. Vortexshedding from a square by Clements 21).

A vortex with strength $\Gamma = \frac{1}{2} U_1^2 \cdot dt$ (with dt the timestep of the procedure) was then placed exactly at the separation point. In spite of the fact that the Kutta-condition was not satisfied and in spite of the arbitrariness of the distance Y_I Clements claimed good qualitative results and a fair prediction of experimental kwown Strouhal numbers and velocityprofiles. The RMS-values of the fluctuating velocities in his model were higher than determined experimentally. In a later study Clements 25) modified his introduction point in order to cause finite velocities at the

square´s edge and thus satisfying the Kutta-condition. Other examples of studies that used this shedding procedure are those of Kiya 28), who studied the vortexshedding (of discrete vortices) from an inclined plate in a shear flow, Kamemoto 39), who showed in his study that the choice of the timestep can influence the flow-characteristics and Nagano 63), who used close approach vortex-amalgamation to prevent chaos in his study of the flow past a prism. All these studies used conformal mapping and mirrorvortices to satisfy $\vec{u}\cdot\vec{n} = 0$. They all found qualitative similarity with experimental results and a good prediction of drag- and lift forces or Strouhalnumbers. Quantities as intensities of fluctuating velocities or pressuredistributions on the surface were not well predicted.

Clements 25) Stansby 55) and Cheer 71) simulated the flow past a circular cylinder with the vortexmethod. Clements and Stansby didn´t satisfy the no-slip condition and satisfied the $\vec{u}\cdot\vec{n} = 0$ condition with conformal mapping and mirrorvortices. They used as an (arbitrary) criterion to find the separation point a certain distance from the point on the cylindersurface where the induced velocity had a maximum. The shedding rate $d\Gamma/dt$ was determined by evaluating the velocities at (again) a more or less arbitrary distance from the separation point. The major justification given for these procedures is the qualitative nice result it gives.

Cheer 71) modelled the no-slip condition on the cylinder with small sheet vortices, thus creating a simulated boundarylayer. To the velocities of the sheetvortices he added a random walk component (see next paragraph) to simulate the diffusive effect of viscosity. Outside this layer the flow was simulated with discrete vortices. When the vortexsheets crossed a given boundary they were smoothly changed in discrete vortices and vice-versa. $\vec{U}\cdot\vec{n} = 0$ is satisfied by conformal mapping and mirrorvortices. This procedure produced separation without assumptions made for the separation point. Drag- and lift coefficients are in good agreement with experimental results.

Graham 32) and Disselhorst 41) present shedding algorithms that make use of a continuous short vortexsheet that is connected to the separationpoint. Further downstream the vorticity of this sheet is transformed to pointvortices. The vorticitdistribution on this sheet is chosen such that the Kutta-condition is satisfied.

4.7 Viscosity in the Vortexmethod

The effect of molecular viscosity in a flow is to diffuse or spread out concentrations of vorticity, see equation 2.3.6.
Chorin 79) suggested that this diffusive effect could be simulated in a vortexmethod by giving each timestep the velocities of the vortices a random walk component. When u_i denotes the velocity induced on vortex i at z_i at time t_i the new vortexposition at t_i+dt is given by:

$$z_i(t+dt) = z_i(t) + u_i \cdot dt + w \qquad (4.7.1)$$

The components of w are independent random Gaussian variables with a mean of zero and a variance that is given by:

$$\text{Variance} = 2\nu\, dt \quad \text{or} \quad \frac{2}{Re} \cdot U \cdot L \cdot dt \qquad (4.7.2)$$

where L is a lengthscale of the flow, ν is the kinematic viscosity, Re the Reynoldsnumber and U the main stream velocity.
Milinazzo & Saffman 29) examined the validity of this idea by trying to model the well kwown problem of the decay of a circular finite sized vortex with N discrete vortices with random walk.
The exact solution for the square of the radius of gyration of such a vortex is:

$$A(t) = A_o + 4\nu \cdot t \qquad (4.7.3)$$

where t denotes time and ν the kinematic viscosity. Milinazzo & Saffman defined an error as:

$$\varepsilon = \frac{(A_{vort} - A_o - 4\nu \cdot t)}{4\nu t} \qquad (4.7.4)$$

where A_{vort} denotes A calculated by the vortex method.
Milinazzo & Saffman let the whole vortex rotate three times around its own axis and then found an error ε of 20% for N=50 and 10% for N=1000. This result suggested that the error decreased like $N^{-1/2}$. Since computation times increase with N^2 it is very expensive to reduce this error. They concluded that the random walk idea was only moderately useful. This vue was strongly attacked by Chorin 38) who criticised Milinazzo & Saffman's way of defining an error.

Milinazzo & Saffman also used the "Cloud in Cell" method (see paragraph 4.9) to calculate the deacay of the circular vortex. They found errors of the same order as before but computing costs were much lower.

4.8 A vortexmethod for flows with densitydifferences and surface tension effects

Zalosh 27) formulated a vortexmethod in which the evolution of the vortexsheet is influenced by the stabilizing effects of buoyancy and surface tension. These effects play a role when the vortexsheet separates two flows with different density.
One can define a critical velocitydifference ΔU_{crit} across the sheet. When the velocity difference $\Delta U > \Delta U_{crit}$ then disturbances on the sheet will grow. If $\Delta U < \Delta U_{crit}$ then the disturbance of the sheet will merely oscillate. Zalosh gave this critical velocity difference as:

$$\Delta U_{crit} = \sqrt{\frac{2(\rho_1+\rho_2)}{\rho_1\rho_2}} \cdot \sqrt{\sigma \cdot g\,(\rho_2-\rho_1)} \qquad (4.8.1)$$

where σ = the surfacetension, ρ_1 and ρ_2 the two densities and g the gravityaccelaration.
He derived an expression for the change of the vorticitystrength's of the vortices representing a sheet between two fluids of different density. The expression for vortex i with strength Γ_i is given by:

$$\frac{d\Gamma_i}{dt} = \frac{2(\rho_2-\rho_1)}{\rho_1+\rho_2} \cdot \Delta s_i \left(g \sin\theta_i + \frac{dV_{is}}{dt}\right) - \frac{2\sigma}{(\rho_1+\rho_2)} \cdot \Delta s_i \left(\frac{\partial R_i}{\partial s}\right)^{-1} \qquad (4.8.2)$$

where R_i denotes the local radius of curvature of the sheet, s the pathlength along the sheet, θ_i local inclination of the sheet with respect to the horizon and Δs_i the length of the sheet that is represented by vortex i.
Zalosh simulated the Kelvin Helmholtz instability with this vortexmethod and found growthrates that are consistent with experimental observations of the initially linear rate of spread of turbulent mixing layers.
Bromilov 77) used equation 4.8.2 in combination with a repositioning procedure (similar to that of Fink & Soh) to model the shear-layer, that develops from a starting flow past a wedge and that separates two fluids of different density. Some of his results are presented in figure 4.8.1. He found that the spreadingrate of his

results were in good agreement with the experimentally determined spread of Brown & Roshko 3).

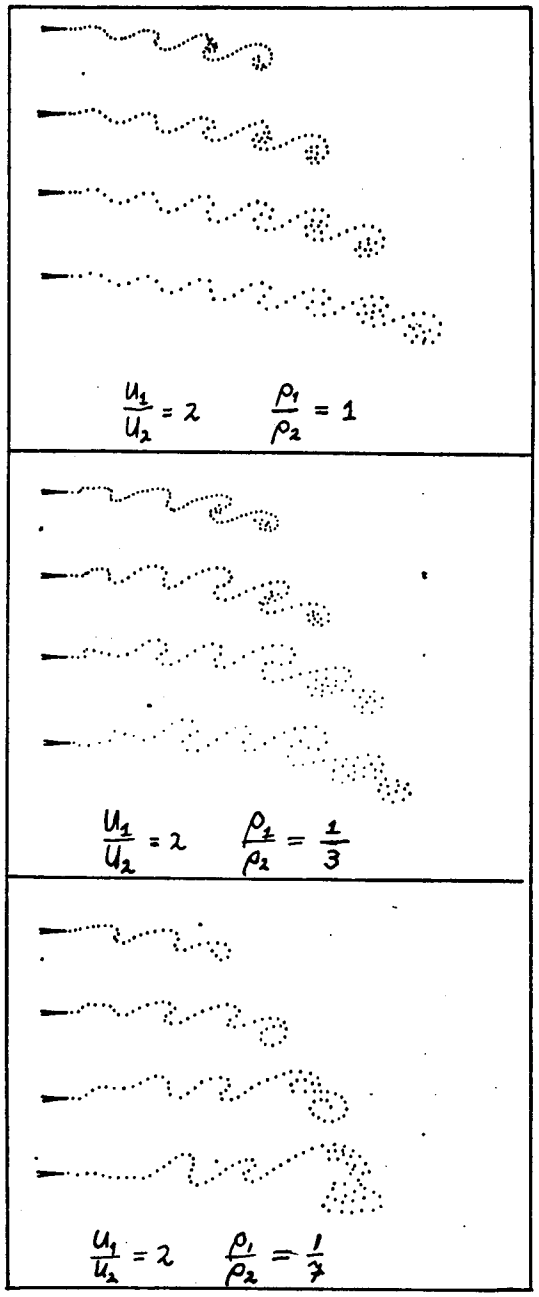

Fig.4.8.1 Shearlayers, represented by pointvortices, between fluids of different densities, by Bromilov 77)

4.9 The Cloud in Cell vortexmethod (C.I.C.)

Christiansen 78) introduced the Cloud in Cell vortexmethod for fluid flow. This method is an hybrid between an Eulerian gridmethod and the Lagrangian point vortex method. The basic equations are:

The Poisson equation:

$$\vec{\nabla}^2 \psi = -\vec{\omega} \tag{4.9.1}$$

where $\vec{\omega}$ denotes the vorticity and ψ the streamfunction, which is related to the velocity by:

$$u = \frac{\partial \psi}{\partial y} \quad , \quad v = -\frac{\partial \psi}{\partial x} \tag{4.9.2}$$

The Euler equation:

$$\frac{\partial \omega}{\partial t} + u \cdot \frac{\partial \omega}{\partial x} + v \cdot \frac{\partial \omega}{\partial y} \tag{4.9.3}$$

The vorticity in the flowfield is represented by N pointvortices with strength Γ_i. A finite difference approximation of the Poisson equation on a rectangular grid ($x_o + (i-1)H_x$, $y_o + (j-1)H_y$; $1<=i<=N_x$, $1<j<=N_y$) with gridspacings H_x and H_y is given by:

$$\frac{(\psi_{i+1,j} - 2\psi_{i,j} + \psi_{i-1,j})}{H_x^2} + \frac{(\psi_{i,j+1} - 2\psi_{i,j} + \psi_{i,j-1})}{H_y^2} = -\omega_{ij} \tag{4.9.4}$$

Because one can write for the whole flowfield $\sum_{n=1}^{N} \Gamma_n = \iint \vec{\omega} \cdot d\vec{A}$ it seems a good idea to assign values to $\omega(k)$ at the gridpoints following a procedure af area weighting:

$$\omega(k) = A_k \cdot \Gamma_n / H_x \cdot H_y \tag{4.9.5}$$

where A_k are the areas shown in figure 4.9.1.

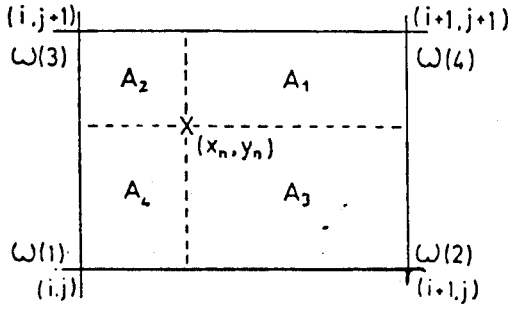

Fig. 4.9.1 Gridelement in the CIC - vortexmethod

Now, with $\omega_{i,j}$ known, equation 4.9.4. can be solved with the help of a fast Poisson solver. Outof the calculated $\psi_{i,j}$ the velocities in the gridpoints can easily be calculated with a central difference scheme:

$$u_{ij} = (\psi_{i,j+1} - \psi_{i,j-1}) / 2 H_y$$
$$v_{ij} = -(\psi_{i+1,j} - \psi_{i-1,j}) / 2 H_x \qquad (4.9.6)$$

The velocity of the pointvortex can then be calculated with:

$$u_n = \sum_{k=1}^{4} u(k) A_k / H_x H_y \qquad (4.9.7)$$

The pointvortices are subsequently convected following a simple Euler scheme x(t+dt)=x(t) + u(t)·dt in which dt is chosen to satisfy:

$$dt < Min(n) \left\{ \frac{H_x}{u_n}, \frac{H_y}{v_n} \right\} \qquad (4.9.8)$$

Boundaryconditions must be given at the gridedge for an unique solution. An example is the setting of the streamfunction ψ_{ij}. The big advantage of the CIC-method is the computational efficiency. The computation-time is about proportional with the number of pointvortices. Application indicate that CIC is about 20 times faster for N=1000 than the point- or discrete vortexmethod. Baker 42) applied the "Cloud in Cell"-technique to the Kelvin-Helmholtz instability. He found that the sheet develops small scale instabilities of the order of gridspacing. According to Baker this is due to the anisotropic redistribution process. The large scale disturbances had growth-rates in good agreement with non-linear theory. He also applied CIC to Kaden's problem.

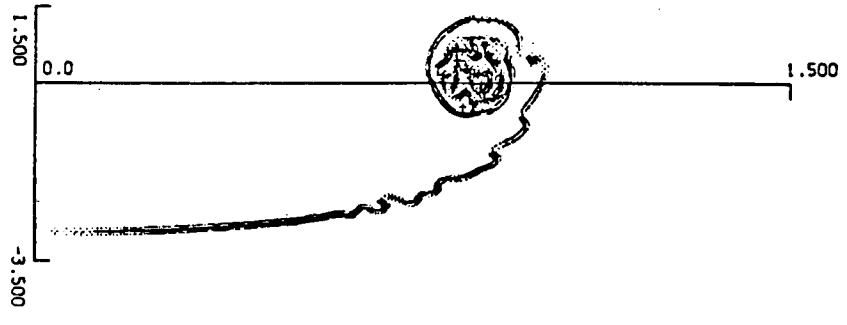

Fig.4.9.2 CIC-vortexmethod solution of Kaden's problem, Baker 42)

Again the small-scale instabilities developped, see figure 4.9.2. The large scale motion was in good agreement with the similarity-solution, see equation 4.2.8.
The conclusion can be that the CIC-vortexmethod is able to predict large scale vortexmotions at a considerable lower computational cost. An exact error analysis is not available yet.

4.10 Comparison of the vortexmethod mixing layer and experiments

In this paragraph an investigation by Ashurst is presented, that compared the two dimensional plane mixing layer modelled with a discrete vortexmethod with experimental results of Winant & Browand 4), Brown & Roshko 3) and Browand & Weidman 6). The set-up of the experiment was essentially the same as drawn in figure 2.1.2. In this investigation discrete vortices with random walk were used. According to Ashurst there are three parameters that define the ideal mixinglayer: 1) The velocitydifference $\Delta U = (U_2 - U_1)$, 2) The average velocity $\bar{U} = 0.5(U_1 + U_2)$ and the kinematic viscosity ν. Good experimental techniques eliminate other effects. The splitterplate was represented by a uniform sheet of vorticity represented by a row of discrete vortices with spacing L/M and of strength $\Gamma = \Delta U\ L/M$ where L is the lengthscale and M the number of vortices per lengthscale.. The average velocity was produced with the addition of a linear potential throughout the system. Each timestep a vortex was convected into the flow with the proper vorticity production rate $d\Gamma/dt = \bar{U}\Delta U$. Thus $L/M = \bar{U}dt$. The timestep was selected to be 0.05, after looking at the displacement for each timestep on computer generated movies.
The preliminary results for the mixing layer indicated that the random walk provides the laminar sqrt(x) growth rate of momentumthickness with a transition to the turbulent linear growth. Leaving out the random walk component still gave a transition to linear growth but the early growth differs clearly from the sqrt(x) growth rate. Thus the experimentally observed linear growth of the mixing layer is a consequence of the Euler equation. The approach to linear growth rate occurred at about the same location as the waterchannel results of Winant & Browand 4). The vorticitythickness growth rate was equal to the one found by Brown & Roshko 3). Computer generated movies of the vortex motion clearly revealed vorticity coalescence and the large scale vortex pairing. Figure 4.10.1 presents streakline plots of the discrete vortices. From these pictures Ashurst concluded that
vortex pairing is identical to mixing layer growth and is very important to the entrainment process of the surrounding non-turbulent fluid.

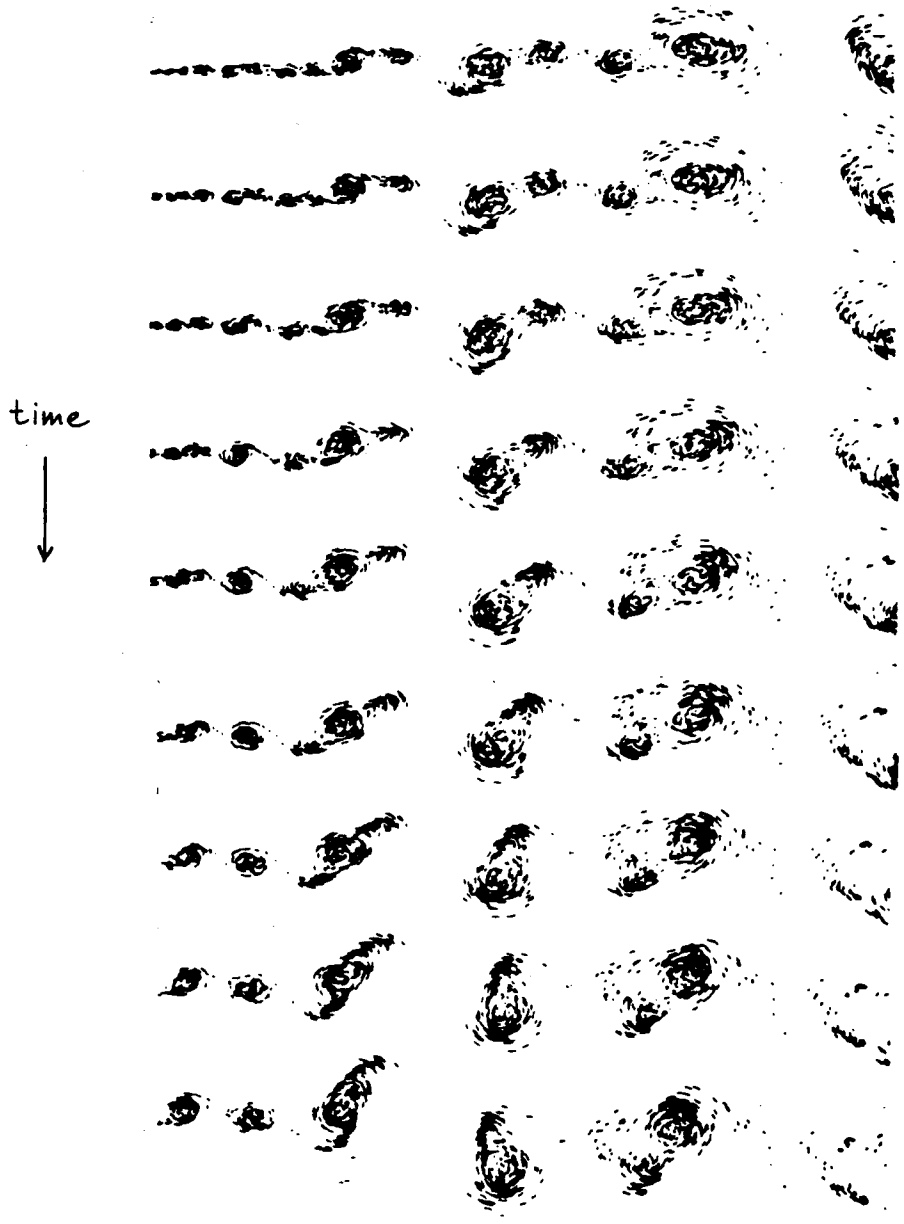

Fig.4.10.1 Streakline plots of each discrete vortex for a unit time with respect to the average velocity. The Reynoldsnumber ($\Delta u \cdot L/\nu$) is 1000.

One of the numerical simulations was done to correspond with the experimental condition of the Water channel of Browand & Weidman 6). The numerical results for the Reynoldsstress were twice the experimental value found by Browand & Weidman 6).

The experimental RMS velocity fluctuations in the y-direction were twice as large as those in the x-direxion. The numerical RMS velocity fluctuations were equal in both directions and even a little larger than the maximum experimental ones.
In a second calculation aging of the discrete vortices was included by reducing the vortex interaction according to the exact solution for a single isolated vortex in a viscous fluid, see equation 4.7.3. The overall effect was however not an exact solution of the Navier Stokes equation. The discrete vortex velocity field U(r,t) was now a fuction of distance r from the vortexcenter and the age t of the vortex:

$$U(r,t) = \frac{\Gamma}{2\pi r} \cdot \left(1 - \exp\left(-r^2/4\nu t\right)\right) \qquad (4.10.1)$$

where ν denotes the kinematic viscosity.
The results of the aging were dramatic in the sense that now both the Reynolds stress and the two components of the RMS-velocity fluctuations were in good agreement with experiment.
Ashurst performed another calculation at the much higher Reynoldsnumber of 25000 in order to compare its results with the experiment of Brown & Roshko. The growth-rate of the vorticitythickness now exceeded the experimental one with 16%. The calculation included the aging effect. The reynoldsstress and the longitudinal RMS velocity fluctuations showed good agreement with experiment, however the normal velocity fluctuations were 50 % larger. A possibility for the disagreement is the lack of the space dimension in the numerical simulation. Shadowgraphs indicated the existence of three dimensinal Taylor type vortices (see also chapter 2) with axes of rotation in the flow direction. It was felt that these Taylor vortices could produce the experimentally observed normal (and spanwise) fluctuations while not affecting the longitudinal fluctuations.
Ashurst concluded that the two-dimensional discrete vortexmethod simulation of the free mixing layer showed excellent agreement with moderate Reynolds number flows if the diffusion and decay of vorticity were included.
In a later article by Ashurst et al.50), in which an experimental and a CIC-vortex method investigation of the two-dimensional flow over a backward facing step are compared Ashurst et al. concluded that to improve vortex dynamics results, a model of dissipation caused by small scale three dimensional vorticity should be added to the two-dimensional calculation or a full three-dimensional discrete vortex dynamics calculation should be done.

4.11 Conclusion

The vortex method is a useful and promising addition to existing turbulence models. Majda & Beale (par 4.4) summed up the nice features of the vortexmethod:
-The vortices (vortex filaments in a three dimensional vortexmethod) closely mimic the physical mechanisms of the flow.
-The vortexmethod is very adaptive. Vortices concentrate in the areas with steep gradients.
-The vortexmethod is not troubled by numerical viscosity
-It can be designed to have arbitrary high accuracy in solving the Euler equation.
With relatively little effort "extra's" (viscosity, density differences, dissipation) can be build in. Even the disadvantage of a computation time, that is proportional with the square of the number of vortices, has been solved in the hybrid 'Cloud in Cel' vortexmethod. There is however no established error analysis for the CIC-vortexmethod.
The two dimensional vortexmethod has however a limited applicability in simulating experiments. Comparison with gross experimental features, such as drag, lift or strouhal numbers, is not conclusive. Moreover one must distinguish between a method to model turbulent flow (in most cases a three dimensional phenomenon) and a method to approximate an exactly two dimensional flow. The two-dimensional vortex method, in particular the discrete vortex method, is only reliable in modelling those flows that are dominated by two dimensional large scale inviscid phenomena. The initial part of the turbulent mixing, where the Kelvin Helmholtz instability dominates, is an example of such a flow. Real progress can only be expected from a three dimensional vortexmethod. Discussion of three dimensional vortexmethods is however outside the scope of this study but several literature references are listed. (e.g. Callegari et al. 35; Acton 46); Leonard 51); Kida 53); Beale 58); Beale 59) and Robinson 65)

CHAPTER 5 A VORTEXMETHOD FOR MIXING IN CONFINED FLOWS

5.1 Introduction

In this chapter a 2-D point vortex method for confined mixing will be described. In the previous chapter many methods have been described to improve the accuracy of vortexmethods. Only a few of these methods have been implemented in the vortexmodel that is here presented. This is due to a lack of time and to the fact that some of the improvements only came to the attention of the author just before writing this report.
Nevertheless the here descibed vortexmodel is a flexible basis for further development.
The essential problems of a 2-D vortexmethod describing confined mixing are:

1) To satisfy the boundaryconditions on the walls of the geometry

2) To find a physically satisfying vortexshedding algorithm

3) To prevent the growth of numerical errors and errors caused by the discretization process.

Because these problems are essentially the same for different geometries first the solution to them will be treated for the splitter-plate geometry, see figure 5.1.1 The advantage of this geometry above the A-type geometry is that conformal mapping of the splitter plate geometry is relatively simple.
This geometry consists outof two infinite parallel flat plates and a half infinite flat plate in the middle of these two, see figure 5.1.1.
At the end of the semi-infinite plate, when the two non-vortex flows U_H and U_L have different speeds, a vortexsheet will seperate.

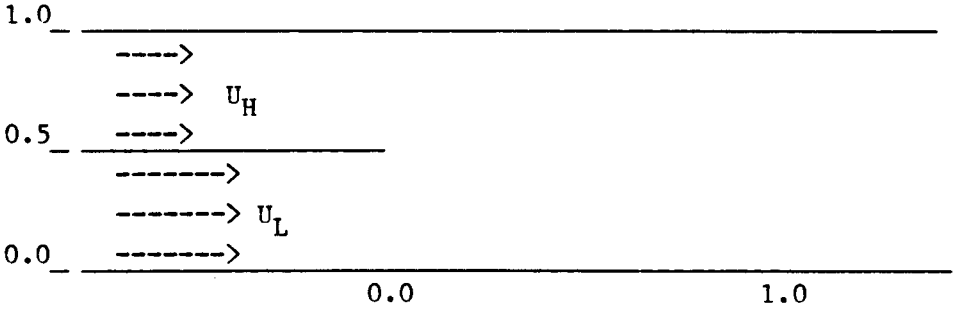

Fig.5.1.1 Splitter-plate geometry with the irrotational main flow

Paragraph 5.2 presents the Schwartz-Christoffel transformation, that transforms the geometry of figure 5.1.1 to the upper half plane and it gives the equation of motion for the pointvortices in this geometry.
In paragraph 5.3 the vortex shedding problem will be treated.
In paragraph 5.4 some inital results will be presented. Since they show the typical chaotic behaviour of Rosenhead's point vortex-method a redistribution technique to combat this chaos will be described.
In paragraph 5.5 an amalgamation technique will be presented. This technique aims to give a better representation of the highly rolled up regions of the vortexsheet and to reduce calculation time.
Paragraph 5.6 will outline the structure of the program VORTEX that solves the equation of motion of paragraph 5.2 together with the shedding algorithm of paragraph 5.3 and the redistribution technique of paragraph 5.4.
Paragraph 5.7 shows the effects that forcing (deliberate disturbances in the main flow) has on the development of the vortexsheet.
Paragraph 5.8 gives a short look at the influence of the velocity ratio parameter λ^* $(=U_L - U_H)/(U_L + U_H)$ on the growth of the mixinglayer (vortexsheet).
How to change the above pointvortex model to acommodate for the an A-type geometry, see figure 5.1.2, will be the subject of paragraph 5.9.

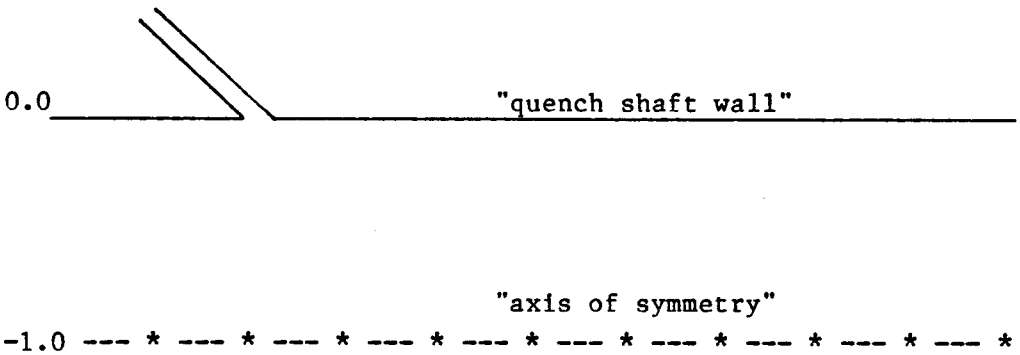

Fig.5.1.2 The A-type geometry

Finally some conclusions are presented in paragraph 5.9.

5.2 The equation of motion in the splitter plate geometry.

Because the vortexmethod essentially is an inviscid flowmodel the only boundary condition on the wall that has to be satisfied is $\vec{U}\cdot\vec{n} = 0$, the inpenetrability of the wall. In a 2-D flow above an infinite flat plate this boundary condition can easily be satisfied by introducing mirrorvortices, see par.4.5. By way of a so called Schwartz Christoffel transformation (Batchelor 22) it is possible to project geometries on a half plane bounded by a flat surface. For the splitterplate geometry the Schwartz Christoffel transformation is given by:

$$\frac{dz}{d\zeta} = \frac{\zeta}{\pi(\zeta+1)(\zeta-1)} \qquad (5.2.1)$$

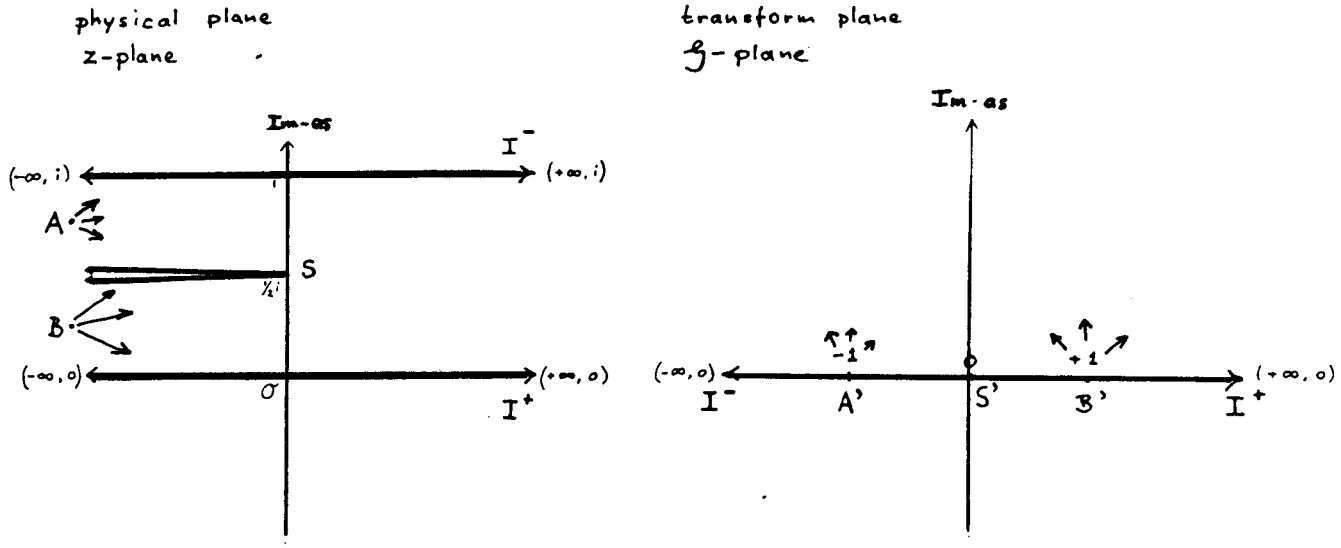

Fig.5.2.1 The Schwartz Christoffel transformation of the splitter plate geometry in the physical z-plane to the flat surface geometry in the transform ζ -plane.

In the points A´ and B´ sources provide the main irrotational fluid flows U_L and U_H. In the ζ -plane A´ and B´ are on the real axis in the points -1 and +1, their transformed positions in the z-plane are at $-\infty$ respectively above and under the splitter plate.

The differential equation 5.2.1 has the following solution:

$$z = \frac{1}{2\pi} \ln(\zeta^2 - 1) \qquad (5.2.2)$$

With the help of this equation vortexpositions in the upper ζ -plane can easily be transformed to the z-plane.

The vortexsheet, shedding from point S = (0,1/2i) in the physical plane will shed in the ζ -plane from S' = (0,0) in the direction of the positive imaginary axis.
Mirrorvortices whose strength is opposite to that of the point vortices in the upper ζ -plane are introduced at their complex conjugated positions.
The complex velocity potential in the ζ -plane at a point ζ_p (see also equation 4.5.4) is given by:

$$\left.\frac{dw}{d\zeta}\right|_{\zeta_p} = \frac{1}{2\pi}\left\{\frac{U_H}{(\zeta_p+1)} + \frac{U_L}{(\zeta_p-1)}\right\} + \sum_{j=1}^{N} \frac{i\Gamma_j}{2\pi}\cdot\left\{\frac{-1}{(\zeta_p-\zeta_j)} + \frac{1}{(\zeta_p-\zeta_j^*)}\right\} \quad (5.2.3)$$

where: ζ_j is the position of the vortex j in the upper half plane and ζ_j^* the complex conjugated of ζ_j.

In paragraph 4.5 the general equation of motion of the point vortices are given. By substituting the above equations 5.2.1 ($\frac{dz}{d\zeta}$) and 5.2.3 ($dw/d\zeta$) into equation 4.5.3 we obtain the velocity of the pointvortices in the z-plane in terms of their position in the ζ -plane:

$$\frac{dz_i^*}{dt} = \frac{1}{2}\left(U_H\frac{(\zeta_i-1)}{\zeta_i} + U_L\frac{(\zeta_i+1)}{\zeta_i}\right) - \frac{i\Gamma_i}{4}\left(1+\frac{1}{\zeta_i^2}\right) + \frac{(\zeta_i+1)(\zeta_i-1)}{\zeta_i}\cdot\left\{\sum_{\substack{j=1\\ j\neq i}}^{N}\frac{-i\Gamma_j}{2(\zeta_i-\zeta_j)} + \sum_{j=1}^{N}\frac{i\Gamma_j}{2(\zeta_i-\zeta_j^*)}\right\} \quad (5.2.4)$$

where ζ_i is the transformed z_i-position.
The evolution of the vortexsheet in space can now easily be calculate by way of a simple Euler scheme:

$$z_i(t+dt) = z_i(t) + \left(\frac{dz_i}{dt}\right)\cdot dt \quad (5.2.5)$$

where dt is the timestep of the procedure.
The timestep dt usually is determined by test-calculations.
In paragraph 5.4 an example is given of the evolution of the vortexsheet for different timesteps (the largest timestep is divided by two and so on).

5.3 Vortex shedding from a wedge and a plate

To introduce vorticity in the flow a vortexmodel, that aims to model the physics of this introduction, must contain a shedding mechanism. The most important condition determining the shedding mechanism is the Kutta condition see par 4.6. To satisfy this

condition most authors introduce a pointvortex at an arbitrary spot with a vortexstrength that satisfies the kutta condition, which means that it causes a zero velocity in the origin of the ζ-plane, see figure 5.3.1 and paragraph 4.6:

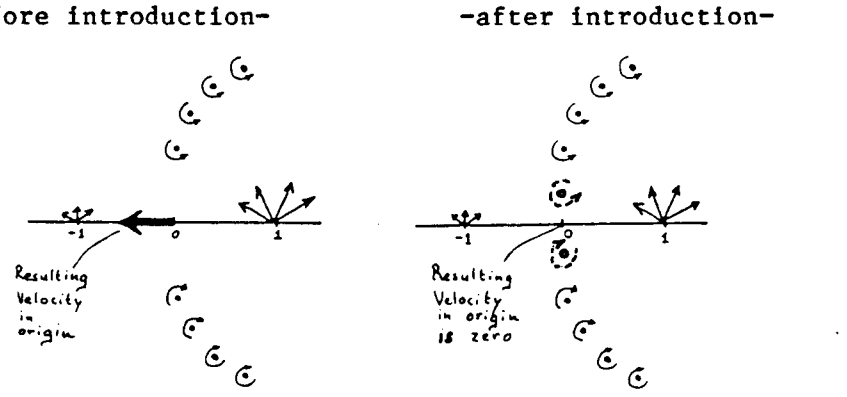

Fig.5.3.1 The shedding mechanism with pointvortex introduction.

This method was also tried in the present investigation. It appeared that different choices of introductionpoint caused different instabilities in the vortexsheet. Another 'unphysical' feature of this method is that between the introduction point and the shedding point high velocities normal to the vortexsheet occur. There is a lot of 'leaking' between the two streams.

It was therefore decided to model the first part of the vortexsheet with a vortexsegment with a constant vorticity distribution, see also Disselhorst 41) & Graham 32).
The sheddingmechanism with a vortexsegment is presented here for the more general shedding from a wedge. The flat plate is a special case from this.
In the complex plane a sharp edge can be transformed to a flat plate with the transformation $z = \zeta^{\lambda}$, see figure 5.3.2.

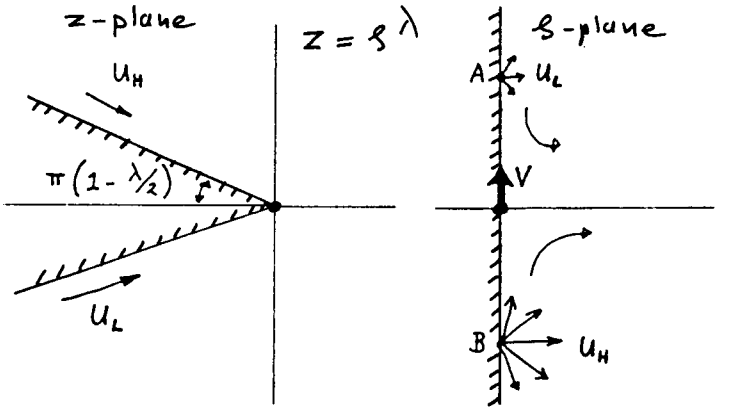

Fig.5.3.2 The transformation of a wedge from the z-plane to the ζ-plane.

The velocity V is the velocity in the origin of the ζ-plane in the absence of the vortexsegment. It is caused by the sources in A and B and by the pointvortices and their mirror vortices that were shed in an earlier phase. To satisfy the kuttacondition (V=0) a vortexsegment will be introduced.
The following assumptions are made about the vortexsegment:

- -It leaves the side of the wedge withe the highest velocity tangentially.
- -It is straight. This seems a reasonable condition when the length of the vortexsegment S_z is smaller than the average distance between the vortices.
- -In the physical z-plane the segment has a constant vorticitydistribution. This means $\gamma = d\Gamma/d|z| = \text{constant}$.
- -It is connected to the origin.

It is easy to see that $\beta = (\frac{\pi}{\lambda} - \frac{\pi}{2})$ is the angle between the segment and the ζ-axis. One can derive (see appendix 2) that the following relation must be true in order to satisfy the Kutta condition:

$$V = \frac{\lambda \cos\beta}{\pi(\lambda-1)} \cdot \gamma \cdot S_z^{1-1/\lambda} \qquad (5.3.2)$$

where S_z is the length of the segment in the z-plane and γ its vorticity strength (dC/ds).
To calculate the convection of this vortexsegment it is replaced by a pointvortex with strength $\gamma \circ S_z$ positioned on the midpoint of the segment.
The sheddingrate $d\Gamma/dt$ is:

$$\frac{d\Gamma}{dt} = \frac{1}{2}(u^- + u^+)(u^- - u^+) \qquad (5.3.3)$$

where u^+ and u^- are defined as:

$$u^+ = \lim_{z \to 0} \left(\frac{dw}{dz}\right)^* \qquad (5.3.4.a)$$

$$u^- = \lim_{z \to 0} \left(\frac{dw}{dz}\right)^* \qquad (5.3.4.b)$$

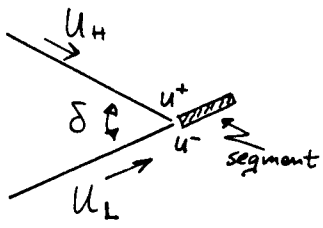

When $\delta = (2-\lambda)\pi > 0$ and $U_H < U_L$ then $u^+ = 0$.

In this case ($\delta > 0$) $d\Gamma/dt$ is given by:

$$\frac{d\Gamma}{dt} = + \tfrac{1}{2} u^{-2} = \tfrac{1}{2} u_L^2 \qquad (5.3.5)$$

The convectionvelocity of the vorticity near the edge is U_c. U_c is given by (see also Graham 32):

$$\begin{aligned} \delta > 0 \; : \quad & u_c = \tfrac{1}{2} u^- \\ \delta = 0 \; : \quad & u_c = \tfrac{1}{2}(u^- + u^+) \end{aligned} \qquad (5.3.6)$$

Then for $\delta > 0$ one finds:

$$u_c = \tfrac{1}{2} \gamma \qquad (5.3.7)$$

$$s_z = u_c \, dt \qquad (5.3.8)$$

When $\delta = 0$ the situation is little more complicated. One can derive that u^+ and u^- are given by:

$$\left.\begin{aligned} u^+ &= u_c - \tfrac{1}{2}\gamma \\ u^- &= u_c + \tfrac{1}{2}\gamma \end{aligned}\right\} \gamma = u^- - u^+ \qquad (5.3.9)$$

and that U_c in this situation is given by:

$$u_c = \tfrac{1}{2}(u_H + u_L) \qquad (5.3.10)$$

The segment, after the first timestep, is transformed in a point-vortex that is convected from the middlepoint of the segment. In the description of the splitter plate vortexsheet of the folowing paragraphs the above way of shedding vorticity is always used.

5.4 Redistribution

The necessaty of a technique that produces a more realistic flow than can be obtained with an unmodified (Rosenhead) point vortex procedure and that reduces the digital Kelvin Helmholtz instability found by Moore 54) (paragraph 4.3) is clearly demonstrated in figure 5.4.1. The unmodified point vortex method for confined parallel mixing, as presented in paragraph 5.2. is there applied to a starting flow: $t<0$ U_L and $U_H = 0$, $t=>0$ $U_L=0.4$ and $U_H=0.2$. This means that the velocity ratio parameter λ^*, defined by Brown & Rosko 3) as $(U_L-U_H)/(U_L+U_H)$, is equal to 1/3.
An dimensionless time dt^* is defined as:

$$t^* = \frac{\bar{U} \cdot t}{L} \qquad (5.4.1)$$

where $\bar{U}$ is the average velocity $.5(U_L+U_H)$, t is the time and L is a lengthscale. The width of the outflow channel (L) is 1.
The moment of the evolution of the sheet in figure 5.4.1 is $t^*=1.2$. The dimensionless timestep dt^* is respectively for picture 1 to 4 equal to 0.03,0.015,0.0075 and 0.00375. Picture 5 is produced under the same conditions as picture 2 but including the redistribution technique that will be described in this paragraph.
Because every timestep one vortex is shed from the splitter plate the number of point vortices in picture 2 is twice the number of pointvortices in picture 1 and so on. As Hama & Burke 18) and other authors have reported chaos increases with decreasing timestep and discretization mesh.
From pictures like this the timestep used for most calculations has been found. It appeared that a timestep of $dt^* = 0.015$ produced the same results as shorter timesteps did except in the inner region of (Kaden's) the starting spiral.
Since the interest of this paper is focussed on the mixinglayer this was not thought to be of importance.

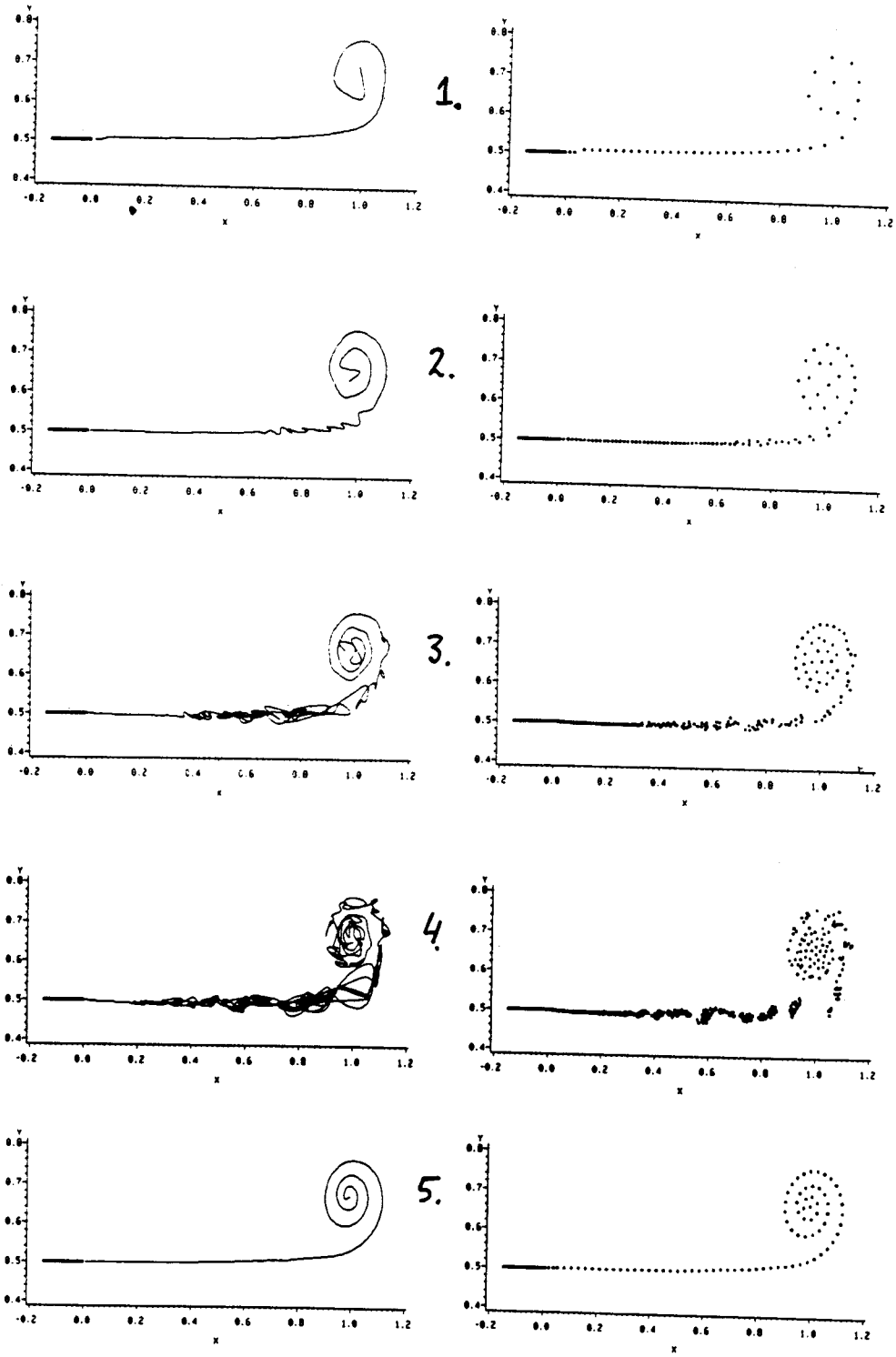

Fig.5.4.1 Development of a vortexsheet for a confined starting flow from a splitter plate. In each picture both the point-vortices connected by a cubic spline (IBM-procedure) as the pointvortices themselves are shown. The moment in time is $t^*=1.2$ but the timesteps used to reach this point are different.
Unmodified pointvortex procedure: 1. $dt^*=0.03$
2. $dt^*=0.015$ 3. $dt^*=0.0075$ 4. $dt^*=0.00375$
Point vortex method with redistribution: 5. $dt^*=0.015$

The aim of redistribution is to represent the vortexsheet with a new set of pointvortices in such a way that the discrete Kelvin Helmholtz instability is surpressed but the same sheet remains represented. The redistribution technique presented here is a variant of the one Bromilov 77) used. It is very similar to the repositioning technique that Fink & Soh 40) used.
Consider a vortexsheet represented by $N-N_o$ vortices. The s-parameter gives the pathlength along a cubic spline function through the pointvortices (see appendix 4), starting with vortex N_o and going till vortex N. The s-position of vortex i is given by s_i and its vortexstrength by Γ_i. The cumulative vorticity $C(s_i)$ is defined by:

$$C(s_{N_o}) = \frac{1}{2}\Gamma_{N_o} \qquad (5.4.1)$$

$$C(s_i) = \frac{1}{2}\Gamma_i + \sum_{j=N_o}^{i-1}\Gamma_j$$

Along the splinefunction the redistributed vortexpositions s_i' are such that the distances between neighbouring vortices are equal:

$$s_i' = s_{N_o} + (i-N_o)\cdot\left(\frac{S_N - S_{N_o}}{N - N_o}\right) \qquad i=N_o,\ldots,N \qquad (5.4.2)$$

The midpoints between the redistributed vortices are:

$$M_i = S_N + (i - N_o + 1/2)\cdot\left(\frac{S_N - S_{N_o}}{N - N_o}\right) \quad i=N_o,\ldots,N-1 \qquad (5.4.3)$$

As is demonstrated in figure 5.4.2 one can define a continuous function C(s) by interpolating $C(s_i)$ as a function of s.
The redistributed vortex strengths are calculated from:

$$\Gamma'_{N_o} = C(M_{N_o}) \qquad (5.4.5.a)$$

$$\Gamma'_i = C(M_{i+1}) - C(M_i) \qquad i = N_o+1 \ldots N-1 \qquad (5.4.5.b)$$

$$\Gamma'_N = \sum_{j=N_o}^{N}\Gamma_j - C(M_{N-1}) \qquad (5.4.5.c)$$

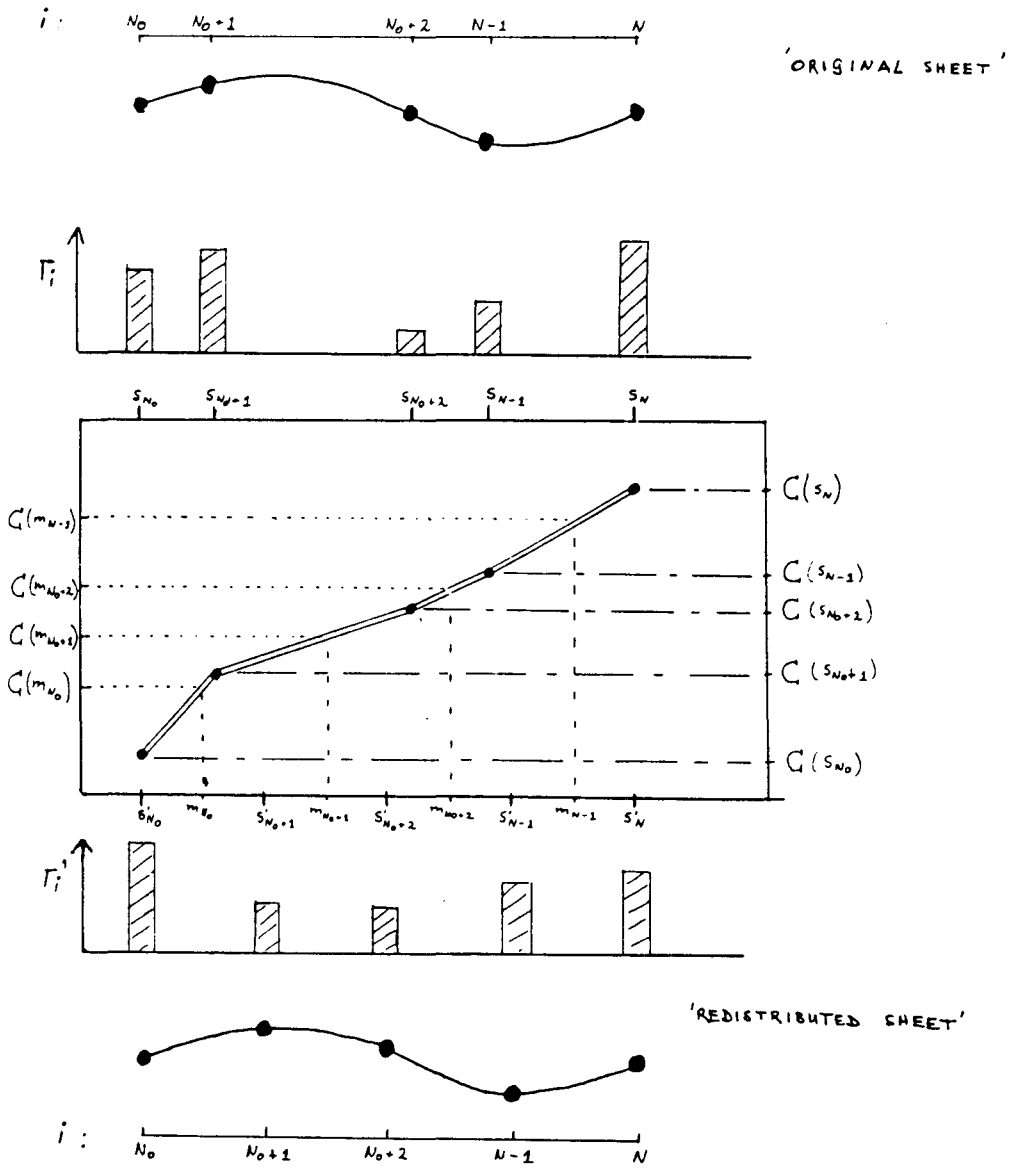

Fig.5.4.2 The redistribution technique

In figure 5.4.3 an example in given of the redistribution technique. The sheet in the first picture, represented by the pointvortices on the triangle positions, is redistributed starting at the third vortex (N_o=3). In the other pictures the original cumulative vorticity C(s) and the redistributed cumulative vorticity C(s´) and the vortex strenghts before and after distribution are given.

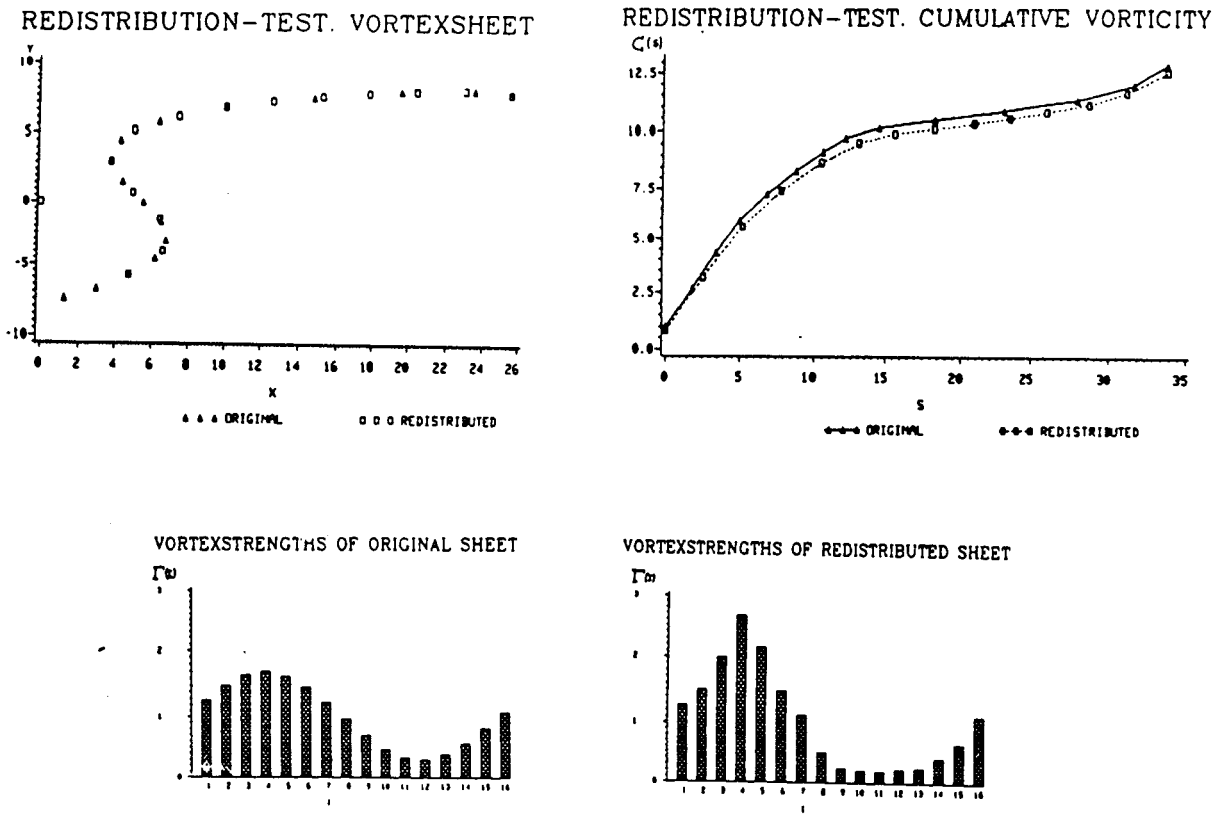

Fig.5.4.3 Example of redistribution

A disadvantage of the redistribution technique is the large amount of computation time needed to implement it. A run of 100 timesteps with redistribution took almost four times the amount of processing units as the same run without redistribution. This is mainly due to the evaluation of the splinefunction.
It was therfore decided to study the effect of not using redistribution every timestep. In figure 5.4.4 the results are shown for the same flow as shown in figure 5.4.1.
In the upper picture redistribution was applied every timestep, in the second picture every two timesteps and in the third picture every four timesteps.

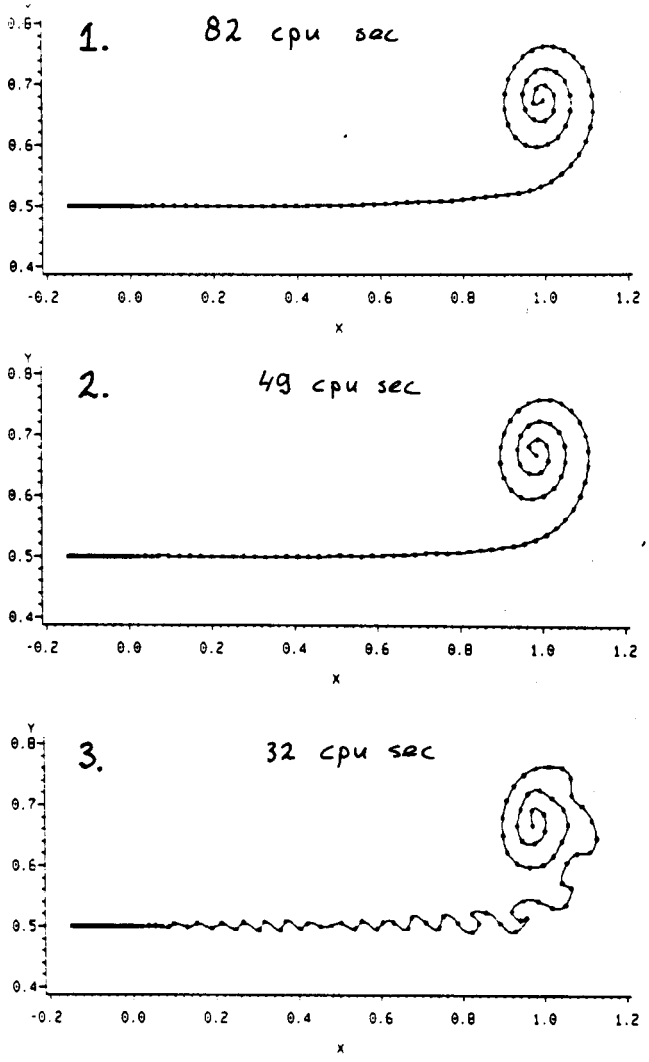

Fig. 5.4.4 Effect of the intermittent use of redistribution on the calculation time and the vortexsheet evolution. Intermittency (I) is: Picture 1: I=1 Picture 2: I=2 Picture 3: I=4

Remarkable in figure 5.4.4 are the spurious waves that develop in picture 3. Moore 54) found under certain conditions the same kind of waves when using Fink & Soh's procedure of repositioning. An explanation is not known. The conclusion is that to follow the development of the mixing layer it is sufficient to apply redistribution every two timesteps. This saves about 40 % of the calculation cost.

Another comparison of the development of a vortexsheet with and without redistribution is presented in figure 5.4.5. It is the development of the Kelvin Helmholtz instability on a finite vortexsheet. To see what the effect of different timesteps and a finer discretization are these parameters were also varied.

At $t^*=0$ the sheet, consisting of equal strength pointvortices, had

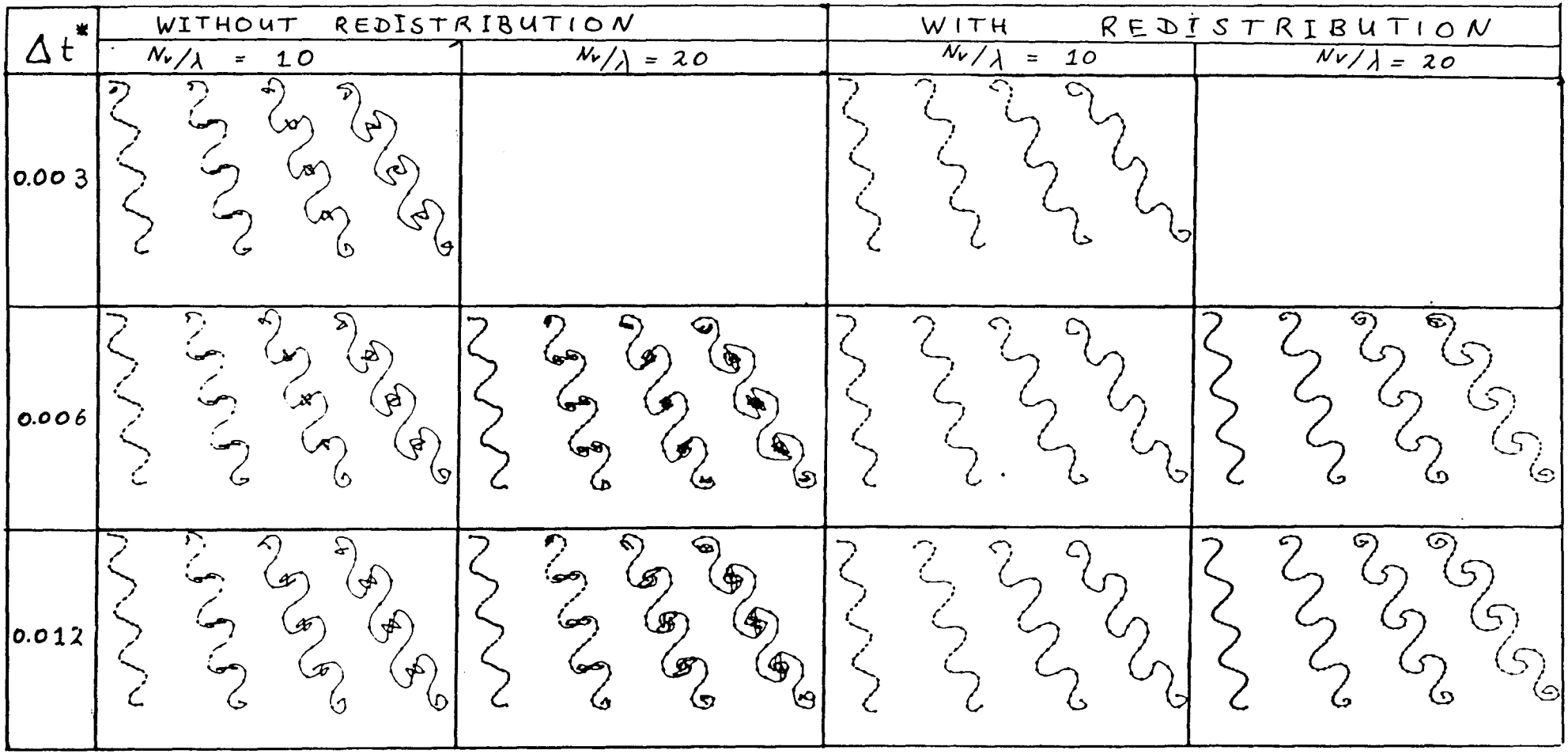

Fig.5.4.5. The Kelvin-Helmholtz intability for a finite vortexsheet.
Four moments in time are shown: $t^* = 0.4\ \ 0.8\ \ 1.2\ \ 1.6$

sinusoidal disturbance. The length of the sheet was 4 wavelength and the starting amplitude was 10% of the wavelength. Exponential growth rates of the amplitude can therefore not be expected.
The timestep is now non-dimensionalised with the velocity difference across the sheet and as length scale the wavelength λ is chosen. For each condition four moments in time are shown: $t^* = 0.4$, 0.8,1.2 and 1.6. The number of vortices per wavelenght is 10 or 20. Clearly visible is the chaos that develops in the roll-up region when no redistribution is applied. Remarkable however is the fact, at least in the timeperiod observed here, that the chaos doesn't seem to influence the size and form of the large scale structures very much.
Another conclusion that can be made from figure 5.4.5 is that 10 vortices per wavelength is not enough to model the roll-up region for an extended period of time.

5.5 Amalgamation

In an attempt to reduce calculation time and to prevent unphysical behaviour that, in spite of the redistribution technique, can occur in regions where vortices from different arms of the roll-up spiral can come close to eachother a variant of the amalgamation technique, described by Bromilov 77) has been tried in the mixing layer simulation.
This amalgamation technique is aimed therefore at amalgamating the inner vortices of the roll-up region into one vortex. This is justified by the fact that at a distance of several vortexspacings the cluster of vortices in the roll-up region seems to behave like one vortex, see Maskew 30).
After each interval of T_a timesteps the algorithm cheques if the sheet has started to roll up (whether $x_{i+1} < x_i$ for any i) and on the onset of rolling up determines the lower and upper points p_l and p_u, between which rolling up is taking place, see figure 5.5.1.

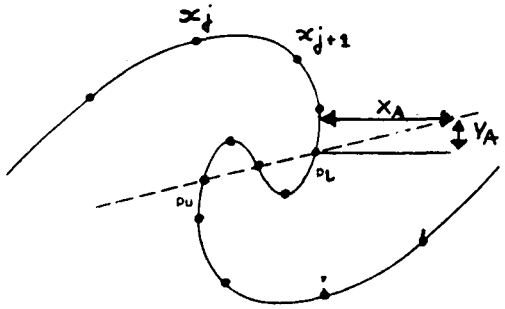

Fig.5.5.1 Illustration with the amalgamation algorithm.

If the points p_l and p_u are found and the ratio $|v_A/x_A|$ is lower than a predetermined value r_a and the number of vortices between p_l and p_u is larger than a predetermined value m_a amalgamation of these vortices takes place into one vortex, positioned at their center of vorticity and with their combined strenghts.

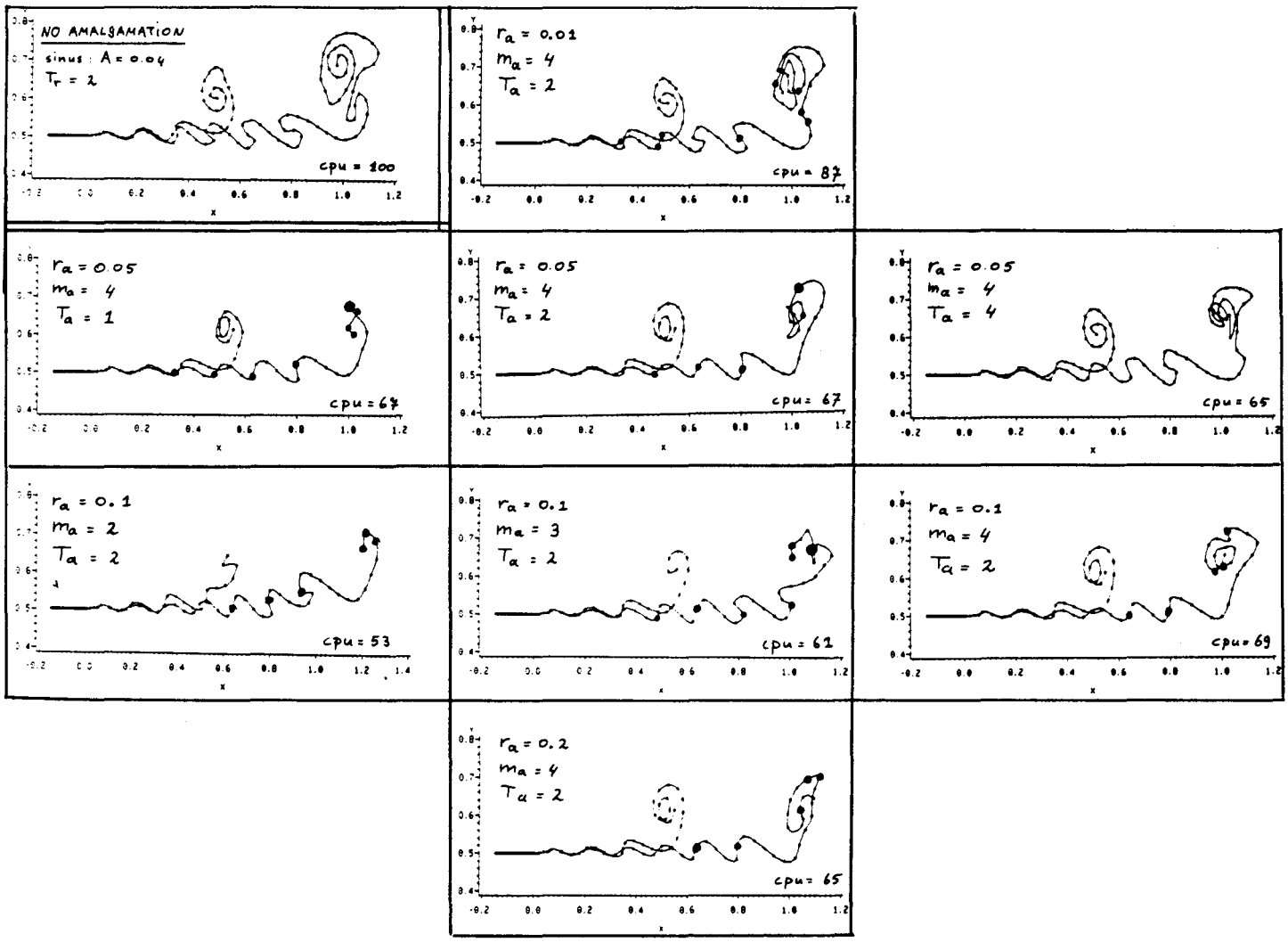

Fig.5.5.2 The effect of the parameters T_a, r_a and m_a on amalgamation. In each picture the same sheet is shown at two different points in time: t^*=0.6 and 1.2. The picture in the upper left corner is made with the same conditions but without amalgamation.
In the lower right corner the calculation time is compared with the no-amalgamation run (CPU=100).
dt^*=0.015 and λ^*=1/3. Vortices, whose strength is clearly larger than that of their neighbours are more clearly marked.

The results of this amalgamation procedure, as presented in figure 5.2.2., are not very satisfactory. In nearly every amalgamated situation the sheet crosses itself. Moreover it is very inconvenient to have an amalgamation procedure that is dependent on three aribitrary parameters. It is possible that the failure of this amalgamation technique is related to the redistribution technique. Lack of time prevented an extensive study of this.
The conclusion is that this amalgamtion procedure is unreliable and that creating a good physically sound amalgamation procedure is not easy since the introduction of spurious effects is difficult to prevent.

5.6 The structure of the program VORTEX.

In this paragraph the structure of the program VORTEX, used to calculate the development of the vortex sheet will be presented. The names of the different subroutines together with an explanation of their function will be given.
In an initial version of the program at a certain timestep t, when the vortex positions were known as well in the ζ -plane as in the z-plane the vortices were convected in the z-plane with the velocity given by equation 5.2.4. The new positions in the z -plane were then tranformed to the ζ -plane. This gave no problems because the transformation of the confined splitterplate geometry to the upper half plane was analytically known (equation 5.2.2). Since the author's vortex method was meaned to describe the A-type flow, of which the Schwarz Christoffel transformation has no analytic solution, an alternative approach was devised. The essence of this new approach is that convection of the pointvortices is done in the ζ -plane.
The 'unphysical' convectionspeed of a pointvortex in the ζ -plane is given by:

$$\frac{d\zeta_i^*}{dt} = \frac{dz_i^*}{dt} \cdot \left(\frac{d\zeta}{dz}\right)_i^* \qquad (5.6.1)$$

If this equation is substituted in the equation for dz_i^*/dt (4.5.3) the 'speed' of vortex i in the ζ -plane follows:

$$\frac{d\zeta_i^*}{dt} = \left|\frac{d\zeta}{dz}\right|_i^2 \cdot \left\{ \frac{dw}{d\zeta} + \frac{i\Gamma_i}{2\pi} \cdot \frac{1}{(\zeta-\zeta_i)} + \frac{i\Gamma_i}{4\pi} \frac{\left(\frac{\partial^2 z}{\partial \zeta^2}\right)}{\left(\frac{\partial z}{\partial \zeta}\right)} \right\}_{\zeta \to \zeta_i} \qquad (5.6.2)$$

For the confined splitter-plate geometry $|d\zeta/dz|^2$ can easily be determined:

$$\left|\frac{d\zeta}{dz}\right|^2 = \left|\frac{\pi(\zeta^2-1)}{\zeta}\right|^2 \qquad (5.6.3)$$

In principal this means that one only have to know the differential part of the Schwartz-Christoffel $dz/d\zeta$, which in most cases is easy to obtain, in order to calculate the movement of the vortices in the ζ-plane. The cumbersome numerical transformation of these position to the physical z-plane can then be postponed till the timestep one really is interested to see the vortexpositios.
A consequence of this procedure is a change of the redistribution algorithm. This algorithm redistributes the vortices along the sheet to have equal spacing. Since most Schwarz-Christoffel transformation are not linear, equal spacing in the ζ-plane doesn't mean equal spacing in the z-plane. In the ζ-plane the vortices must be redistributed along the cubic spline curve through the pointvortices according to:

$$s(i) = \frac{\sum_{j=N_0+1}^{i} \left|\frac{d\zeta}{dz}\right|_{\zeta_j}}{\sum_{j=N_0+1}^{N} \left|\frac{d\zeta}{dz}\right|_{\zeta_j}} \cdot S_{total} \qquad (5.6.4)$$

where s(i) denotes the pathlenght along the sheet from vortex N_0 to vortex i and where S_{total} denotes the total pathlength along the sheet in the ζ-plane.
The consequence is a simplification of the structure of VORTEX.
In figure 5.6.1 a schematic flow scheme is presented with in capitals the subroutines involved. All subroutines whose function lies in the area of output (selection of data to store, making plotfiles etc.) are not mentioned.
VORTEX is an interactive program that uses the subroutine INIT (initialisations) to asks all kin of questions at the user.
In INIT one can for example choose between a starting flow or a condition in which alraedy a vortexsheet is present which satisfies the Kutta-condition. Moreover it asks which kind of output is desired, if amalgamation or redistribution must be performed.
The meaning of the other subroutines follows readily from the short description in the flowscheme of figure 5.6.1.

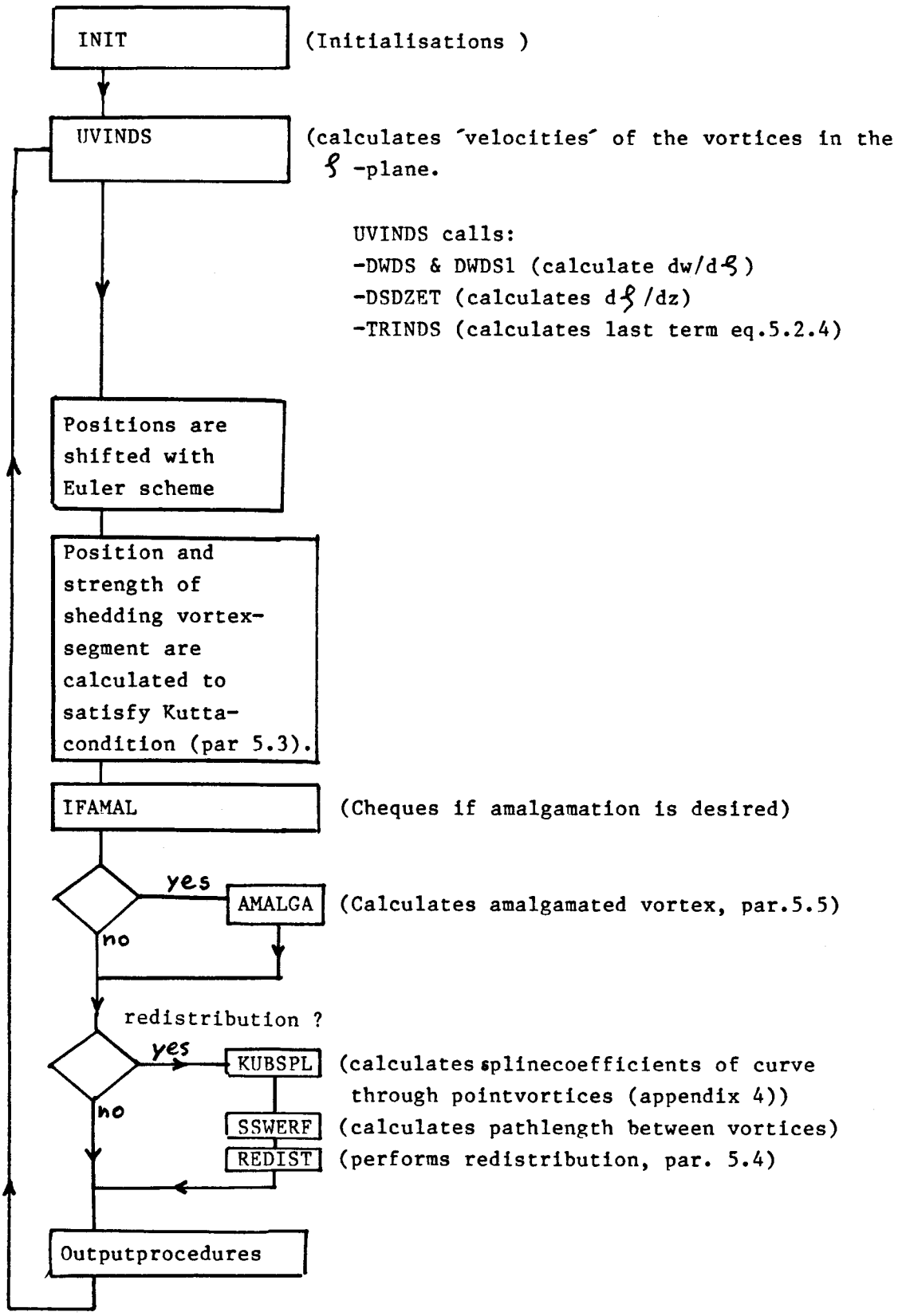

Fig.5.6.1 The flowscheme of the program VORTEX

5.7 The forced mixing layer

In chapter 2 it became clear that the conditions in the outer flow, especially near the separation point, have a big influence on the development of the mixing layer. Some authors even stated that it is impossible to create an experimental mixing layer that is not infuenced by some kind of disturbance.
In calculations with VORTEX however, when no artificial outside disturbances were introduced, the vortexsheet behaved unrealistically quiet and smooth, see figure 5.7.1.

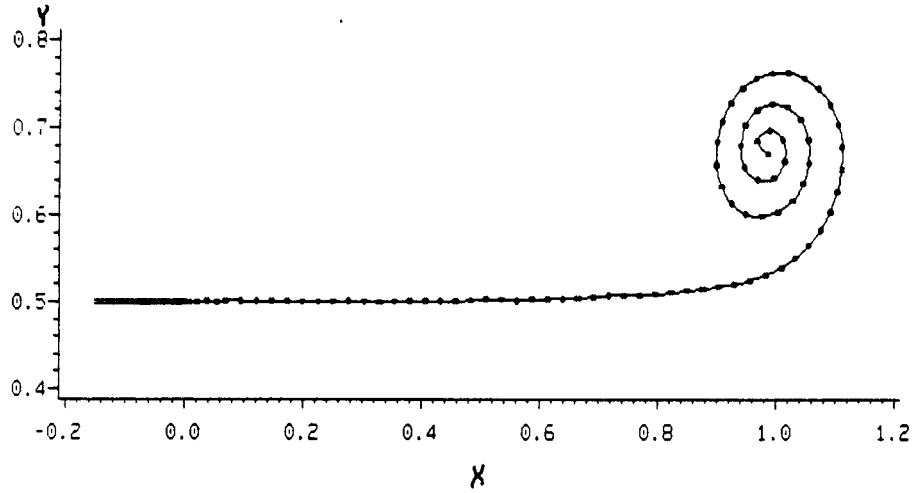

Fig. 5.7.1. Development of the vortexsheet. t^*=1.2 dt^*=0.015. λ^*=1/3. No outside disturbances are applied.

It was therefoe decided to simulate these 'inevitable' disturbances by adding a fluctuating signal to the irrotational main flows U_H and U_L. In figure 5.6.1. the effect of sinusoidal disturbances is presented for different amplitudes A of the disturbance. This diturbance is given by:

$$U_H = 0.2(1+A)\cos\left(\frac{2\pi P_d}{dt^*}\right)$$
$$U_L = 0.4(1+A)\sin\left(\frac{2\pi P_d}{dt^*}\right) \qquad (5.7.1)$$

where P_d is the period of the disturbance in number of timesteps dt^*. Redistribution was applied only every two timesteps.
In figure 5.7.2. P_d was 10.
The results are qualitatively in good agreement with experimental results, which show that forcing of the mixing layer:
- causes the mixinglayer to resonate with the forcing frequency
- increases the growthrate of the mixinglayer width.

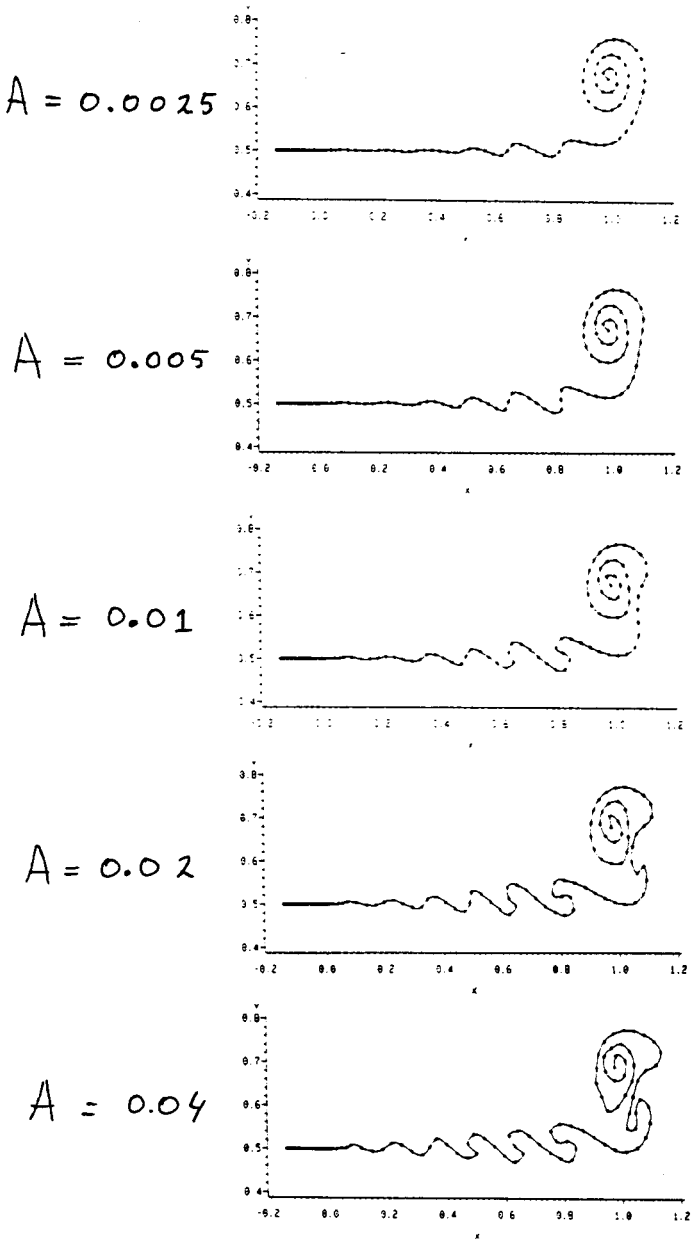

Fig.5.7.2 Forcing of the mixing layer for different amplitude A of the forcing-sinus. t^*=1.2 dt^*=0.015 and P_d=10

Non-coherent disturbances appear to have less influence on the mixing layer growth rate than the coherent forcing of figure 5.7.2. In figure 5.7.3 the influence of a sinusoidal disturbance with an amplitude of 1% of the mean is compared with a random disturbance and a pseudo-turbulent disturbance that have a maximum amplitude of 1% of the mean. The pseudo-turbulence was created by applying a digital low-pass filter to a random signal. Its powerspectrum is also given in figure 5.7.2.

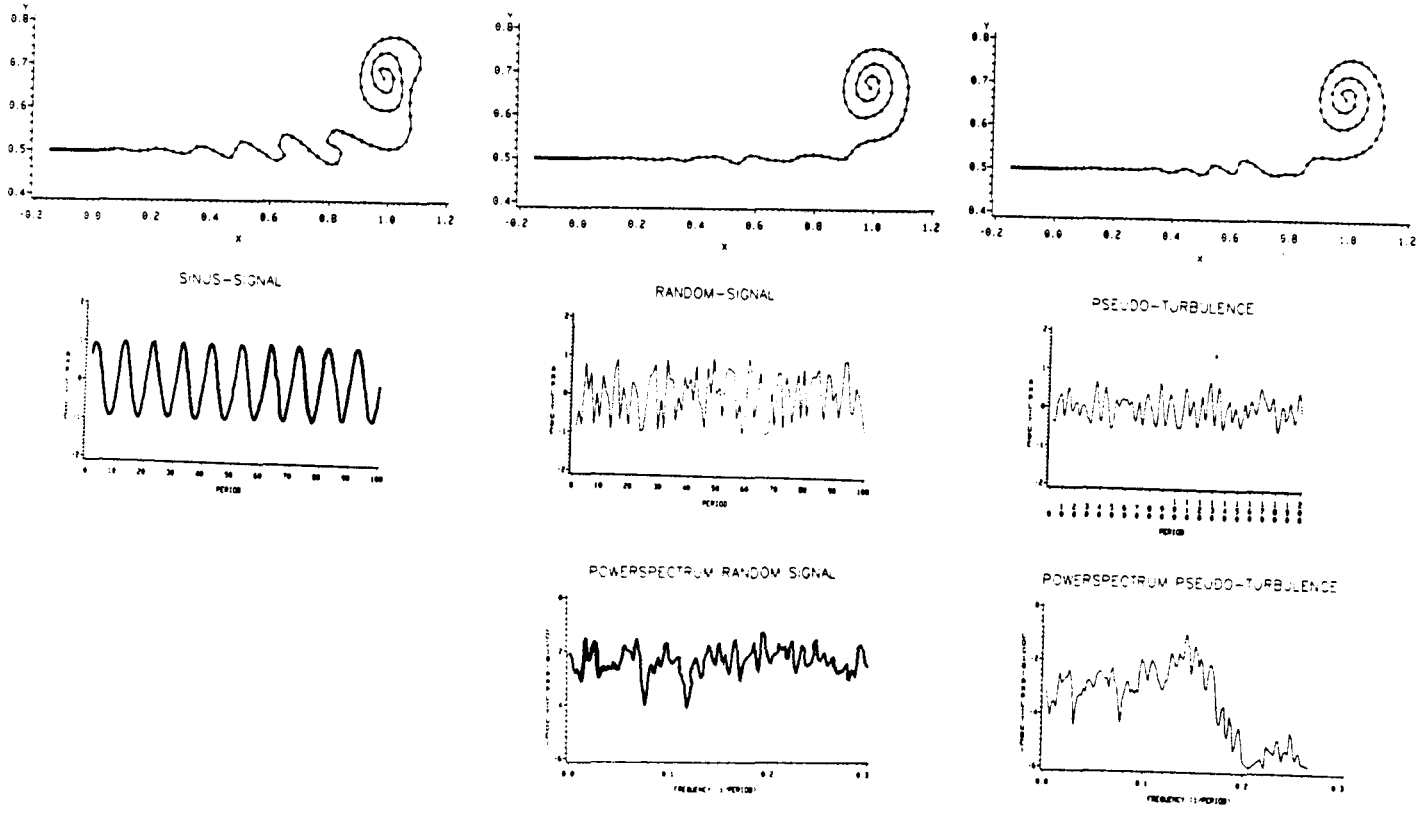

Fig.5.7.2 Comparison of the effect of different types of disturbances in the main flow on the vortexsheet development. Conditions are the same as in figure 5.7.1.

The conclusion of this paragraph is that a mixing layer model by means of a pointvortexmethod needs artificial disturbances in order to create realistic results.

5.8 Changing the velocityratio

Brown & Roshko 3) showed in their experiments that increasing the velocity ratio parameter λ^* cased the growth rate of the mixinglayer width to increase. This effect can also been seen in our pointvortexmodel, see fig.5.8.1. In this picture three values of λ^* (λ^* =1/3 , λ^* =1/2 , λ^* =2/3) were compared. An exact analysis of the mixinglayergrowth is hampered (especially for λ^* =2/3 by the dominating Kaden spiral caused by the fact that we observe a starting flow. In all three pictures an artificial pseudo turbulent signal was applied on the main stream with an maximum amplitude of 2% of the mean.

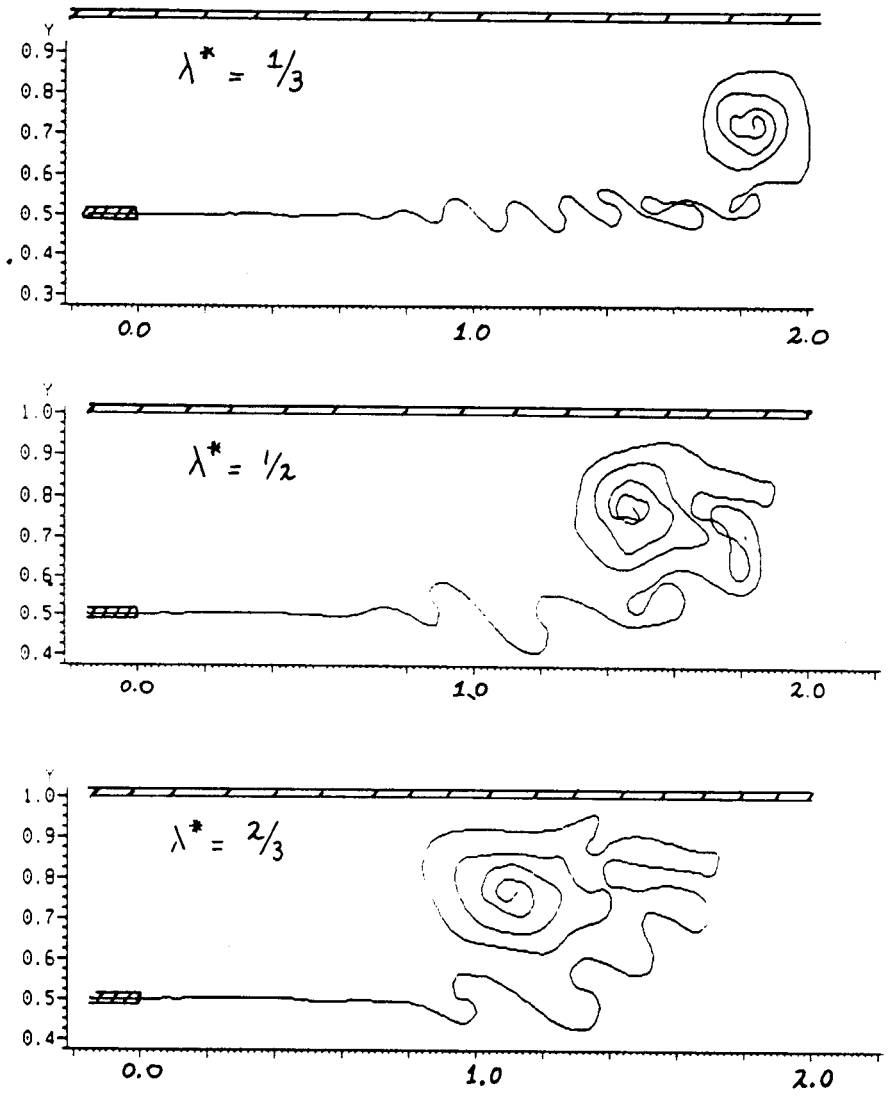

Fig.5.8.1 Influence of changing λ^* on the development of the mixinglayer. With pseudoturbulence : max = 2 %

5.9 The A-type geometry

The original aim of this work was to model the flow in A-type mixing geometry with the vortexmethod. To acomplish this the splitter-plate model has to be extended. In figure 5.9.1. is an picture of a possible result of a vortexmethod for the A-type mixing geometry is given. In the geometry is assumed that the flow in the A-type quench may be assumed symmetric so only one half of the quenchshaft has to be modelled.

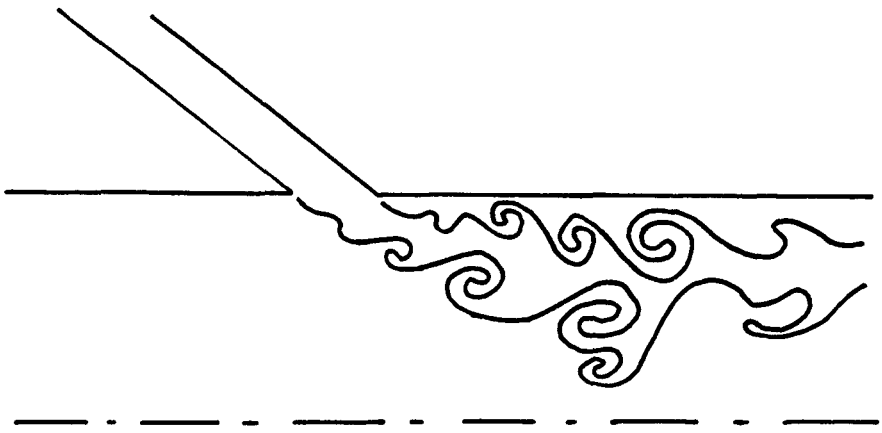

Fig.5.9.1 Possible result of a vortexmethod for the A-type flow

At least the following extensions must be added to the present plane mixing layer point vortex model:

- A new Schwartz-Christoffel transformation, to transform ζ-positions to z-positions, must be used in order to be able to satisfy the boundary conditions with mirrorvortices.
- The shedding mechanism must be adapted for a wedge flow.
- Provisions must be make to convect a second vortexsheet see figure 5.9.1. This could mean for example that the close approach algorithm of Maskew 30) (see paragraph 4.3.) must be included.
- A procedure must be created that handles vortices that cross the boundary (make them disappear, bounce them back ?)
- The algorithm of Zalosh 27) (see paragraph 4.8), to model densitydifferences, must be included.

Probably it is a good idea to change the vortexmethod from a point vortex method with redistribution into a discrete vortex method or a "cloud in Cell"-vortexmethod. This would reduce computationtime considerably. The "random walk" approach to viscosity of Chorin 79) or the "aging" algorithm of Ashurst 31) could be tried.

Some preliminary calculations have been done on the Schwarz Christoffel transformation needed for the A-type geometry. The Schwarz Christoffel transformation belonging to the $\alpha=30^{\circ}$ - quench is given by:

$$\frac{dz}{d\zeta} = \frac{\zeta^{5/6}(\zeta+1)}{(\zeta-p_1)(\zeta-p_2)} \qquad (5.9.1)$$

where p_1 and p_2 determine the diameter-slitwidth ratio and the relative position of the two separation points, see also fig.5.9.2.

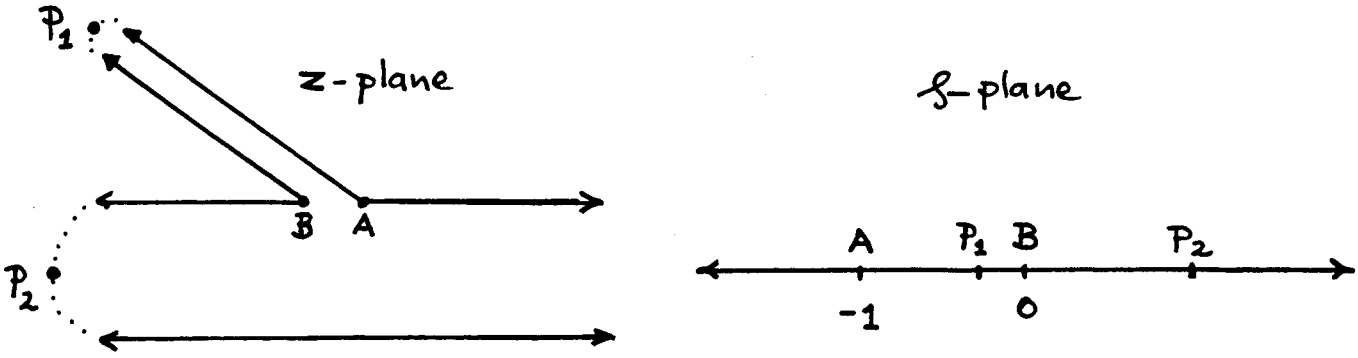

Fig.5.9.2 The Schwarz-Christoffel transformation of the A-type geometry.

In figure 5.9.3. some results have been given of the numerical solution of equation 5.9.1. The choice of p_1 and p_2 were:

$p_1 = -0.157$

$p_2 = 4.0$

The picture shows how straight lines along the real and imaginary axis of the ζ -plane are transformed to the z-plane.

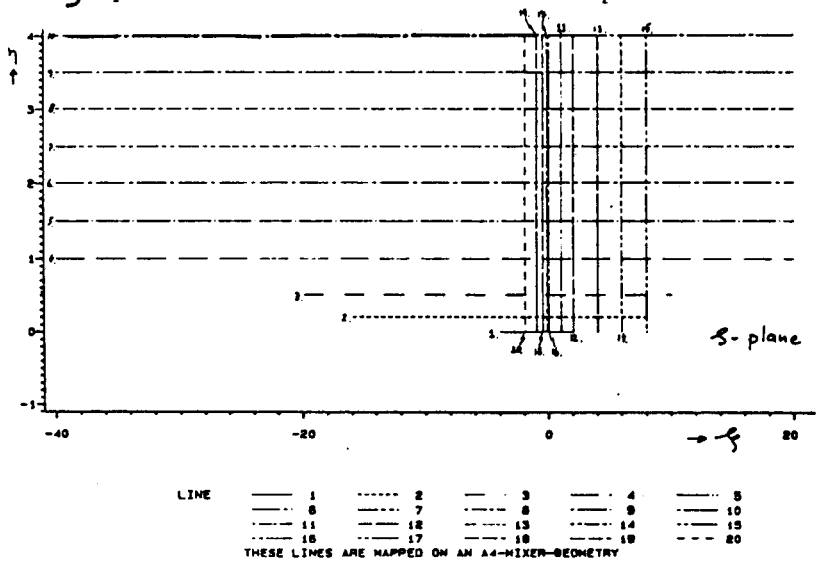

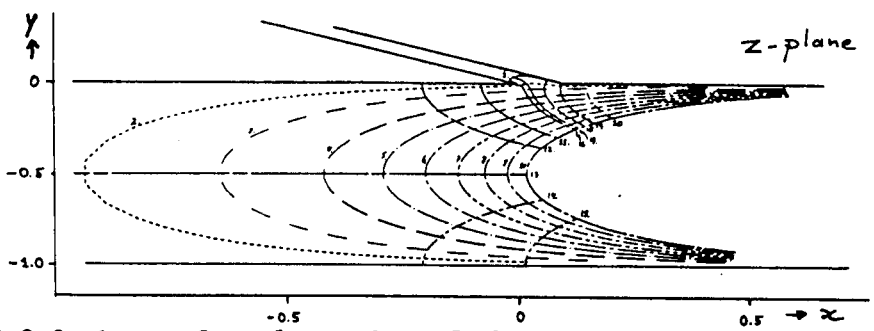

Fig.5.9.3 The conformal mapping of the A-type geometry with the Schwarz Christoffel transformation of equation 5.9.1.

5.10 Conclusions

In this chapter a point vortex method for the confined plane mixing layer has been constructed. The redistribution technique to surpress the chaos-causing discrete Kelvin Helmholtz instability proved succesful. It appeared to be possible to simulate, at least qualitatively, some experimental features of the mixing layer.
A more close analysis could maybe also prove quantitative agreement.
This model can be considered as a first step on the way of modelling the A-type quench flow with a vortexmethod but many steps lay still ahead.

PART B THE QUENCH TEST UNIT

CHAPTER 6 DESIGN OF THE QUENCH TEST UNIT

6.1 Introduction

The purpose of the Quench-Test-Unit (Q.T.U.) is to have a scale-model of a real quench in which the aerodynamic performance of this real quench can be tested. In order to satisfy this purpose the Quench-Test-Unit must meet three requirements:

1) The flowconditions in the Q.T.U. must be the same as in an actual quench.

2) The Q.T.U. must be designed in such a way that changing the main parameters (slitwidth S and flowangle α) can be done easily.

3) The Q.T.U. must be designed in such a way that it is easily accessible to instruments with which the fluid dynamic behavior can be tested.

In this chapter it will be described how the design that meets the above requirements looks like. In paragraph 6.2.2 will be described what the important flowparameters are and which conditions they force on the design of the Q.T.U.
The density-ratio condition is met by using a very cold gas. How this cold gas can be produced is described in paragraph 6.2.3.
In the Q.T.U. it is tried not only to model the flowconditions in the quench as good as is possible but also is tried to simulate the flow in the reactorvessel before the quench. The determining factor here is the burner-flow. In paragraph 6.2.4 will be described how these burners are modelled.
In paragraph 6.2.5 is described how the test-section itself (part of Q.T.U were the hot and cold flow meet) is designed.
In paragraph 6.2.6 finally all the elements, described in paragraph 6.2.2 to 6.2.5, are put together to form the complete flowscheme of the experiment.

6.2 Simulating the flow; requirements.

-Actual circumstances-
The conditions existing in the actual quench are described schematically in figure 6.2.1 and tabel 6.2.2:

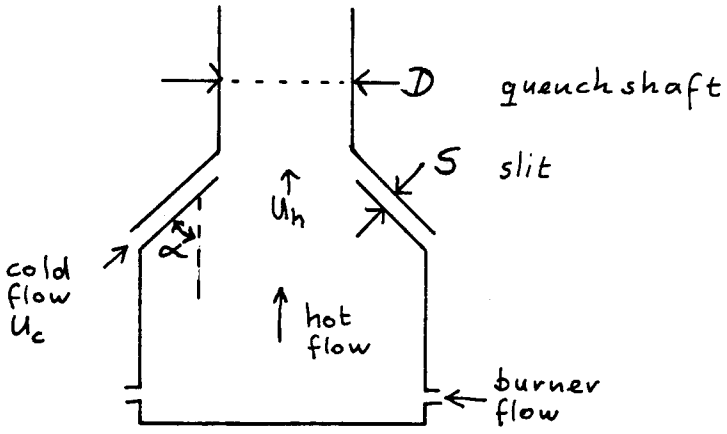

Fig.6.2.1 Schematic picture of Quench-Test-Unit

HOT FLOW	COLD FLOW
U_h = ca. 5 m/s	U_c = 5 - 60 m/s (to be determined)
D = ca. 0.4 m	S = 1 - 12 mm (to be determined)
ρ_h = ca. 3 kg/m_3	ρ_c = ca. 12 kg/m_3
p_h = 25 bar	p_c = 25 bar
T_h = 1800 K	T_c = ca. 450 K
$\dot{M}_h$ = ca. 1.9 kg/sec =	$\dot{M}_c$ = ca. 1.9 kg/sec
$Re_h > 5\ 10_4$	$Re_c > 5\ 10_4$

Tabel 6.2.2 Physical parameters of the actual quench

-Total dimensions-
The geometry of the Q.T.U. is the same as the actual geometry, but is scaled down in order to have a lower throughput. To be able to simulate actual flowconditions as well as possible the reactorvessel with the four burners are included in the flowmodel. For economic reasons scaling down to very small dimensions is attractive. However because of the requirement of accessibility for experiments it was decided to set a lower limit to the diameter of the quenchshaft (D):

$$D >= 0.1 \text{ m} \qquad (6.2.1)$$

All other dimensions follow from this dimension.

-Density ratios-
The density ratio between the hot reactorgas and the cold quenchgas must be the same as in the actual quench:.

$$\frac{\rho_c}{\rho_h} = 4 \qquad (6.2.2)$$

This ratio is so high that it is not possible to use liquids to simulate the reactor- and quenchgas. The following possibilities are thinkable:

1) A combination of a cold and a hot gas.

2) A combination of a high and a low molecular weight gas.

Because of economic and safety reasons the solution finally chosen is to use cold nitrogen (T=80 K) to simulate the quenchgas, and to use slightly heated nitrogen (T=320 K) to simulate the reactorgas. How to produce this low-temperature nitrogen-gas in sufficient amounts will be the subject of paragraph 6.3.

-Mass Flow Ratio-
The massflow-ratio between both fluids must be the same as in the actual quench, this is:

$$\dot{M}_c \; / \; \dot{M}_h = 1 \qquad (6.2.3)$$

-Compressibility-
The velocities in the Q.T.U. can be more or less chosen freely but they must not be so high that compressibility-effects start playing a role. A criterion for this is $M^2 < \sigma(0.1)$ where M is the machnumber of the flow. The highest velocities are in the annular slit, so that the above criterium becomes:

$$U_c < 0.3 * \text{velocity of sound} = \text{ca. } 60 \text{ m/s} \qquad (6.2.4)$$

-Viscosity-
In the actual coal-gasifier and quench the throughput is so large that the flow is fully turbulent. The Reynoldsnumber in the quenchshaft is estimated to be more than 10^5. It is not necessary to require the same values in the Ouench Test Unit as long as the

Reynoldsnumber is sufficiently large, say $3 \cdot 10^4$. The Reynoldsnumber in the slit must be based on the hydraulic diameter of the annulus, being 2S. The ratio of the slit- and shaft-Reynoldsnumber can now be written as:

$$\frac{Re_c}{Re_h} = \frac{\mu_h}{\mu_c} \cdot \frac{\dot{M}_c}{\dot{M}_h} \qquad (6.2.5)$$

This means, with $\dot{M}_h = \dot{M}_c$, $\mu_c = 6 \cdot 10^{-6} \frac{kg}{m \cdot s}$, $\mu_h = 20 \cdot 10^{-6} \frac{kg}{m \cdot s}$, that $Re_c/Re_h \sim 2$. This means that by satisfying the condition $Re_h > 3 \cdot 10^4$ for the hot flow automatically this condition is fulfilled for the cold flow. The minimum required massflow to satisfy this condition for the hot flow is given by:

$$\dot{M}_{h,min} = \frac{\pi}{4} \cdot Re_{h,min} \cdot D \cdot \mu_h \cong 0.05 \ kg/sec. \qquad (6.2.6)$$

This value for $\dot{M}_h$ doesn't violate the compressibility-requirement (6.2.3) upto a velocity-ratio $U_c/U_h = 12$. This is amply sufficient.

-Buoyancy-

If the velocities in the quench are small and the diameter is large buoyancy-effects can play a role. A characteristic quantity for this effect is the Froude-number:

$$Fr = \frac{U^2}{g \cdot D} \qquad (6.2.7)$$

where g is the gravity constant.
To investigate the effect of buoyancy the Froude number of the experiment should have the same value as in the actual quench.
If a turn-down ratio (the ratio between the minimal massflow and the nominal massflow) of 50 % is taken into account the lowest value of Fr in a large scaled up quench is around 1.
This value cannot easily be accommodated for in the Q.T.U. unless very large amounts of gas are used. Fr can be written as:

$$Fr = \alpha^* \cdot \frac{Re_h^5}{\dot{M}_h^3} \qquad (6.2.8)$$

with $\alpha^* = \left(\frac{\pi}{4}\right)^3 \cdot \frac{\mu_h^5}{\rho_h^2 \cdot g} \cong 10^{-25}$ in the Q.T.U.

This means that the massflow $\dot{M}_h$ ($Re_h = 3 \cdot 10^4$ and Fr = 1) must be four times as high as required by the viscosity-condition (6.2.6).
It is not necessary to do detailed measurements on this value of Fr=1. Only when mixing is slow and density differences are persistent (H-type quench) it can be necessary to see if complications will occur on this value of Fr=1. For that case the Re-condition is released a bit and we require $Re_h < 1.5\ 10^4$. Then the required massflow is equal to the requirement set by the viscosity condition (6.2.6), i.e. $\dot{M}_h = .05$ kg/sec. To be able to get Re so low with the same massflow the quenchshaftdiameter D must be enlarged with a factor 2. This means that the design of the Q.T.U. must be such that such an enlargement is possible.

6.3 Production of cold gas

In this paragraph the productionmethod of the cold gas will be described. The cold gasflow must meet the following requirements:

(1) Massflow $\dot{M}_c = 0.05 - 0.1$ kg/sec
(2) Temperature T_c = ca. 80 K
(3) Running-time under constant conditions should be at least 20 minutes.

The low temperature is reached by using the evaporation heat of liquid nitrogen. Three ways of using this principle have been studied:

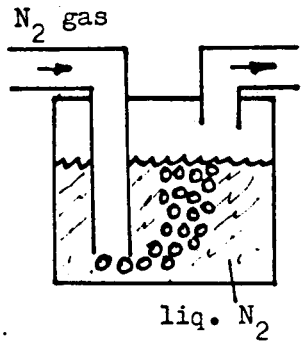

(1) The **bubble-bath** principle involves bubbling room-temperature nitrogen through a liquid nitrogen bath. Calculations showed that heat transfer from gas to liquid is amply sufficient to produce a 77 K gas. A disadvantage of this was that existing cryogenic vessels had to be rebuild at high cost to acommodate the pipediameters for sufficiently large massflow. Another disadvantage is the possible entrainment of liquid nitrogen droplets in the gasflow.

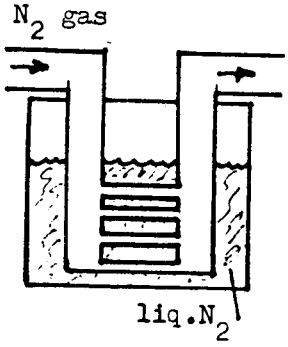

(2) The **closed heat exchanger** principle would solve this last, but not the first problem mentioned above.

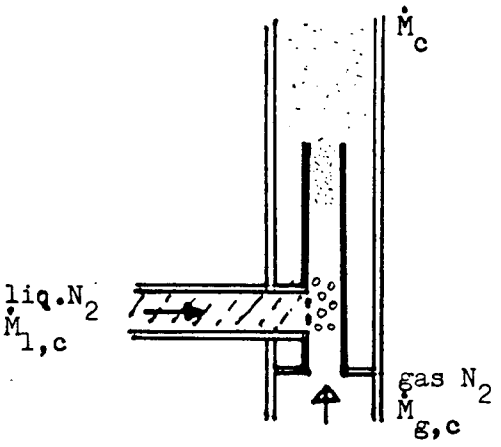

(3) So finally the solution chosen was to **spray** liquid nitrogen in a fast turbulent gasflow. When a droplet with diameter d_o suddenly is brought in a flow with speed U_o this droplet will experience a very large acceleration. When these acceleration forces are sufficiently greater than the surface tension, holding the droplet together, the droplet will break up. According to Hinze 57) this will happen when the Weber number of the droplet is greater than 13. The Weber number of a droplet is defined as:

$$We_{droplet} = \frac{\rho_g \cdot U_o^2 \cdot D_o}{\sigma_d} \qquad (6.3.1)$$

where D_o is the diameter of the droplet, ρ_g the density of the gasflow, U_o the velocity of the gasflow relative to the droplet and σ_d is the surface tension of liquid nitrogen.
Ferment 18) found that the final diameter of the droplets is given by:

$$D_{final} = \frac{1}{\sqrt{We_{droplet}}} \cdot D_o \qquad (6.3.2)$$

These relations (6.3.1 and 6.3.2) are presented grphically in figure 6.3.1. for $\sigma_d = 9\ 10^{-3}$ kg/s^2 and $\rho_g = 1.2$ kg/m^3.

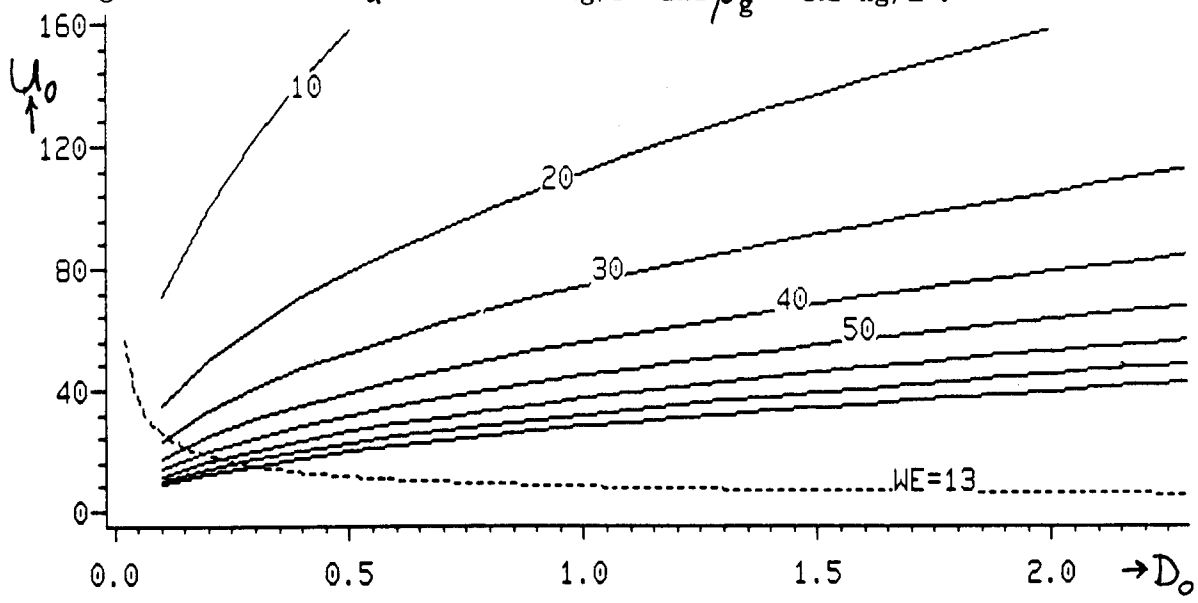

Fig.6.3.1 Final drop diameter (in μm) as a function of the initial drop diameter D_o (in mm) and the velocity U_o (in m/s)

The gas velocity U_o is determined by the massflow $\dot{M}_{g,c}$ and the diameter D_t of the tube in which the liquid nitrogen spray is injected. Under normal working conditions the diameter D_t was chosen such that the velocity U_o is greater than 60 m/s.
With the initial droplet diameter D_o smaller than 1 mm this choice garantees a final drop diameter of less than 40 μm.
The evaporation speed of such a droplet is determined by the temperature difference ΔT between the droplet and the surrounding gas and by the heat exchange factor α_e between droplet and gas.
We try to establish an upper limit for the evaporation length, i.e. the length the droplet has travelled before total evaporation.
When the radius of the drop is R, the evaporation heat of liquid nitrogen is H_{evap}, its density is ρ_l and the average travelling speed of the droplet is U_d we can write the rate of change of the radius dR travelling a distance dz as:

$$\frac{dR}{dz} = \frac{-\alpha_e}{\rho_l \, H_{evap} \, U_d} \cdot \Delta T \qquad (6.3.3)$$

The difficulty in solving this equation is that both α_e and ΔT are dependent on z. Since we are only interested in the lower limit of dR/dz we fill in the minimum values for α_e and ΔT.
The heatexchange factor α is given by:

$$\alpha_e = \frac{\lambda}{2R} \cdot Nu \qquad (6.3.4)$$

where λ is the heatconductivity of N_2 and Nu is the nusselt number for a sphere. It is well known that the Nusselt number of a sphere in the limit for $Re \rightarrow 0$ is equal to 2.
Aiming at a final low temperature of 90 K $\Delta T > 13$ K. With a droplet speed $U_d < 20$ m/s a liquid nitrogen drop of 40 μ m always has evaporated before it has travelled 3 m. In the design this worst case evaporation length of 3m is used.
To establish the average travelling speed of the droplet < 20 m/s the tube diameter D_t expands after some distance in a wider tube, see figure 6.3.2.

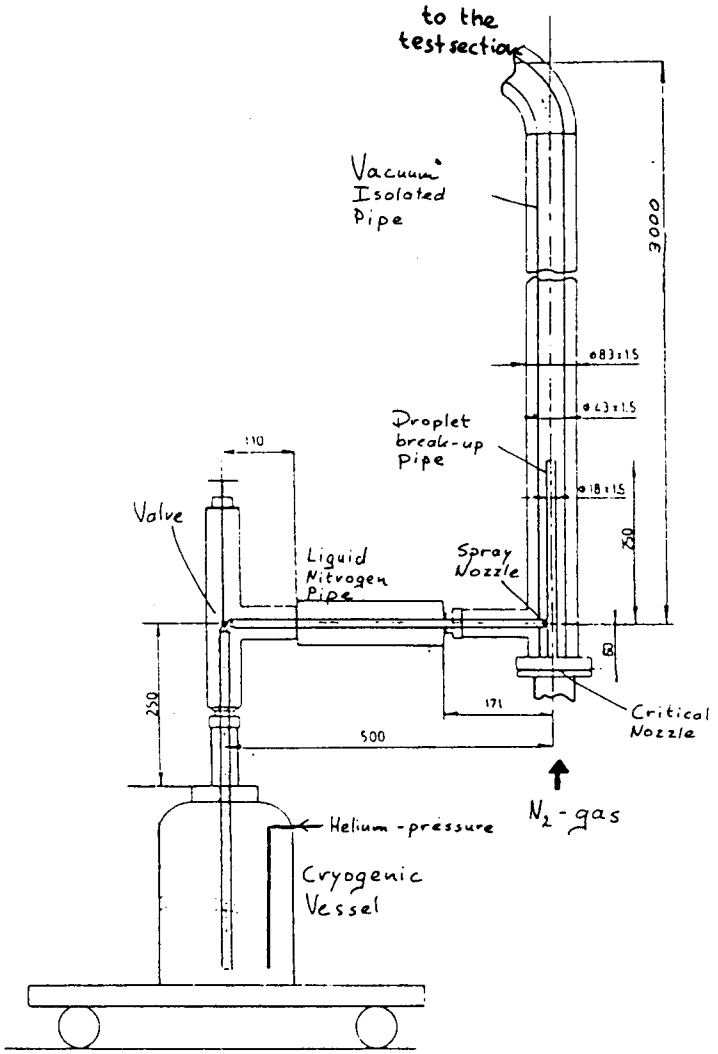

Fig.6.3.2 The design of the cold nitrogen producing part of the Q.T.U.

6.4 Modelling the burners

In the quench test unit the aerodynamic properties of the hot flow entering the quench are simulated by modelling the burners and the reactor vessel through which this gas flows in a actual coal gasification plant.
The reactor vessel is modelled by geometrically scaling it down, see par.6.2. The modelling of the burnerflow is not so straightforward. The important parameter is the equivalent momentum diameter D_{eq}:

$$D_{eq} = \frac{\dot{M}_o}{\sqrt{\frac{\pi}{4} \cdot \dot{J}_o \cdot \rho_\infty}} \qquad (6.4.1)$$

in which $\dot{J}_o$ and $\dot{M}_o$ are the momentumflow and the massflow through the burner and ρ_∞ is the ambient density in the reactor.
The physical meaning of D_{eq} is that it determines the entraining capacity of a jet. For a round jet Ricou & Spalding 85) found empirically:

$$\frac{d\dot{M}_{entrained}}{dx} = 0.28 \frac{\dot{M}_o}{D_{eq}} \qquad (6.4.2)$$

When $D_{reactor}$ is the diameter of the reaction vessel the scale rule for the burners is given by:

$$\left.\frac{D_{eq}}{D_{reactor}}\right|_{EXPERIMENT} = \left.\frac{D_{eq}}{D_{reactor}}\right|_{ACTUAL} \qquad (6.4.3)$$

For the actual coal gasification plant for one burner $\alpha^* = .25$ à .35. This means that a burner in the Q.T.U. must have a diameter such that the gasvelocity U_b is given by:

$$U_b = \frac{\dot{M}_o}{\rho_\infty \cdot 0.32 \cdot \alpha^* \cdot D_{reactor}} \qquad (6.4.3)$$

with $\alpha^* = 0.25$ a 0.35
Under normal running conditions U_b must be between 10 and 20 m/sec.

6.5 The Testsection

The testsection of the Quench Test Unit is the part where the hot and the cold flow meet. This part must meet the following (more or less contradictory) requirements:

1) Adjustable D and α
   The slitwidth D and the flowangle α must be easily variable

   Solution
   Chosen is for a system that allows varying the slitwidth D continuously by turning the nuts (1), see figure 6.5.1. The variation of the flowangle α is a little more complicated. It

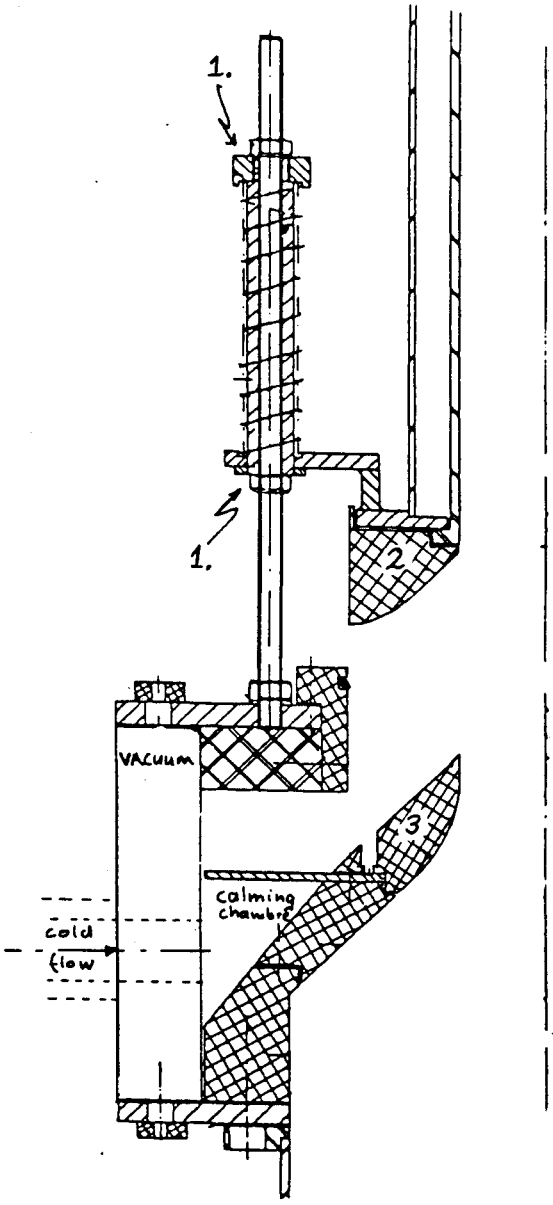

requires changing the pieces (2) and (3) (45°) and replace them by for example pieces (4) and (5) (15°).

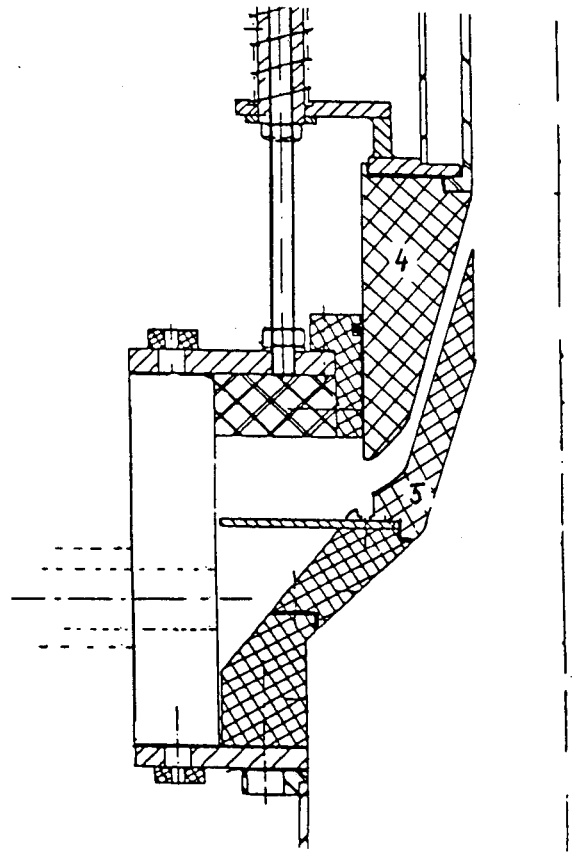

Fig 6.5.1 Two examples of the Testsection (α=45° and α=15°)

2) Material

The density ratio of the hot and the cold gas on the moment they meet should be 4. This means that the heat conductivity of the material keeping the cold and hot flow apart should be very low. The material should also be resistant to high temperature differences (250K), it must be easy to mould and it should have a low thermal expansion coefficient.

Solution

The chosen material is Celeron, a phenol raisin with cotton. It is relatively cheap, very strong and has attractive properties:

- Thermal expansion coefficient: $\alpha = 2 \cdot 10^{-5}\ K^{-1}$
- Heatconductivity: $\alpha = 0.34$ W/m K

These properties guarantee that under normal stationary operating conditions the temperature influence of the two streams on eachother is negligable (<1%)

3) Uniform flow distribution

The cold flow must be tangentially evenly distributed. Therefore we need a calming chambre with some kind of flowresistance that forces the flow around the inner tube. Also the cooling down of the whole testsection should not take to long.
This means that the whole calming chambre must have a small heatcapacity and a very good insulation from the environment.

Solution

A distribution plate (1) (see fig.6.5.2) in the middle of the calming chambre takes care of a good tangential distribution of the cold gas, coming outof a vacuum isolated pipe (2). In this plate holes are evenly distributed. The total area of these holes (including a contraction factor of 0.6) is about half the area of the cold gas pipe (2).

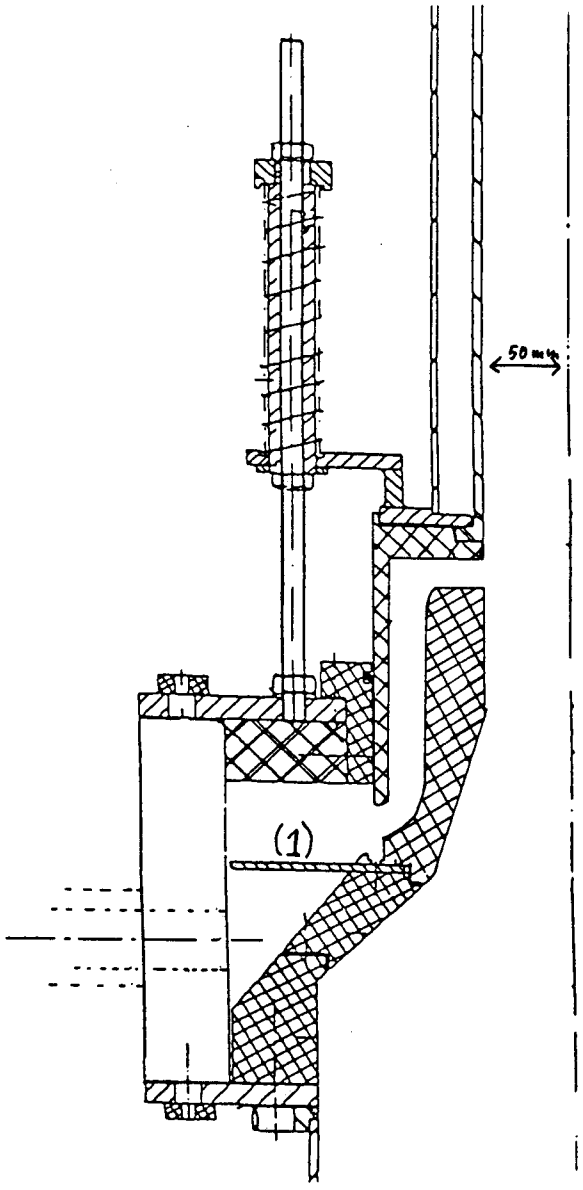

Fig.6.5.2 The Testsection ($\alpha = 90^{\circ}$)

Those parts of the calming chambre that can be vacuum isolated (3) are so isolated. This kind of insulation offers the lowest heatcapacity and the best insulation. The upper part of the calming chambre (4) must remain removable to allow for the 25 cm diameter quench shaft. Isolation there (5) is provided for by a piece of roofmate (λ= ca. 0.02 J/K m). The inner side of the suschambre is the celeron piece (6)

4) The 25-cm quench

The design of the testsection must be such that it is possible to install a quench with a diameter of 25 cm instead of the normal 10 cm quench. See for an explanation paragraph 6.2.

Solution

In figure 6.5.3 the modifications are shown to allow for a 25-cm quench.

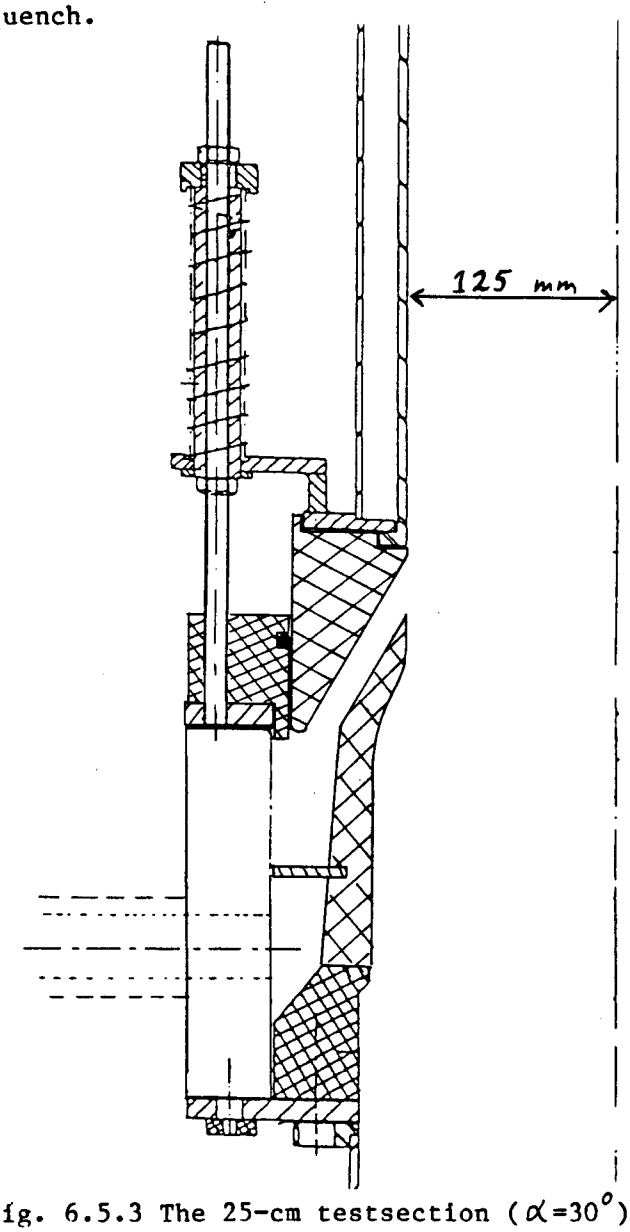

Fig. 6.5.3 The 25-cm testsection (α=30°)

6.6 Flowscheme of the Quench Test Unit

In this paragraph the (gas-)flowscheme of the complete Quench Test Unit will be described. This includes a description of the important parameters and their mutual dependence. In fig. 6.6.1 a schematic representation of the flowscheme is given.
In the scheme the symbols are drawn that are used to point out the different temperatures, pressures and massflows. Going from left to right the flowsystem consists outof the following items:

1) The nitrogengas supply. The pressure is ca. 14 bar.

2) A backpressure regulator. With this regulator one can choose the initial pressure P_i. The temperature of the gas is given by T_i.

3) The gasflow splits in two parts. One part will, after heating, form the hot flow. Its massflow is $\dot{M}_h$. The other part (massflow = $\dot{M}_{c,g}$) will form in combination with liquid nitrogen (massflow = $\dot{M}_{c,l}$) the cold flow (massflow = $\dot{M}_c$).

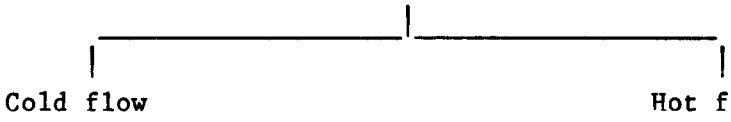

4) The gasflow is restricted by a critical nozzle with a diameter $D_{c,cr}$.

4) The gasflow is restricted by a critical nozzle with a diameter $D_{h,cr}$.

Through a critical nozzle the massflow, when the pressure before the nozzle is more than ca. two times the pressure after the nozzle (and critical flow is assured), only depends on the diameter of the nozzle and the upstream pressure P_i. This dependence is given by:

$$\dot{M}_{critical} = P_i^{8/7} \cdot D_{cr}^{2} \qquad (6.6.1)$$

This means that by choosing a ratio $D_{c,cr}/D_{h,cr}$ one fixes the massflow ratio $\dot{M}_{c,g}/\dot{M}_h$:

$$\frac{\dot{M}_{c,g}}{\dot{M}_h} = \left\{\frac{D_{c,cr}}{D_{h,cr}}\right\}^{2} \qquad (6.6.2)$$

5) After the critical nozzle liquid nitrogen is sprayed into the gasflow (par.4.3). The massflow $\dot{M}_{c,l}$ can be determined by adjusting the He-pressure on the cryogenic vessel. Helium is chosen because it remains gaseous at the boiling temperature of liquid nitrogen.

6) Through the vacuum isolated raiser pipe the cold flow enters the calming chambre and via the distribution plate enters the testsection.

5) After the critical nozzle the gasflow, which is at the initial temperature T_i, can be heated with a 10 kW electrical heater. (Enough to heat 10 gr/s N_2 to 100 ^{o}C.)

6) At this point steam can be injected into the hot flow.

7) After splitting into four pipes the hot flow supplies the four burners.

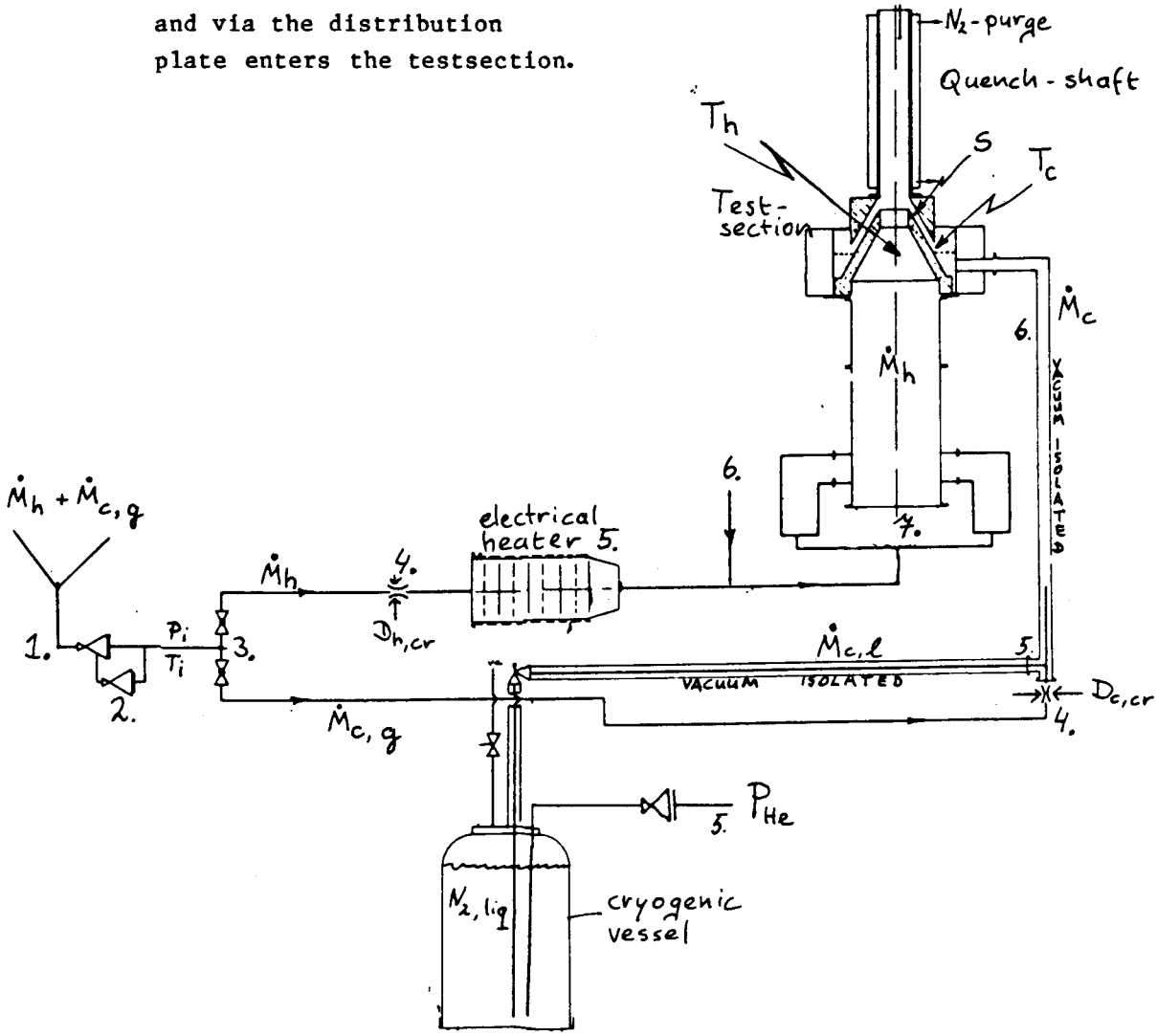

Fig. 6.6.1 Schematic plan of flow with important parameters.

Suppose a run is planned with the following requirements:

1- The massflow ratio $\dot{M}_c/\dot{M}_h$ must be 1.
2- The massflows $\dot{M}_c = \dot{M}_h = 0.05$ kg/s
3- The densityratio $\rho_c/\rho_h = 4$. ($T_h = 360$ K ; $T_c = 90$ K)

The chosen low temperature T_c determines the massflow ratio $\dot{M}_{c,g}/\dot{M}_{c,1} = \vartheta$:

$$\vartheta = \frac{c_p (T_c - 77) + H_{evap}}{c_p (T_i - T_c)} \qquad (6.6.3)$$

The critical nozzle diameter ratio $D_{c,cr}/D_{h,cr}$ one has to choose depends on ϑ:

$$\frac{D_{c,cr}}{D_{h,cr}} = \sqrt{\frac{\vartheta}{1+\vartheta}} \qquad (6.6.4)$$

The value of D_{cr} should be chosen such that:
- there is critical flow through the critical nozzle
- the initial pressures needed are not to high

Now the initial pressure P_i can be adjusted to supply the right amount of gas ($\dot{M}_{c,g} + \dot{M}_h$).
The helium pressure must be adjusted until enough liquid nitrogen is pushed through the spray nozzle (5) to cool the cold flow down to the chosen temperature T_c.
As an extra illustration in figure 6.6.2. a photograph of the reactor vessel, the testsection and the measuring instruments is presented.

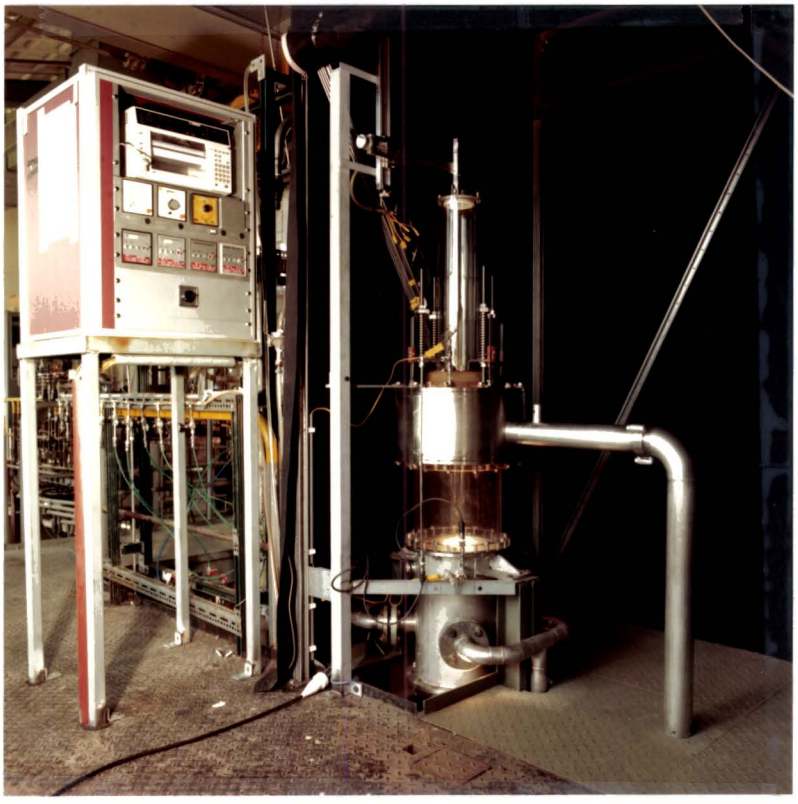

Fig.6.6.2 Photograph of part of the O.T.U.

CHAPTER 7 EXPERIMENTS

7.1 Introduction

The goal of experiments in the quench test unit is to find the optimal flowangle α and slitwidth S. Optimal is:

1) The α,S combination that causes minimal fouling of the quenchshaft,

If this goal can be reached and there is still some freedom in the choice of α and S, the second goal becomes the determination of:

2) The α,S combination that causes maximum mixingspeed.

To be able to answer these questions fully one should have to know the ashparticle trajectories and their individual temperature histories. This can only be done by simulating the actual fouling process in an experiment. Particles are then needed that have the right size distribution, thermodynamical and cohesive properties so they behave as the actual ashparticles. This can not be considered as a realistic option.
Finally it was decided to judge the performance of the quench with the help of the following three techniques:

1) Flow visualisation
2) Slow temperature measurements
3) Fast temperature measurements

Several other techniques, like measuring break through times with the help of tracers, or velocity measurement with the help of laser doppler anemometry were considered. Due to financial and practical problems these ideas were not further pursued.
In the next three paragraphs the three above mentioned techniques will be discussed and some examples of results will be given.

7.2 Visualisation

The aim of visualisation in the Q.T.U. is to support the temperature measurements and to offer a fast method to judge the quench performance.
A secondary aim is the detection of coherent structures and their comparison with vortexmethod results.
To visualize a flow one can choose from several alternatives.
If the aim is to freeze on a picture one flowcondition of the Q.T.U., due to rather high velocities in the quenchshaft (5-40 m/s), a very fast method is needed. For the condition in the Q.T.U. two methods seem suited:

1) Shadowgraph- or Schlieren photography

2) Photography with light scattered from particles that follow the flow.

The first method is based on the fact that the optical pathlength depends on the gasdensity. Because of the high density differences in the quench flow this method seems viable. Several problems however must be overcome. Interpretation of Schlieren- or shadowgraph results are not easy. The fact that lightrays used to obtain these results have to pass two concentric transparant walls and a cilindrical flow makes this interpretation probably very hard.

In this investigation the second method, use of light scattering particles, was used. The quality of this visualisationmethod depends on three independent elements:

1) Quality of illumination
2) Quality of scattering particles
3) Quality of photography

These elements will be discussed seperately.

Illumination

Illumination was provided for by a laserbeam and a rotating mirror. The laser illuminated from below through the reactor vessel a plane through the axis of symmetry of the quenchshaft, see figure 7.2.1. Fiedler 13) et.al. have described this rotating mirror system. During the experiment the testsection was screened from disturbing lightsources. Only light coming from the scattering particles could reach the lens of the camera.

First the shutter of the camera is opened. While the shutter is open the rotating mirror will sweep the laserbeam once through the area under observation, see fig.7.2.1. After this one sweep the shutter is closed.

The scattering particles are several orders smaller than the laser beam diameter. The time that one particle is illuminated by the laserbeam therefore only depends on the speed with which the beam sweeps through the observation area. In the photographs shown in figure 7.2.2-7.2.24 this speed was ca. 33 m/s. The beamdiameter is around 1 mm and the maximum flowspeed is around 20 m/s. This means that a particle will never travel further than 1 mm while being illuminated and thus sharp pictures are ensured.

A small disadvantage of this method is that the pictures are distorted. There is time lag of around 1/300 sec. between the illumination of the far left and the far right side of the photo. In this time particles travel 1 to 3 cm.

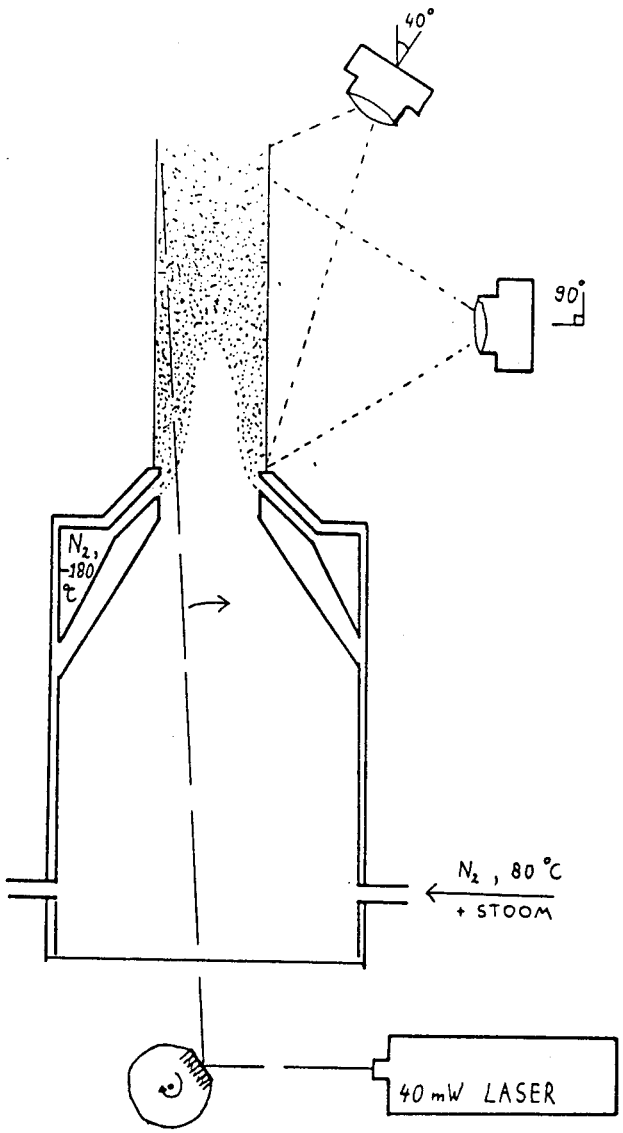

Fig.7.2.1 Set up of the visualisation experiment in the Q.T.U.

Scattering particles

The choice of scattering particles appeared to be very important for the final result. Because only a low intensity laser was available (40 mW) and beacause of the relative high speeds a lot of particles with good scattering efficiency were needed.

The best reults were obtained with condensationdroplets that were formed when the hot flow, to which steam was added (par.6.5), mixed with the cold flow. The result was that the parts where mixing had taken place contained a thick fog. Three examples of pictures thus taken are presented in fig.7.2.2., 7.2.3 and 7.2.4

Fig. 7.2.2.
Visualisation in the Q.T.U.
α=90° and S= 0.6 mm

Remarkable is the quick mixing. After only one diameter no dark hot spots are present anymore.

Fig.7.2.3.
Visualisation in the Q.T.U.
α=90 and S= 4.4 mm

In this picture one can see that the hot flow reaches the wall about 3 diameters above the slit. This penomena could be the reason that the H-type quench sometimes was fouled.

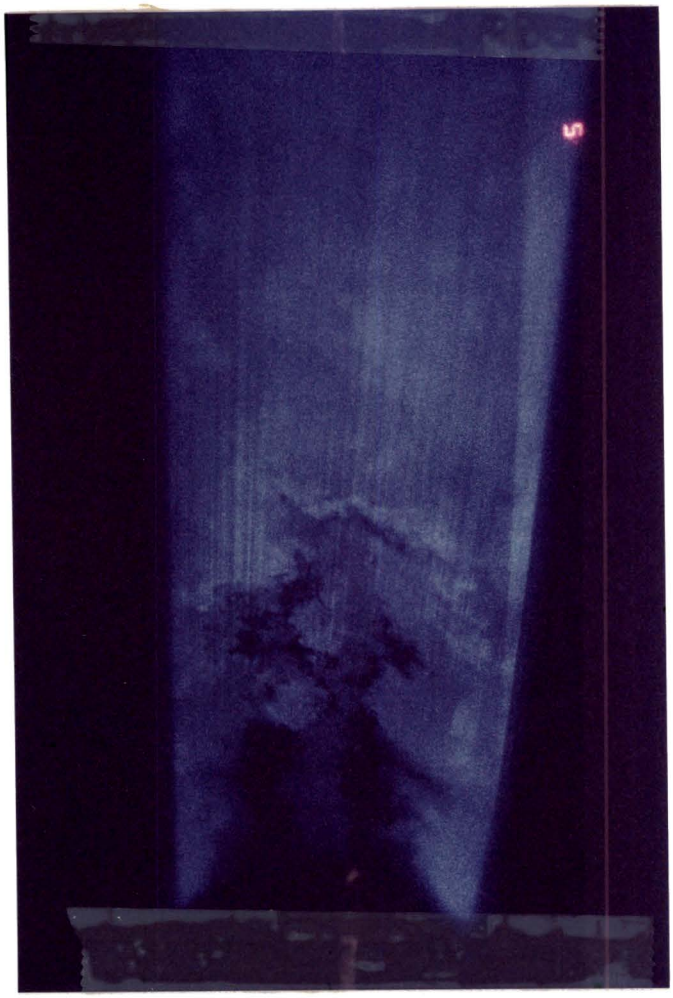

Fig.7.2.4
Visualisation in the Q.T.U.
$\alpha = 90^{o}$ and S $\cong$ 1 mm

In this photograph the cold flow seems to recirculate down the centre of the pipe. This was also observed in some of the slow temperature measurements, see figure 7.5.1.

This visualisation method however needs a lot of extra research before it is really trustworthy. The particle size distribution, the condensationprocess (possibly homogeneous nucleation) and the exact amount of vapor in the hot nitrogen are not well known. Results at the T.H.Eindhoven, with fog created for visualisation, suggest a particle size distribution with a maximum at ca. 3μm. This kind of particles are able to follow details in the quenchflow of 0.5 mm.
The amount of steam added to the hot flow was determined by the quality of visualisation. Too little steam resulted in too low light intensities, too much steam resulted in a too thick fog and in a fouling of the quenchshaft. It may be very interesting to use this iceforming on the quenchshaft and even upstream of the slit as a way to simulate the fouling process in the actual quench. This option however needs a lot of extra considering. It is very well possible that the heat release in the condensation process when using a very high vaporconcentration influences the flow.
Estimation of the amount of steam used during visualisation indicates that de temperature is only raised a few degrees.

When comparing the visualisation results with the temperature measurements no contradictions are observed.

Photography

The biggest problem in recording visualisation results with photography were the extremely low light intensities coming from the 40 mW laser, the only one that was available.
This problem was tackled in three ways:

1) The photographic film used was very sensitive. It appeared that Kodak Ectachrome, illuminated as a 6400 ASA film, gave reasonable results.
2) The most light sensitive lens, that was readily available, was used. The ratio of the focal distance f and the aperture D was: $f/D = 1.4$
3) The camera was positioned in a forward scattering angle of 40° with respect to the direction of the laserbeam, see figure 7.2.1. At this angle the lightintensity, scattered from water droplets of a few micron, is much higher than at 90° looking angle. A disadvantage of this cameraposition is the non-constant distance between lens and subject resulting in diminished resolution.

Conclusion

It can be concluded that it is possible to do flowvisualisation in the Q.T.U. with the help of a laserbeam and condensing steam.
For the moment one has to be careful interpretating thusfar obtained results because of lack of quantitative information of some of the parameters and their influence on the flow and the visualisation process. It can however be concluded that this visualisation technique is a helpful tool in judging quenchperformance and in preselecting ares in the quench that are interesting for further investigation.
Major improvements can be expected when using more defined scattering particles. A more powerful laser would improve the flexibility of parameter choice.

7.3 Slow Temperature Measurements

With a rake (figure 7.3.1) of 10 Chromium-Alumel-Thermocouples (thickness=0.5mm) slow temperature measurements were done in the quenchshaft. The rake was moved to different x-positions (relative to the slit). In this way it was possible to determine the average temperatures in the whole quenchshaft.

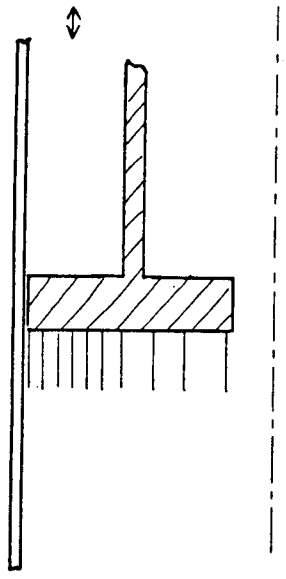

Fig.7.3.1 The thermocouple rake in the quenchshaft

The data were recorded on a Yew recorder. At each position the temperature was recorded about six times in half a minute thus allowing an estimation of the average temperature. After entering (by hand) this data in a computer it is possible to create an isotherm plot. Instead of the temperature the dimensionless parameter φ will be used:

$$\varphi = \frac{T(x,y) - T_{mix}}{T_h - T_{mix}} \qquad (7.3.1)$$

where the mixing temperature T_{mix} is defined as:

$$T_{mix} = \frac{\dot{M}_c T_c + \dot{M}_h T_h}{\dot{M}_c + \dot{M}_h} \qquad (7.3.2)$$

When the hot and the cold massflows are equal the mixingparameter is between -1 and +1. An example of results of this kind of measurements are shown in figure 7.3.2. Shown are the results of $\alpha = 45^o$ S = 3mm quench. The area of concern is shown in the upper picture.

The results are presented in two ways. In the first contourplot of the vertical coordinate is y/R with R the radius of the quench shaft. In the second contourplot the vertical coordinate is the square of y/R. In this plot the areas between the φ-contours are proportional with the volume of the nitrogen that has a φ-value between that of the contours. At the right side the positions of the thermocouples are designated with arrows.

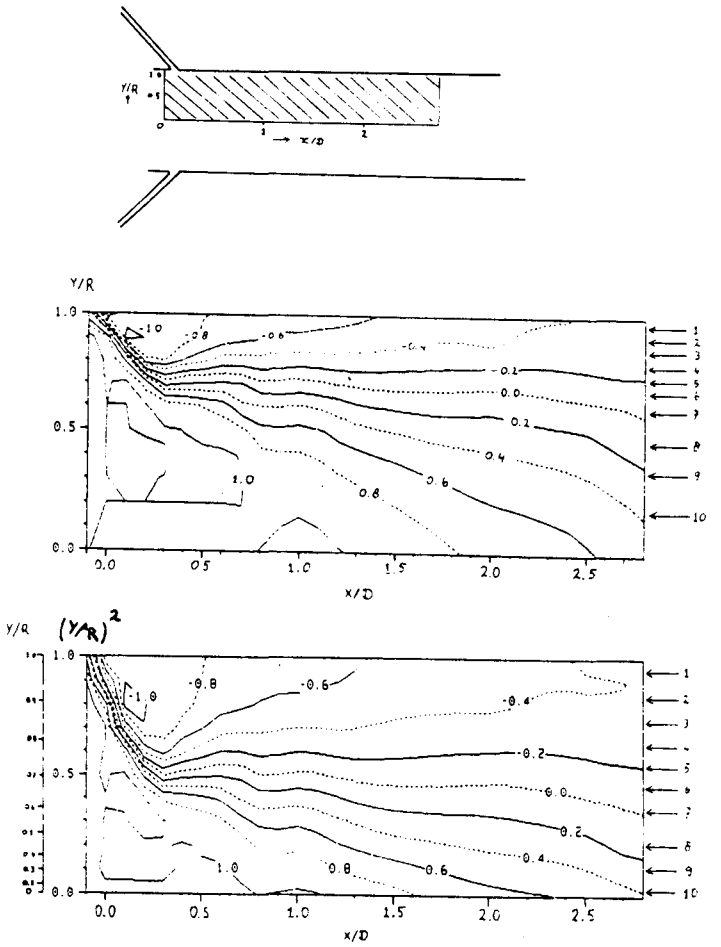

Fig.7.3.2 φ-contour plots of the 45°,3mm quench.
M_h= 45 g/s M_c= 41 g/s T_h= 350 K T_c= 93 K

It was feared that the very high temperature gradients existing in the quench could influence the accuracy of the thermocouples. The all important temperature of the tip of the couple could be influenced by heatconduction through the mantle of the thermocouple. A correction was calculated, based on the Nu-number of the couple, the heatconductivity of its steel mantle and of the surrounding gas. It appeared that the influence of heatconduction through the steel mantle is restricted to a length of about 5 mm. As can be seen in figure 7.3.3 the effect of this correction seems to be minimal and only noticable in the very high gradient areas.

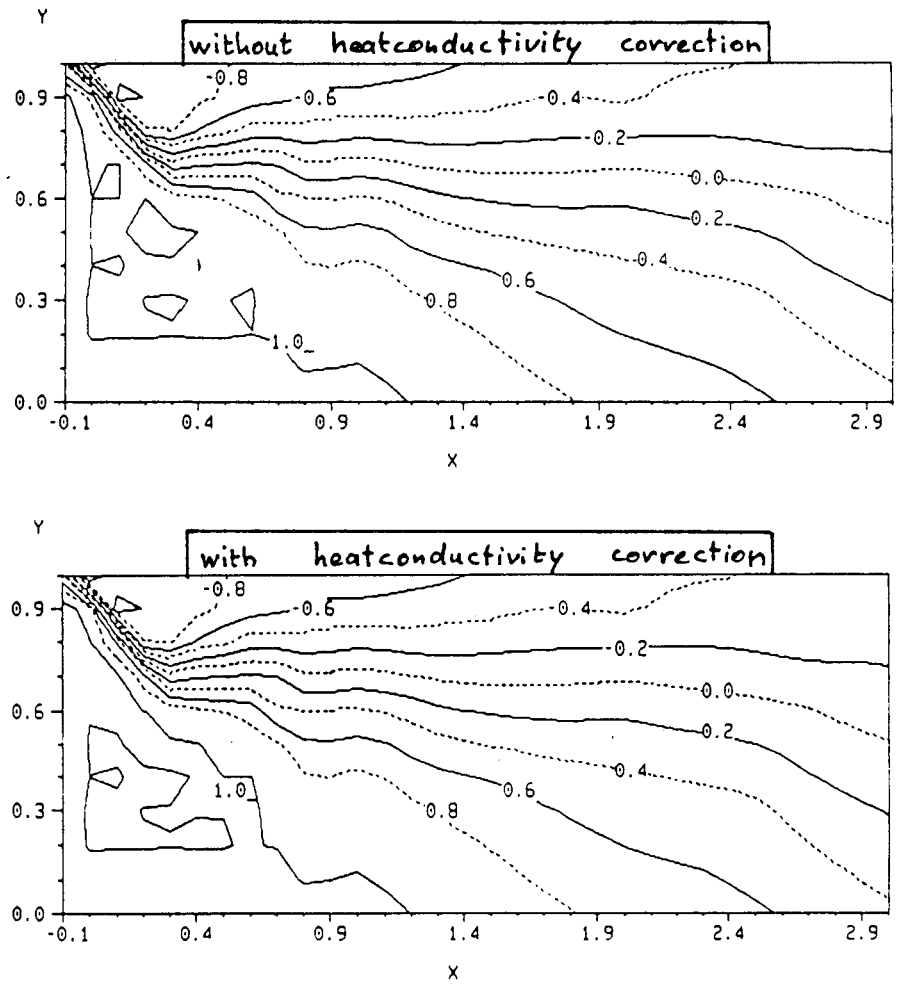

Fig.7.3.3 The effect of a correction for heatconduction through the thermocouple mantle of the slow temperature measurements results. Flowcondition are as in figure 7.3.2

7.4 Fast Temperature Measurements

With the use of constant current anemometry (CCA) it is possible to measure very fast fluctuating temperatures. CCA is based on measuring the resistance of a very thin wire. This wire has a diameter of 1 μm and a length of 1 mm and is fixed to the end of fork shaped probe. The current through the wire is so small that it doesn't influence the temperature of the wire and therefore the wire has the temperature of the surrounding fluid.
According to its supplier (DANTEC) its frequencyresponse starts going down only after 3kHz. Measurements in the quench showed

rising speeds of 100 ^{o}C in 0.1 msec. With the help of a DIFA transiscope (a digital oscilloscope) it was possible to sample the signal and record it on a floppydisk. The samplefrequency used was 12500 Hz and one measurement contained 64k samples. This means a measurement time of ca. 5 seconds. In a later stage these measurements can be analyzed with an HP-9845 computer.
In figure 7.4.1 an example is given of a part of a temperature signal and of a temperature distribution P(T) of the complete 64k samples of this signal.

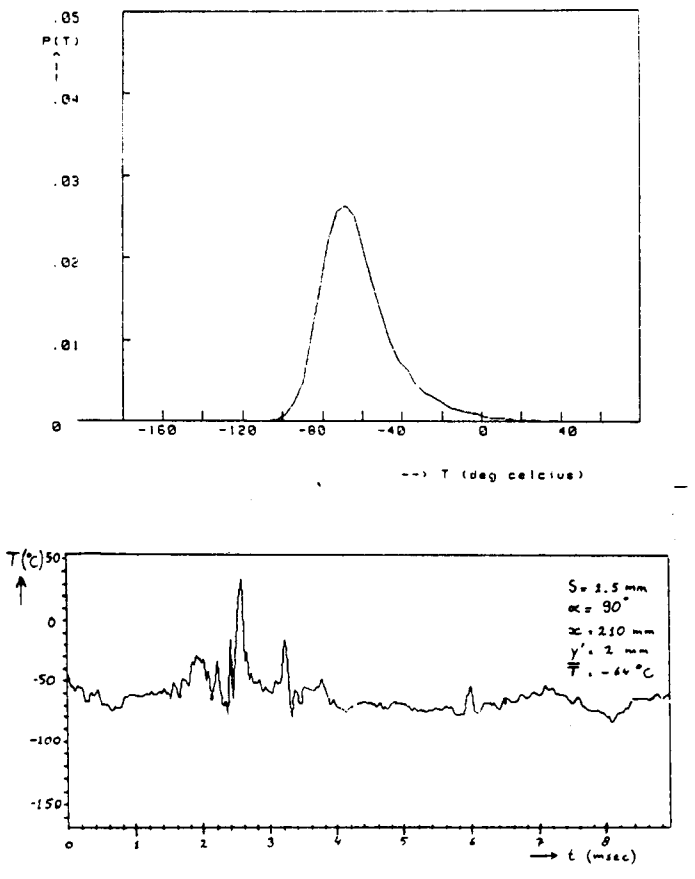

Fig.7.4.1 Fast temperature distribution and signal.

This measurement was taken at 2 mm from the quench shaft wall at a height of 210 mm above the slit. The temperature of the cold flow T_c was ca. -180 ^{o}Cand the temperature of the hot flow was ca. 80 ^{o}C. Remarkable is the high peak in the signal. Its top is more than 100 ^{o}C higher than the average temperature at that position. Its width suggests a gaspocket with a dimension of ca. 1 cm. From the distribution one can see that there is a chance of ca. 2 % that temperatures above 0 ^{o}C reach the shaft wall at this point.
These results coincide very well with some of the visualisation results in which dark spots (hot, no condensation droplets containing fluid pockets) seem to reach the quench shaftwall.
The temperature signal of figure 7.4.2 is taken at 25 mm from the

quenchshaft wall and ca. 50 mm above the slit. The position appears to be in the border of the cold jet. The intermittent structure of the signal very strongly suggest that at this position coherent structures determine the flow. Another indication for coherent structures is the fact that near -120 ^{o}C the distribution has a maximum. This suggests a bimodal distribution, which is typical for coherent structures.

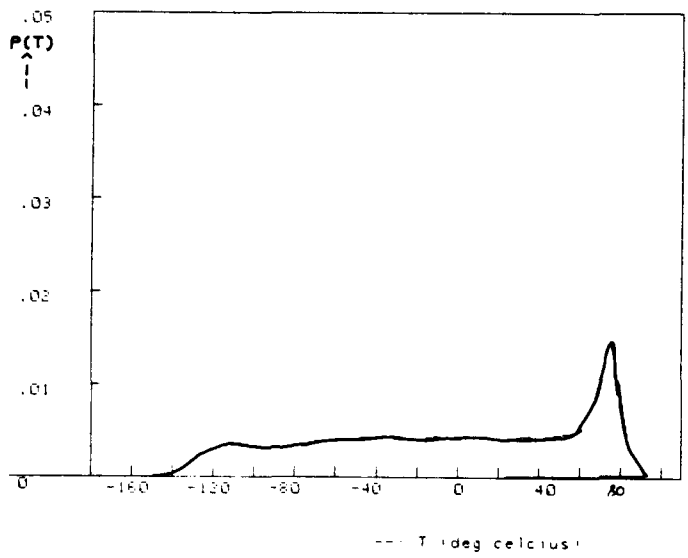

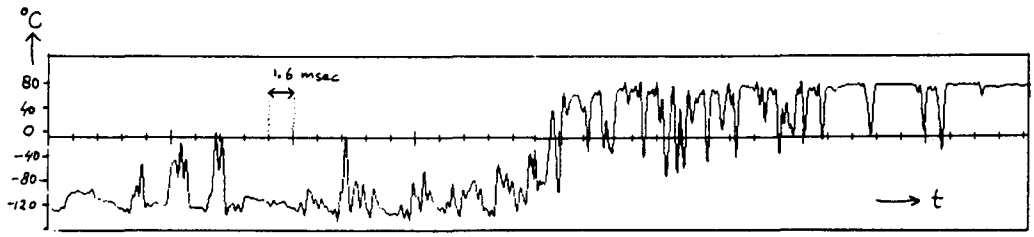

Fig.7.4.2 Fast temperature distribution and signal

7.5 A comparison with the results from a K-ε Model

As was mentioned in paragraph 2.1 one of the modern models for turbulence is the so-called K-ε model. This model is based on a decomposition of every turbulent quantity (velocity, temperature, etc.) in its average and its fluctuating part. Then transport

equation are formulated for all these parts. By making certain suppositions concerning turbulent energy (K) and dissipation (ε) these eqation (partial differential equations) can be solved numerically.
A commercially available K-ε program is known by the name of FLUENT. Without giving further details or comment about FLUENT a comparison is here presented of an average mixing parameter contour plot produced by FLUENT and one based on Q.T.U. experiments.

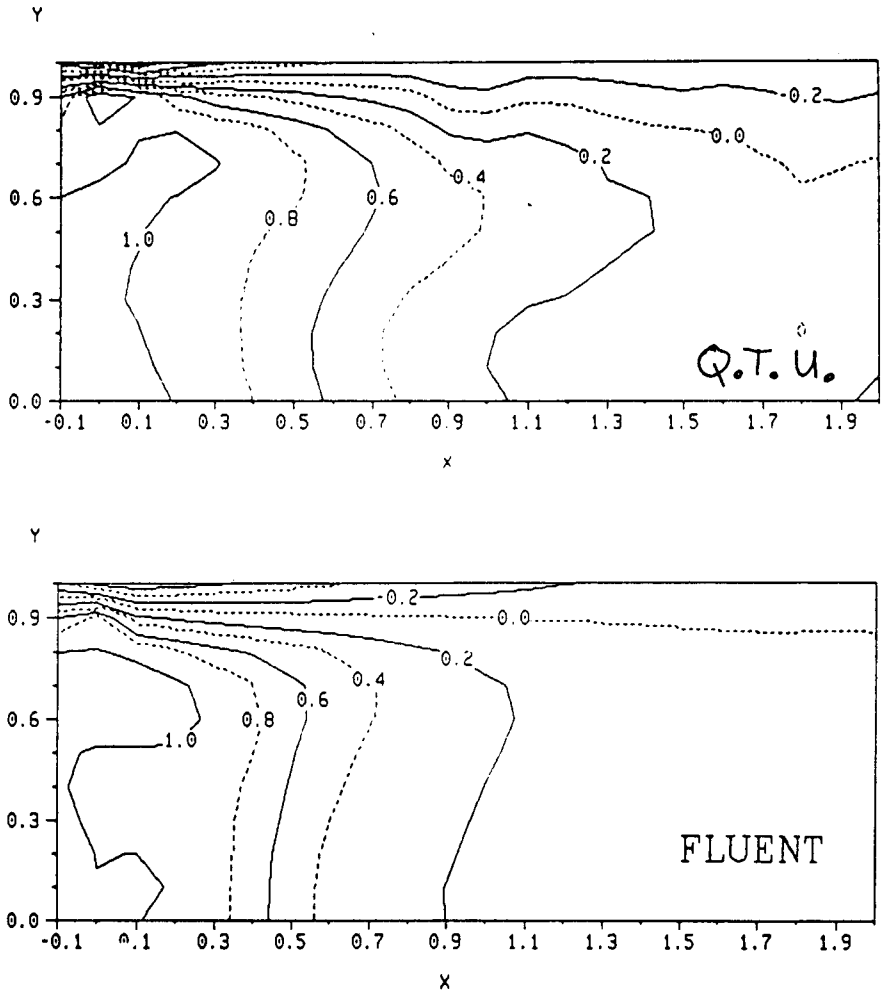

Fig.7.5.1 φ-contour plots. α=30° and S=0.9 mm.

These results concern a quench with a slitwidth S of 0.9 mm and a flowangle α of 30°. The massflows and the hot and cold temperatures are a little different from most other examples: M_c = 0.041 kg/s $\dot{M}_h$ = 0.045kg/s T_c = -165 °C and T_h = 20 °C.
The experimental result shows that the cold flow acts as a wall jet till ca. 1.5 D above the slit and then it recirculates down the center of the quenchshaft. This behavior of the cold flow is also predicted by the K-ε model.
It therefore seems possible that a K-ε model is able to predict

average temperature fields of the A-type quench. Thus it can help selecting the right experiments. The fast temperature results and the temperature distribution presented in par.7.4 can never be predicted by a K- ε model because the distribution of the fluctuating quantities has to be specified in the input of the K-ε model. The results from the fast temperature measurements suggest that coherent structures are an important factor of the flow. Only a model with sufficient temperal resolution can reveal such structures. Examples of such models are 'large eddy simulation' and the 'vortexmethod'.

PART C CONCLUSION

In part A of this thesis a description of the experimental plane mixing layer was given. The conclusion was that the initial region of the mixing layer is strongly dominated by the Kelvin-Helmholtz instability, which in this case is a large scale two dimensional inviscid effect. In a later stadium of the mixing layer, probably because of small scale three dimensional turbulence, large scale three dimensional effects (e.g.streamwise Taylorvortices) start to play an important role.
This conclusion has consequences for the ability of the two-dimensional vortexmethod to model the mixing layer. It became clear that the two dimensional vortexmethod is a very good method to describe flows that are dominated by large scale two dimensional "coherent structures". Its advantages above other methods lay in its close mimicry of physical phenomena in the flow, its adaptivity and its lack of numerical viscosity. Even for flows, where small-scale three dimensional turbulence has some importance the two dimensional vortexmethod (with some modifications) can be applied. The above mentioned condition for the applicability of the two dimensional vortexmethod are satisfied by the first part of the mixing layer (region 1 and 2 of figure 2.3.1) This means that only the first say 10 to 20 slit diameters of the A-type quench mixing layer can be modelled by a two dimensional mixing layer. (neglecting the possible distorting effects of the fact that two mixing layers originate in the slit) After this distance three dimensional effects probably have a so great importance that this cannot be incorporated in a two dimensional vortexmethod.
In the experimental part B this thesis showed that it is possible to simulate large density difference in flows experimentally with the use of heated (100 ^{o}C) and cooled (-190 ^{o}C) nitrogen. In fact all experimental techniques used in this work made use of this temperature difference. With the visualisation studies and the slow temperature measurements it was possible to study the time-averaged mixing process. The fast temperature measurements and also the visualisation results can be used to judge time dependent properties of the quench. From the preliminary results it can be concluded that stationary models (K-ϵ method) and other methods that imply Gaussian probability distribution for the fluctuating quantities are not able to predict the aerodynamic properties that are important to the fouling of the quench (probability of a hot particle to reach the quench shaft). Models that could be able to

predict these properties must be timedependent.
Examples are:
- The large eddy simulation.
- The three dimensional vortexmethod

So we end where we started: with the vortexmethod.

LITERATURE

Literature belonging to chapter 2

1) **Michalke, A** 1965 On spatially growing disturbances in an inviscid shear layer. J.Fluid Mech. 23, 521

2) **Bradshaw, P.** 1966 The effect of initial conditions on the development of a free shear layer J.Fluid Mech 26, 225

3) **Brown, G.L. & Roshko, A** 1974 On density effects and large structure in turbulent mixing layers. J.Fluid Mech. 64, 775

4) **Winant, C.D. & Browand, F.K.** 1974 Vortex pairing: the mechanism of turbulent mixing-layer growth at moderate Reynolds numbers. J.Fluid Mech. 63, 237

5) **Hinze, J.O.** 1975 Turbulence. McGraw-Hill,Inc. New-York

6) **Browand, F.K. & Weidman, P.D.** 1976 Large scales in the developing mixing layer. J.Fluid Mech. 76, 127

7) **Chandrsuda, C. & Mehta, R.D. & Weir, A.D. & Bradshaw, P.** 1978 Effect of free-stream turbulence on large structure in turbulent mixing layers. J.Fluid Mech. 85, 693

8) **Wygnanski, D.O. & Oster, D. & Fiedler, H. & Dziomba, B.** 1979 On the perseverance of a quasi-two-dimensional eddy-structure in a turbulent mixing layer J.Fluid Mech. 93, 325

9) **Roshko, A.** 1980 The plane mixing layer, flow visualisation results and three-dimensional effects. In "The role of coherent structures in modelling turbulence and mixing" (ed.J.Jimenez.) Lecture Notes in Physics, vol.136, pp.208, Springer.

10) **Fiedler, H.E. & Dziomba, B. & Mensing, P. & Rosgen, T.** 1980 Strategies in turbulence experiments and modelling. In "The role coherent structures in modelling turbulence and mixing". (ed.J.Jimenez.) Lecture Notes in Physics, vol.136, pp.2??, Springer.

11) **Breidenthal, R.E.** 1981 Structure in turbulent mixing layers and wakes using a chemical reaction. J.Fluid Mech. 116, 1

12) **Hernan, M.A. & Jimenez, J.** 1982 Computer analysis of a high-speed film of the plane turbulent mixing layer. J.Fluid Mech. 119, 323.

13) **Jimenez, J & Cogollos, M & Bernal, L.P.** 1985 A perspective view of the plane mixing layer J.Fluid Mech. 152, 125

14) **Fiedler, H.E. & Mensing, P.** 1985 The plane turbulent shear layer with periodic exitation. J.Fluid Mech. 150, 281

15) **Dziomba, B. & Fiedler, H.E.** 1985 Effect of initial conditions on two-dimensional free shear layers. J.Fluid Mech. 152, 419

Literature belonging to chapter 3

16) **Batchelor, G.K.** 1967 An introduction to Fluid Dynamics Cambridge University Press

Literature belonging to chapter 4

17) **Rosenhead, L.** 1932 The formation of vortices from a surface of discontinuity. Proc.Roy.Soc.Lond. A 134, 170

18) **Hama, F.R. & Burke, E.R.** 1960 On the rolling up of a vortexsheet. Technical note BN-220, AFOSRTN 60-1069, university of Maryland

19) **van de VOOREN, A.T.** 1965 A numerical investigation of the rolling-up of vortexsheets, Rep. TW-21, Dept. of Math., Groningen University, Netherlands

20) **Chorin, A.J. & Bernard, P.S.** 1973 Discretization of a vortexsheet with an example of roll-up. J. of Comp. Physics 13, 423

21) **Clements, R.R.** 1973 An inviscid model of two dimensional vortex shedding. J.Fluid Mech.57, part 2, 321

22) **Damms, S.M. & Kuchemann, D.** 1974 On a vortexsheet model for mixing between two parallel streams. 1. Description of model and experimental evidence. Proc.Roy.Soc.Lond. a339, 451

23) **Fink, P.T. & Soh, W.K.** 1974 Calculation of vortexsheets in unsteady flow and applications in ship hydrodynamics. Proc. of the 10th symp.of Naval Hydrodynamics, 463

24) **Moore, D.W.** 1975 The rolling-up of a semi-infinite vortexsheet Proc.Roy.Soc.Lond. A345, 417

25) **Clements, R.R. & Maull, D.J.** 1975 The representation of sheets of vorticity by discrete vortices. Prog.Aerospace Sci., 16, no.2, 129

26) **Acton, E.** 1976 The modelling of large eddies in a two dimensional shear layer. J.Fluid Mech. 76, part 3, 561

27) **Zalosh, R.G.** 1976 Discretized simulation of vortexsheet evolution with buoyancy and surface tension effects. A.I.A.A. journal, 14, no.11, 1517

28) **Kiya, M. & Aie, M.** 1977 An inviscid numerical simulation of vortex shedding from an inclined plate in shear flow. J.Fluid Mech. 82, part 2, 241

29) **Milanazzo, F. & Saffman, P.G.** 1977 The calculation of large Reynolds number two dimensional flow using discrete vortices with random walk. J.of Comp.Physics 23, 380

30) **Maskew, B.** 1977 Subvortex technique for the close approach to a discretized vortexsheet. J.Aircraft 14, no.2, 188

31) **Ashurst, W.T.** 1977 Numerical simulation of turbulent mixing layers via vortexdynamics. Sand 77-86.13

32) **Graham, J.M.R.** 1977 Vortexshedding from sharp edges. I.C.Aero report 77-06

33) **Hald, O & Del Prete, V.M.** 1978 Convergence of vortexmethods for Euler's equations. Math.of Computation 32, no.143, 791

34) **Moore, D.W.** 1978 The Equation of Motion of a Vortex Layer of Small Thickness. Studies in Appl. Math. 58, 119

35) **Callegari, A.J. & Ting, L.** 1978 Motion of curved vortex filament with decaying vortical core and axial velocity. Siam J.Appl.Math. 35, no. 1, 148

36) **Pullin, D.I.** 1978 The large scale structure of unsteady self-similar rolled up vortexsheets. J.Fluid Mech. 88, part 3, 401

37) **Moore, D.W.** 1978 Vortex Dynamics Sci.Prog.Oxf. 65, 295

38) **Chorin, A.J.** 1978 A comment on the paper: "The calculation of large Reynolds number flow using discrete vortices with random walk" by Milinazzo & Saffman.
Saffman, P.G. Reply to comment.
J. of Comp.Physics 26, 453

39) **Kamemoto, K. & Bearman, P.W.** 1978 The importance of the time-step size and the initial vortexposition in modelling flows with discrete vortices. I.C. Aero Tech. Note 78-108

40) **Fink, P.T. & Soh, W.H.** 1978 A new approach to roll-up calculations of vortexsheets. Proc.Roy.Soc.Lond. A362, 195

41) **Disselhorst, J.H.M.** 1978 Acoustic resonance in open tubes Phd - thesis , Technical university Twente, Netherlands

42) **Baker, G.R.** 1979 The "Cloud in Cell" technique applied to the roll-up of vortexsheets. J.of Comp.Physics 32, 76

43) **Moore, D.W.** 1979 The spontaneous appearance of a singularity in the shape of an evolving vortexsheet. Proc.Roy.Soc.Lond. A 365, 105

44) **Saffman, P.G. & Baker, G.R.** 1979 Vortex interactions. In: Ann.Rev.Fluid.Mech. 1979, 11, 95

45) **Ferziger, J.H.** 1980 Energetics of vortex roll-up and pairing. Phys.Fluids 23, 1

46) **Acton, E.** 1980 A modelling of large eddies in axisymmetric jet. J.of Fluid Mech. 98, part 1, 1

47) **Bearman, P.W. & Graham, J.M.R.** 1980 Vortex shedding from bluff bodies in oscillatory flow: A report on Euromech.119 J.Fluid Mech. 99, part 2, 225

48) **Baker, G.R.** 1980 A test of the method of Fink & Soh for following vortexsheet motion. J.Fluid Mech. 100. part 1, 200

49) **Chorin, A.J.** 1980 Vortex models and boundary layer instability. Siam J.Sci.Stat.Comput. 1, no.1, 1

50) **Ashurst, W.T. & Durst, F. & Tropea, C.** 1980 Experiment and discrete vortex dynamics simulation. AGARD, conf.proc. 29. "Computation of viscous-inviscid interactions".

51) **Leonard, A** 1980 Vortex methods for flow simulation. J.of Comp. Physics 37, 289

52) **Schwartz, L.W.** 1981 A semi-analytic approach to the self-induced motion of vortex sheets. J.Fluid Mech. 111, 475

53) **Kida, S.P** 1981 A vortex filament moving without change of form. J.Fluid Mech. 112, 397

54) **Moore, D.W.** 1981 On the point vortex method. Siam.J.Sci.Stat.Comput. 2, no.1, 65

55) **Stansby, P.K.** 1981 A numerical study of vortexshedding from one and two circular cylinders. Aero.Q.

56) **Laan, D.J.** 1981 Vortex-simulatie van stromingen. Thesis Technical University Delft, Netherlands

57) **Majda, A.J. & Beale, J.T.** 1982 The design and numerical analysis of vortexmethods. Transonic, shock and multidimensional flows: advances in scientific computation

58) **Beale, J.T. & Majda, A.** 1982 Vortex methods. 1: Convergence in three dimensions. Math. of Comput. 39, no. 159, 1

59) **Beale, J.T. & Majda, A.** 1982 Vortex methods. 2: Higher order accuracy in two and three dimensions. Math. of Comput. 39, no. 159, 29

60) **Hoeijmakers, H.W.M. & Vaatstra, W.** 1981 A higher order panel method applied to vortex sheet roll-up. NLR MP 81059 U Also in 1982: A.I.A.A. journal 21, no. 4, 516

61) **Nakamura, Y & Leonard, A. & Spalart, P.** 1982 Vortex simulation of an inviscid shear layer. A.I.A.A.-82-0948.

62) **Shirahata, H. & Daiguji, H.** 1982 An analysis of unsteady diagonal cascade flow using a discrete vortex method. Bulletin of the J.S.M.E. 25, no. 201, 334

63) **Nagano, S. & Naito, M. & Takata, H.** 1982 A numerical analysis of two dimensional flow past a rectangular prism by a discrete vortex model. Computers & Fluids 10, no. 4, 243

64) **Meiron, D.I. & Baker, G.R. & Orszag, S.A.** 1982 Analytic structure of vortex sheet dynamics. Part 1: Kelvin Helmholtz instability. J.Fluid Mech. 114, 283

65) **Robinson, A.C. & Saffman, P.G.** 1982 Three dimensional stability of vortex arrays. J.Fluid Mech. 125, 411

66) **Bromilov, I.G. & Clements, R.R.** 1982 Some techniques for extending the application of the discrete vortexmethod for flow simulation. Aero.Q. 33, 73

67) **Chorin, A.J.** 1982 The evolution of a turbulent vortex. Commun. Math. Phys. 83, 517

68) **Zhen Huan Teng** 1982 Elliptic Vortexmethod for incompressible flow at high Reynolds number. J.of Comp. Phys. 46, 54

69) **Bromilov, I.G. & Clements, R.R.** 1983 A discrete vortex simulation of Kelvin Helmholtz instability. A.I.A.A. journal 21, no. 9, 1345

70) **Inamuro, T. & Adachi, T. & Sakata, H.** 1983 A numerical analysis of unsteady separated flow by a vortex shedding model. Bulletin of JSME 26, no. 222, 2106

71) **Cheer, A.Y.** 1983 Numerical study of incompressible slightly viscous flow past blunt bodies and aerofoils. Siam. J.Sci.Stat.Comput. 4, no. 4, 685

72) **Bromilov, I.G. & Clements, R.R.** 1984 A numerical study of vortex interaction. J.Fluid Mech. 146, 331

73) **Meiron, D.I. & Saffman, P.G. & Schatzman, J.C.** 1984 The linear two dimensional stability of finite cored vortices. J.Fluid Mech. 147, 187

74) **Melander, M.V. & Styczek, A.S. & Zabusky, N.J.** 1984 Elliptically desingularized vortex model for the two-dimensional Euler equations. Physical Review Letters 53, no. 13, 1222,

75) **Higdon, J.J.L. & Pozrikidis, C.** 1985 The self-induced motion of vortexsheets. J.Fluid Mech. 150, 203

76) **Pozrikidis, C. & Higdon, J.J.L.** 1985 Non-linear Kelvin-Helmholtz instability of a finite vortex layer. J.Fluid Mech. 157, 225

77) **Bromilov, I.G.** 1982 Discrete vortex methods applied to flows fundamental to a jet engine. Phd - thesis Dept. of Engineering Mathematics, University of Bristol

78) **Christiansen, J.P.** 1973 Numerical simulation of hydrodynamics by the method of point vortices. J.of Comp.Physics 13,363

79) **Chorin, A.J.** 1973 Numerical study of slightly viscous flow J.Fluid Mech. 57, 785

Literature belonging to chapter 6

80) **Hinze, J.O.** 1955 Fundamentals of the Hydrodynamic Mechanism of Splitting in Dispersion Processes. A.I.Ch.E. Journal, Vol.1, no.3, 289

81) **Ferment, J** 1984 Afstudeerverslag H.T.S. Alkmaar no. 5-E-84

82) **Beek, W.J. & Muttzall, K.M.K.** 1975 Transport Phenomena, John Wiley & Sons Ltd.

83) **Frossling, N.** 1938 Gerlands Beitr. Geophys., 52, 170

84) **Sjenitzer, F.** 1962, The evaporation of a liquid spray injected in a stream of gas. Chemical Engineering Science, Vol.17, 309

85) **Ricou, F.P. & Spalding, D.B.** 1960 Measurements of entrainment by axisymmetrical turbulent jets. J.Fluid Mech. 57, 785

APPENDIX 1

Transformation Induced Velocity

The following relations exist between points in the ζ-plane and the z-plane:

$$z = z(\zeta) \qquad z_i = z(\zeta_i) \qquad 1.$$

$$\zeta = \zeta(z) \qquad \zeta_i = \zeta(z_i) \qquad 2.$$

The complex conjugate of the velocity induced on vortex i in the z-plane is given by:

$$\left(\frac{dz_i}{dt}\right)^* = \lim_{z \to z_i} \left\{ \frac{dw}{dz} + \frac{i\Gamma_i}{2\pi} \cdot \frac{1}{(z - z_i)} \right\} \qquad 3.$$

The goal of this excercise is to write this velocity as a function of the complex velocity potential and the vortexposition i in the ζ-plane. We therefore multiply equation 3. with $d\zeta/dz$ and add and subtract the following term: $(i\Gamma_i/2\pi) \cdot (1/(\zeta - \zeta_i))$
The result is:

$$\left(\frac{dz_i}{dt}\right)^* = \lim_{z \to z_i} \left\{ \frac{d\zeta}{dz} \cdot \left(\frac{dw}{d\zeta} + \frac{i\Gamma_i}{2\pi} \frac{1}{(\zeta - \zeta_i)} + \frac{i\Gamma_i}{2\pi} \cdot \left(\frac{1}{(z - z_i)} \frac{dz}{d\zeta} - \frac{1}{(\zeta - \zeta_i)} \right) \right) \right\} \qquad 4.$$

In order to rewrite this equation we need the Taylor expansions of z_i and ζ_i and two relations that follow from these expansions:

$$z_i = z + (\zeta_i - \zeta) \left.\frac{dz}{d\zeta}\right|_\zeta + \frac{1}{2}(\zeta_i - \zeta)^2 \left.\frac{d^2z}{d\zeta^2}\right|_\zeta + O(\zeta - \zeta_i)^3 \qquad 5.$$

$$\left.\frac{dz}{d\zeta}\right|_\zeta = \left(\frac{z - z_i}{\zeta - \zeta_i}\right) + \frac{1}{2}(\zeta - \zeta_i) \frac{d^2z}{d\zeta^2} + O(\zeta - \zeta_i)^2 \qquad 6.$$

$$\zeta_i = \zeta + (z_i - z) \left.\frac{d\zeta}{dz}\right|_z + O(z_i - z)^2 \qquad 7.$$

$$\left(\frac{\zeta - \zeta_i}{z - z_i}\right) = \left.\frac{d\zeta}{dz}\right|_z - O(z - z_i) \qquad 8.$$

When equations 6. and 7. are substituted in 4. we find:

$$\left(\frac{dz_i}{dt}\right)^* = \lim_{z \to z_i} \left\{ \frac{d\zeta}{dz} \cdot \left(\frac{dw}{d\zeta} + \frac{i\Gamma_i}{2\pi} \cdot \frac{1}{(\zeta - \zeta_i)} + \frac{i\Gamma_i}{2\pi} \cdot \frac{1}{2} \cdot \left(\frac{d\zeta}{dz} - \frac{1}{2}(z - z_i) \frac{d^2\zeta}{dz^2} \right) \frac{d^2z}{d\zeta^2} \right) \right\} \qquad 9.$$

Because of the limit $z \to z_i$ the term $\frac{1}{2}(z - z_i)\, d^2\zeta/dz^2$ is zero and we finally find the wanted relation for dz_i/dt :

$$\left(\frac{dz_i}{dt}\right)^* = \lim_{z \to z_i} \left\{ \frac{d\zeta}{dz} \left(\frac{dw}{d\zeta} + \frac{i\Gamma_i}{2\pi} \cdot \frac{1}{(\zeta - \zeta_i)} \right) + \frac{i\Gamma_i}{4\pi} \cdot \left(\frac{d\zeta}{dz} \right)^2 \cdot \left(\frac{d^2z}{d\zeta^2} \right) \right\} \qquad 10.$$

APPENDIX 2

Shedding from wedges

A vortexsegment with length S_z is being shed from a wedge in the z-plane.

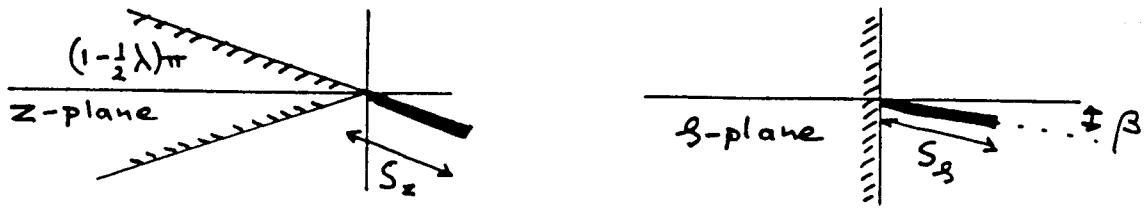

The relation between the z-plane and the ζ-plane is given by:

$$z = \zeta^{\lambda} \qquad 1.$$

When a constant vorticitydistriburion γ is supposed the cumulative vortici starting at the wedgepoint (origin of z-plane) is given by:

$$\Gamma_{cum} = \gamma \cdot |z_{seg}| = \gamma \cdot |\zeta_{seg}|^{\lambda} = \gamma \cdot \zeta_{seg}^{\lambda} \cdot e^{i\lambda\beta} \qquad 2.$$

with z_{seg} : z-coordinate of the segment in the z-plane
ζ_{seg} : ζ-coordinate of the segment in the ζ-plane
$\beta = \pi/\lambda - \pi/2$

Taking the derivative of equation 2. gives:

$$d\Gamma_{cum} = \lambda\gamma \cdot e^{i\beta\lambda} \cdot \zeta_{seg}^{\lambda-1} \, d\zeta_{seg} \qquad 3.$$

The complex velocitypotential $\frac{dw}{d\zeta}\Big|_0$ caused by the vortex segment in the origin of the ζ-plane is given by:

$$\left.\frac{dw}{d\zeta}\right|_{\zeta=0} = \frac{i\lambda\gamma}{2\pi} e^{i\lambda\beta} \int_0^{S_\zeta e^{-\beta i}} \zeta_{seg}^{\lambda-2} \, d\zeta_{seg} \qquad 4.$$

and thus:

$$u - iv = \frac{i\lambda\gamma}{2\pi(\lambda-1)} \cdot S_\zeta^{\lambda-1} \cdot e^{i\beta} \qquad 5.$$

When the mirror vortex segment is also taken into account the velocity v, produced by these two segments , is:

$$V = \frac{-\lambda\gamma}{\pi(\lambda-1)} \cdot \cos\beta \cdot S_\zeta^{\lambda-1} \qquad 6.$$

With $S_\zeta = S_z^{1/\lambda}$ this becomes:

$$V = \frac{-\lambda\gamma\cos\beta}{\pi(\lambda-1)} \cdot S_z^{1-1/\lambda} \cdot \qquad 7.$$

APPENDIX 3

In this appendix it will be shown that there are only two possibilities for the position of a vortexsheet near a sharp edge.

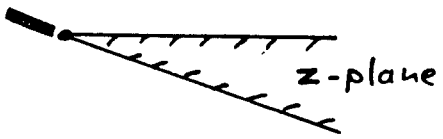

As can be seen in appendix 2 the Shwartz-Christoffel transformation from a wedge to a plate is given by:

$$z = \zeta^{\lambda} \qquad 1.$$

$$\frac{dz}{d\zeta} = \zeta^{\lambda-1} \qquad 2.$$

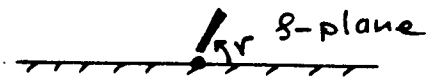

In this appendix the aim is to show that a sheet, shedded from this wedge, has to leave one of the sides of the wedge tangentially.
One assumption is made: The speed of the fluid next to the sheet is directed along the sheet.
In the ζ -plane we define a point P given by: $P: \zeta_p = R \cdot e^{i\alpha}$

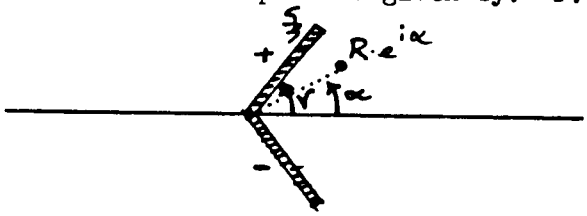

The complex velocity potential in point P is given by:

$$\left.\frac{dw}{d\zeta}\right|_{\zeta=Re^{i\alpha}} = \frac{1}{2\pi i}\left\{ \int_0^{S_\zeta} \frac{d\Gamma^+}{\zeta_{sh}^+ - Re^{i\alpha}} + \int_0^{S_\zeta} \frac{d\Gamma^-}{\zeta_{sh}^- - Re^{i\alpha}} \right\} \qquad 3.$$

With a constant vorticitydistribution along the sheet in the z-plane (γ) we find for the ζ -plane (see appendix 2 equation 2.3.):

$$\frac{d\Gamma^+}{ds} = \lambda\gamma \cdot s^n \;, \quad \frac{d\Gamma^-}{ds} = -\lambda\gamma s^n \;, \quad n = \lambda - 1 \qquad 4.$$

with: $s = |\zeta_{sh}|$ and $\zeta_{sh}^+ = s \cdot e^{i\gamma}$ and $\zeta_{sh}^- = s \cdot e^{-i\gamma}$
Substituting 4. in 3. gives:

$$\left.\frac{dw}{d\zeta}\right|_{\zeta=Re^{i\alpha}} = \frac{\lambda}{2\pi i}\left\{ e^{-i\gamma}\int_0^{S_\zeta} \frac{\gamma s^n ds}{s - Re^{i(\alpha-\gamma)}} - e^{i\gamma}\int_0^{S_\zeta} \frac{\gamma s^n ds}{s - Re^{i(\alpha+\gamma)}} \right\} \qquad 5.$$

Define the integral I_1 as:

$$I_1 \equiv \int_0^{S_\zeta} \frac{s^n}{s - Re^{i\theta}} \quad \text{with} \quad \theta = \begin{matrix} \alpha - \gamma \\ \alpha + \gamma \end{matrix} \qquad 6.$$

$$= \int_0^{S_\zeta} s^{n-1} ds + Re^{i\theta}\int_0^{S_\zeta} \frac{s^{n-1}}{s - Re^{i\theta}} ds \qquad 7.$$

$$= \frac{1}{n} S_\zeta^n + Re^{i\theta}\int_0^{\infty} \frac{s^{n-1}}{s - Re^{i\theta}} ds - \qquad 8.$$

$$Re^{i\theta}\int_B^{\infty} \frac{s^{n-1}}{s - Re^{i\theta}} ds \qquad 9.$$

Define the integral I_2 as:

$$I_2 \equiv \int_0^{\infty} \frac{s^{n-1}}{s - Re^{i\theta}} ds \qquad 10.$$

A3

Define the function g(z):

$$g(z) = \frac{z^{n-1}}{z - Re^{i\theta}} \qquad 11.$$

When g(z) is integrated along the real axis from zero to infinity we find I_2. The curve 1.2.3.4.5. is defined in the figure below. The integral of g(z) around this curve is zero, no singularities are enclosed.
When the wedge has a sharp angle ($n < 1$) and path 2. lies at infinity then the integral of g(z) along path 2. is zero.

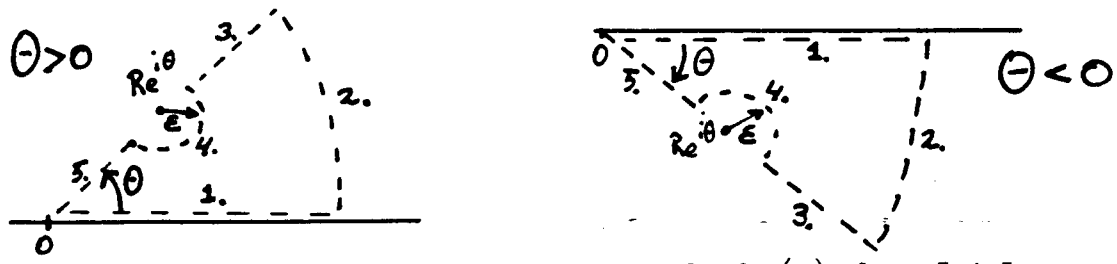

This implies that I_2 is equal to the integral of g(z) along 5.4.3.:
Write z as:

$$z = \tau R e^{i\theta} \qquad 12.$$

Then:

$$I_2 = R^{n-1} e^{i(n-1)\theta} \cdot \overset{(5.4.3)}{\int_0^\infty} \frac{\tau^{n-1} d\tau}{\tau - 1} \qquad 13.$$

When $\varepsilon \to 0$ this integral can be split into the principal value integral and the integral along path 4.:

$$I_2 = R^{n-1} e^{i(n-1)\theta} \cdot \left\{ \overset{(5.3.)}{\int_0^\infty} \frac{\tau^{n-1}}{\tau - 1} d\tau + \overset{4.}{\int} \frac{\tau^{n-1} d\tau}{\tau - 1} \right\} \qquad 14.$$

The integral along path 4. is: $+i\pi$ when $\theta > 0$
$-i\pi$ when $\theta < 0$ 15.

The integral along path 5.-3. has as a solution:

$$\int_0^\infty \frac{\tau^{n-1}}{\tau - 1} d\tau = \pi / \tan((1-n)\pi) \qquad 16.$$

The conclusion is the solution for I_2

$$I_2 = R^{n-1} \cdot e^{i(n-1)\theta} \cdot \left\{ \frac{\pi}{\tan((1-n)\pi)} + \text{sign}(\theta) \cdot \pi i \right\} \qquad 17.$$

When this solution is substituted in the equation for dw/dg (8.) we find:

$$\left.\frac{dw}{dg}\right|_{g=Re^{i\alpha}} = \frac{-\lambda\gamma \sin(\nu)}{n} s_g^n +$$

$$\lambda\gamma R^n \left[e^{-i\nu + i(\alpha-\nu)n} \left(\frac{\pi}{\tan((1-n)\pi)} + \text{sign}(\alpha-\nu)\pi i \right) - e^{i\nu + i(\alpha+\nu)n} \left(\frac{\pi}{\tan((1-n)\pi)} + \text{sign}(\alpha+\nu)\pi i \right) \right] -$$

$$\lambda\gamma R \left[e^{i(\alpha-2\nu)} \int_{s_g}^\infty \frac{s^{n-1} ds}{s - Re^{i(\alpha-\nu)}} - e^{i(\alpha+2\nu)} \int_{s_g}^\infty \frac{s^{n-1} ds}{s - Re^{i(\nu+\alpha)}} \right] \qquad 18.$$

A3

$dw/d\zeta$ is evaluated at $\zeta_{R^-} = R\,e^{ir^-}$ with $r^- = r - \delta$, $\delta \to 0$:

$$\left.\frac{dw}{d\zeta}\right|_{R^-} = \lambda\gamma\left\{\frac{-\sin r}{\pi n}\,\zeta_s^n + R^n e^{irn}\left[\frac{-\sin((n+1)r)}{\tan((1-n)\pi)} - \cos((n+1)r)\right]\right. \qquad 19.$$

$$\left. - R\left[e^{i(-r)}\int_{s_\zeta}^{\infty}\frac{s^{n-1}\,ds}{(s-R)} - e^{i3r}\int_{s_\zeta}^{\infty}\frac{s^{n-1}\,ds}{(s-Re^{i2r})}\right]\right\}$$

The first part of this equation is exactly the velocity V of equation 6., appendix . This means that this velocity is compensated by the sources and other vorticity in the plane, in order to satisfy the Kutta condition.
When $dw/d\zeta$ is multiplied with $d\zeta/dz$ in order to calculate velocities in the z-plane and at the same time $R \to 0$ then the third part of equation 19. goes to zero ($d\zeta/dz \sim R^{-n}$ and $n < 1$)
The only part that remains is:

$$\left.\frac{dw}{d\zeta}\right|_{R^-} = \lambda\gamma R^n e^{irn}\left[\frac{-\sin((n+1)r)}{\tan((1-n)\pi)} - \cos((n+1)r)\right]. \qquad 20.$$

Because the speed of the fluid must be directed along the sheet:

$$\left.\frac{dw}{d\zeta}\right|_{R^-} \cdot e^{ir} \quad \text{must be real} \qquad 21.$$

This means that:

$$e^{i(n+1)r} \cdot \left[\frac{-\sin((n+1)r)}{\tan((1-n)\pi)} - \cos((n+1)r)\right] \quad \text{must be real} \qquad 22.$$

Thus or:

$$e^{i(n+1)r} = \bullet\ \text{Real} \Rightarrow \sin(n+1)r = 0$$

$$\text{with}: \quad 0 < n < 1\ ;\ 0 < r < \pi \Rightarrow r = \frac{\pi}{(n+1)} \qquad 23.$$

or: $[\ldots] = 0$:

$$\tan((1-n)\pi) = -\tan((1+n)r)$$

$$\text{with}: \quad 0 < n < 1\ ;\ 0 < r < \pi \Rightarrow r = \frac{n\pi}{(n+1)} \qquad 24.$$

These two angles can be written as:

$$r = \frac{\pi}{2} \pm \left(\frac{1-n}{1+n}\right)\cdot\frac{\pi}{2} \qquad 25.$$

$$= \frac{\pi}{2} \mp \left(\frac{\pi}{\lambda} - \frac{\pi}{2}\right) \qquad 26.$$

These are exactly the two angles belonging to the sides of the wedge, compare equation 2., appendix .

APPENDIX 4

Cubic Spline Interpolation of pointvortices

The aim is to have available a function $\vec{K}(s)$, where s is the pathlength, that defines a curve that goes through all the pointvortex positions and that has continuous first and second derivatives.
We define a parameter t that, like s, goes and grows along the curve. t has the property that it has the value j when evaluated at vortex j. This means:

$$x_i = x(t=i) \qquad \text{At } s_j: \quad t = j \tag{1.}$$

$$y_i = y(t=i) \tag{2.}$$

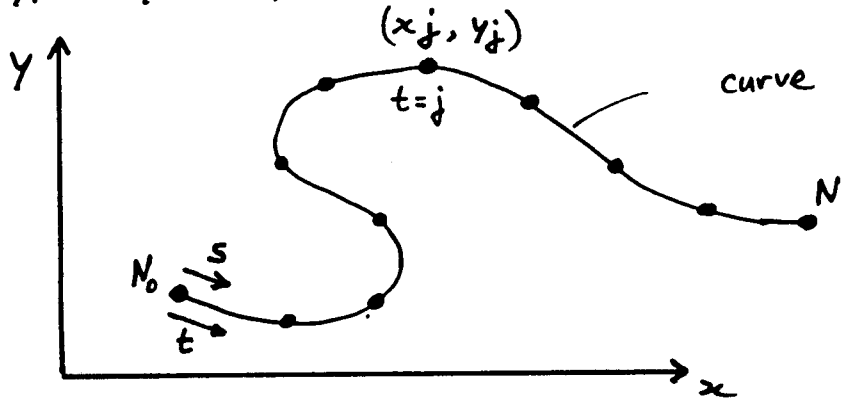

$\vec{K}$ is completely defined by x(t) and y(t). Because both x(t) and y(t) have the property that for each t there is only one x- or y-value. it is possible to make a cubic spline interpolation for x(t) and y(t). All details can be found in 'Numerieke methoden *'.
The essence of this method is that for example x(t) is piecewise described by a set of third order polynomes:

For each $j = N_0, N_0+1, \ldots, N$ with $j \leq t \leq j+1$ x(t) is given by:

$$x(t) = (j+1-t)\left(x_j - \tfrac{1}{6}B_j\left(1-(j+1-t)^2\right)\right) + (t-j)\cdot\left(x_{j+1} - \tfrac{1}{6}B_{j+1}\left(1-(t-j)^2\right)\right) \tag{3.}$$

The factors B_j can be derived from the following set of linear equations:

$$j = N_0+1, \ldots, N-1 \qquad \tfrac{1}{6}\left(B_{j-1} + 4B_j + B_{j+1}\right) = x_{j+1} - 2x_j + x_{j-1} \tag{4.}$$

$$j = N_0 \qquad B_{N_0} = 2B_{N_0+1} - B_{N_0+2} \tag{5.}$$

$$j = N \qquad B_N = 2B_{N-1} - B_{N-2} \tag{6.}$$

In the same way the cubic spline interpolation for y(t) can be determined.
The relation between the parameter t and the pathlength s can be found from:

$$s(t) = \int_{N_0}^{t} \sqrt{y^2(t) + x^2(t)}\, dt \tag{7.}$$

Now x(s) and y(s) are known and thus K(s).

* Numerieke methoden. Lecturebook of the dept. of Mathematics, technical university Eindhoven.